

INFORMATION TO USERS

The most advanced technology has been used to photograph and reproduce this manuscript from the microfilm master. UMI films the text directly from the original or copy submitted. Thus, some thesis and dissertation copies are in typewriter face, while others may be from any type of computer printer.

The quality of this reproduction is dependent upon the quality of the copy submitted. Broken or indistinct print, colored or poor quality illustrations and photographs, print bleedthrough, substandard margins, and improper alignment can adversely affect reproduction.

In the unlikely event that the author did not send UMI a complete manuscript and there are missing pages, these will be noted. Also, if unauthorized copyright material had to be removed, a note will indicate the deletion.

Oversize materials (e.g., maps, drawings, charts) are reproduced by sectioning the original, beginning at the upper left-hand corner and continuing from left to right in equal sections with small overlaps. Each original is also photographed in one exposure and is included in reduced form at the back of the book.

Photographs included in the original manuscript have been reproduced xerographically in this copy. Higher quality 6" x 9" black and white photographic prints are available for any photographs or illustrations appearing in this copy for an additional charge. Contact UMI directly to order.

U·M·I

University Microfilms International
A Bell & Howell Information Company
300 North Zeeb Road, Ann Arbor, MI 48106-1346 USA
313 761-4700 800 521-0600



Order Number 9030578

**Microtubule-based vesicle transport and isolation of a
microtubule-based motor from *Paramecium***

Schroeder, Christopher Carl, Ph.D.

University of Hawaii, 1990

U·M·I
300 N. Zeeb Rd.
Ann Arbor, MI 48106



MICROTUBULE-BASED VESICLE TRANSPORT AND ISOLATION OF A
MICROTUBULE-BASED MOTOR FROM PARAMECIUM

A DISSERTATION SUBMITTED TO THE GRADUATE DIVISION OF THE
UNIVERSITY OF HAWAII IN PARTIAL FULFILLMENT
OF THE REQUIREMENTS FOR THE DEGREE OF

DOCTOR OF PHILOSOPHY

IN MICROBIOLOGY

MAY 1990

By

Christopher C. Schroeder

Dissertation Committee:

Richard D. Allen, Chairman
Agnes K. Fok
Ian R. Gibbons
John B. Hall
Paul Q. Patek

ACKNOWLEDGEMENTS

I would like to sincerely thank Dr. Richard Allen and Dr. Agnes Fok for their guidance, encouragement and support throughout the course of my graduate education. I especially want to express gratitude to Dr. Allen for his insightful guidance in Cell Biology and for emphasizing a multidisciplinary approach in my training. Also, the outstanding technical assistance of Marilyn Ueno, and the friendships of all in our lab are acknowledged.

I wish to thank Dr. Ian Gibbons and the members of his lab, especially Dr. Grace Tang, for helpful discussions concerning dynein biochemistry, for generously supplying me with dynein samples, and for other technical assistance.

I would like to acknowledge the members of my Dissertation Committee for their constructive criticism.

I am grateful to Dr. Bill Saxton for assistance with video microscopy, in vitro motility assays, and other helpful discussions.

I would also like to thank Dr. Marilyn Dunlap and Tina Carvalho of the Biological EM Facility, and Margaret Morimoto, and Betty Ueda of the Microbiology Department office for their assistance from time to time.

Finally, I wish to express sincere appreciation to my wife, Laura, and to my family for their patience, love, understanding, and support of my dreams and goals over the years.

ABSTRACT

Cytoplasmic microtubule-based motility in Paramecium was investigated using a variety of techniques. Vesicle transport along microtubules was directly observed using video enhanced contrast microscopy. The observation of the association of vesicles with microtubules at the ultrastructural level was accomplished with the quick-freeze, deep-etch technique. Finally, a microtubule-based motor from the cytosol was isolated and purified.

Two microtubular structures, the cytopharyngeal microtubular ribbons and the post oral fibers, supported vesicle transport, but the properties of transport along these two microtubular structures were quite different. Each cytopharyngeal microtubular ribbon is composed of 10 - 12 microtubules aligned in a single plane oriented perpendicularly to the oral apparatus. The post oral fibers are composed of several bundles of microtubules which originate at the right side of the oral apparatus and extend to the posterior end of the cell.

Along the microtubular ribbons vesicles moved primarily toward the oral apparatus, a minus-end directed movement, at a rate of approximately 6 $\mu\text{m}/\text{sec}$. Only three populations of vesicles (discoidal vesicles, acidosomes, and 100 nm vesicles) were transported along these microtubules. This transport was smooth, continuous and exclusively on the anterior side of the ribbons. Vesicles occasionally moved away from the oral apparatus, but in this direction they moved only along the posterior side of the microtubular ribbons. The smooth nature and sidedness of transport are unique findings for an in vivo system.

Supporting evidence for the above observations was found at the ultrastructural level. Discoidal vesicles, acidosomes, and 100 nm vesicles were aligned in single file along the anterior side of the microtubular ribbons. Cross bridges were evident in most cases between the vesicle membrane and the microtubules.

Transport along the post oral fibers occurred only during and shortly after digestive vacuole formation and release from the oral apparatus. A distinct on/off switching mechanism was evident. The rate of transport was approximately 20 $\mu\text{m}/\text{sec}$ and exclusively plus-end directed. In contrast to transport along the microtubular ribbons, a heterogeneous population of vesicles were transported along the post oral fibers.

To understand the molecular basis for microtubule-based vesicle transport, a microtubule-based motor was isolated from the cytosol using bovine brain microtubules as an affinity matrix. This motor was found to be a two headed cytoplasmic dynein which closely resembled the cytoplasmic dyneins of higher organisms. The dynein exhibited a microtubule-stimulated ATPase activity and promoted microtubule gliding in an in vitro assay. This cytoplasmic dynein was directly compared to axonemal dyneins from Paramecium and were found to differ by five separate criteria. The criteria were morphology, sedimentation coefficient, polypeptide composition, vanadate cleavage patterns and CTPase/ATPase ratio. Therefore, the cytoplasmic dynein was not an axonemal dynein precursor. This dynein may be the motor that drives the microtubule-based vesicle transport along the ribbons in minus-end directed movements.

TABLE OF CONTENTS

	<u>Page</u>
ACKNOWLEDGEMENTS.....	iii
ABSTRACT.....	iv
LIST OF TABLES.....	vii
LIST OF ILLUSTRATIONS.....	viii
LIST OF ABBREVIATIONS AND SYMBOLS.....	xi
CHAPTER 1. INTRODUCTION AND OBJECTIVES.....	1
CHAPTER 2. LITERATURE REVIEW.....	4
CHAPTER 3. MATERIALS AND METHODS.....	30
CHAPTER 4. RESULTS.....	41
CHAPTER 5. DISCUSSION.....	100
APPENDIX - SUPPLEMENTARY TABLES.....	118
LITERATURE CITED.....	120

LIST OF TABLES

<u>Table</u>		<u>Page</u>
1	ATPase and CTPase activities of cytoplasmic and axonemal dyneins.....	86

APPENDIX TABLES

2	Axenic media formulation.....	118
3	Hook decoration buffer.....	118
4	PEM buffer.....	118
5	Dynein buffer.....	118
6	Dryl's solution.....	119
7	STEN.....	119
8	Column equilibration buffer.....	119

LIST OF ILLUSTRATIONS

<u>Figure</u>	<u>Page</u>
1 Schematic drawing of a microtubule	9
2 Schematic drawings of membrane flow and modifications in the phagosome-lysosome system of <u>Paramecium</u>	26
3 Purification scheme for cytoplasmic dynein from <u>Paramecium</u>	36
4 VECM micrograph of the microtubular ribbons.....	43
5 Low magnification VECM micrograph of identifiable cellular structures in <u>Paramecium</u>	43
6 Beaded appearance of the nascent vacuole.....	45
7 Vesicle transport toward the cytopharynx.....	45
8 Vesicle transport away from the cytopharynx.....	48
9 VECM morphology of vesicles transported along the MTR.....	48
10 Neutral red labelling of acidosomes.....	51
11 QF-DE fracture through the oral region.....	54
12 High magnification of the MTR illustrating the cross-links between the individual microtubules.....	54
13 Thin section micrograph illustrating planar sheet of the MTR.....	54
14 High magnification of the MTR adjacent to the cytopharynx.....	57
15 QF-DE fracture of acidosomes surrounding a nascent digestive vacuole.....	59
16 High magnification of an acidosome that appears firmly bound to the nascent digestive vacuole by short linkers.....	59
17 E fracture face of an acidosome along the MTR.....	61
18 P fracture face of the acidosome.....	61
19 Cross fracture of an acidosome illustrating the unique labyrinthine appearance of the lumen.....	61
20 A very small acidosome which illustrates the wide range of sizes for the acidosomes.....	61

<u>Figure</u>	<u>Page</u>
21 100 nm vesicles.....	64
22 High magnification of 100 nm vesicles.....	64
23 Cross section of the MTR near their origins and viewed from their distal ends toward their origin in the filamentous reticulum.....	67
24 Successive serial sections of a single MT in the proximity of the MTR.....	67
25 Digestive vacuole release from the oral apparatus.....	69
26 VECM micrograph of the postoral fibers.....	71
27 Postoral fiber transport.....	71
28 Digestive vacuole transport and rotation.....	74
29 QF-DE fracture of the postoral fibers.....	77
30 High magnification of a segment of the postoral fibers.....	77
31 Cross section of the postoral fibers distal to, and viewed from their distal ends toward the oral region.....	79
32 Cross section of the postoral fibers near their origin at the oral region.....	79
33 Purification procedure for cytoplasmic dynein.....	82
34 Relative mobilities of sea urchin dynein, <u>Paramecium</u> cytoplasmic dynein, and brain cytoplasmic dynein.....	82
35 Vanadate cleavage of <u>Paramecium</u> cytoplasmic dynein.....	82
36 S value determination for cytoplasmic dynein.....	84
37 Sucrose gradient purification of <u>Paramecium</u> cytoplasmic dynein.....	84
38 MT attachment to coverslip surface.....	88
39 Bending or kinking of a MT.....	88
40 MT gliding.....	90
41 Ultrastructural analysis of cytoplasmic dynein from <u>Paramecium</u>	92

<u>Figure</u>	<u>Page</u>
42 Purification of <u>Paramecium</u> axonemal dyneins.....	94
43 Ultrastructural analysis of axonemal dyneins from <u>Paramecium</u>	97
44 Comparison of vanadate cleavage patterns and intermediate chain composition for the three dynein species.....	99
45 "Channels" created by the MTR	106
46 Dorsal view of vesicle transport toward the oral region.....	108
47 Vesicle transport and associated vacuole growth.....	110

LIST OF ABBREVIATIONS AND SYMBOLS

AMP	adenosine 5'-monophosphate
AMP-PMP	5'-adenylylimidodiphosphate
ATP	adenosine 5'-triphosphate
CaCl ₂	calcium chloride
CEB	column equilibration buffer
cm	centimeter
CTP	cytidine 5'-triphosphate
°C	degrees centigrade
DIC	differential interference contrast
DV	digestive vacuole
EM	electron microscopy
GTP	guanosine 5'-triphosphate
h	hour
ITP	inosine 5'-triphosphate
kD	kilodalton
kV	kilovolt
KCl	potassium chloride
L	liter
M	molar
Mg ²⁺	magnesium ion
min	minute
mg	milligram
ml	milliliter
mM	millimolar
MAPs	microtubule-associated proteins
MT	microtubule
MTR	cytopharyngeal microtubular ribbons
NaCl	sodium chloride
nm	nanometer
QF-DE	quick-freeze, deep-etch
sec	second
TTP	thymidine 5'-triphosphate
UTP	uridine 5'-triphosphate
UV	ultraviolet
VECM	video enhanced contrast microscopy
µm	micrometer
µM	micromolar
>	greater than
%	percent
~	approximately

CHAPTER 1

INTRODUCTION and OBJECTIVES

Recent technological advancements have revolutionized light and electron microscopy as well as the field of cellular motility. Video enhanced contrast microscopy (VECM) has combined the use of high resolution video cameras and digital image processors with conventional light microscopes (Allen et al., 1981). With the proper optics it is now possible to detect single microtubules which are only 25 nm in diameter (10 times smaller than the resolution of the light microscope). This development has sparked a resurgence in use of the light microscope for a wide variety of applications in cell biology.

The impact of the quick-freeze, deep-etch (QF-DE) technique on electron microscopy equals that of VECM on conventional light microscopy. The QF-DE technique preserves ultrastructural details in a near native conformation (Heuser et al., 1979). Rapid freezing is obtained by compressing samples against a copper block cooled to liquid nitrogen (-196° C) or liquid helium (-269° C) temperatures which produces a freezing rate so rapid that damaging ice crystals are not allowed to form. In combination with freeze-fracturing and deep-etching, rapid freezing allows the observation of near-native cellular ultrastructure in three dimensions.

These two technical advances have had a dramatic impact on the study of intracellular motility and on investigations of microtubule-based vesicle transport. The nerve axon has been one of the most popular systems for the study of such vesicle transport. In 1985 Vale and

co-workers identified a force generating enzyme capable of translocating microtubules across a glass surface, as well as polystyrene beads or membranous vesicles along microtubules (Vale et al., 1985a). This force generating enzyme has been named kinesin and has been suggested to play a role in important cellular events, e.g., vesicle transport, expansion of the endoplasmic reticulum and chromosome movements during mitosis.

Cytoplasmic dynein represents another class of novel force generating enzymes presumably involved with microtubule-based vesicle transport (Paschal et al., 1987). However, this protein generates force along microtubules in the opposite direction to that of kinesin. Together these proteins could conceivably mediate all plus- and minus-end directed vesicle transport in cells. Although their widespread distribution supports a universal role in all eukaryotic cells, their occurrence in more species needs to be confirmed to support this idea. Also, their properties and function are not yet fully understood. Problems which remain to be studied include how they are regulated, and how they recognize and bind to vesicular membranes.

The ciliate Paramecium, a "primitive" eukaryote, offers an attractive system for further study of vesicle transport. This organism is large, easily cultured and can be manipulated readily. Its digestive system membranes have been extensively studied and a clear descriptive picture of vesicle transport along microtubules, and membrane flow and recycling has been developed (Allen, 1984; Fok and Allen, 1988). This large body of information already obtained for Paramecium forms a useful basis for further research. Two microtubule-based motile events have been postulated in Paramecium, but the enzymes producing the motive force have not been determined.

The objectives of this research are two-fold. First, I will study the microtubule-based vesicle transport of living Paramecium in as much detail as possible using video microscopy. Particular attention will be paid to the oral-region cytoskeleton and the events leading to digestive vacuole formation. Data will be collected on the morphology, rate of transport, and other prominent features of all vesicles being transported along microtubules within the cell. Corresponding evidence for microtubule-vesicle attachment will be obtained at the ultrastructural level using the QF-DE technique. The data will then be compared to properties of microtubule-based vesicle transport in other systems.

The second objective will be to isolate and characterize a microtubule-based motor from the cytosol of Paramecium. This will be accomplished using protocols established for microtubule-based motors in other systems. Once a motor has been isolated its properties will be characterized with regard to its polypeptide composition, enzymatic properties and morphological characteristics. The Paramecium motor will then be compared to kinesin and to cytoplasmic dyneins from other systems.

CHAPTER 2

LITERATURE REVIEW

I. Overview of vesicle transport

Directed organelle motility occurs in virtually every living eukaryotic cell (Schliwa, 1984). In many cases, microtubules (MTs) provide a framework upon which motility may occur (Schliwa, 1986). These motile events are involved in various cellular activities such as mitosis, pigment granule movements, and axonal transport (Dustin, 1978; Schliwa, 1986; Bershadsky and Vasiliev, 1988). Axonal transport is the most extensively studied system of microtubule-based vesicle transport processes (Grafstein and Forman, 1980), and will be used in this discussion to illustrate several different forms of MT-based vesicle transport.

The nerve axon is particularly suited for vesicle transport studies. The axon and synapse lack any biosynthetic capabilities (Grafstein and Forman, 1980), therefore, cellular materials must be synthesized in the neuronal cell body and transported through the axon. The use of radioactive tracers has revealed two forms of transport: fast and slow axonal transport (Lasek, 1970; Smith, 1971; Ochs and Ranish, 1969). Fast axonal transport through the axon is responsible for the movement of neurotransmitters and other proteins packaged in membrane-bound vesicles (McEwen and Grafstein, 1968). Fast axonal transport proceeds in both anterograde (cell body to synapse) and retrograde (synapse to cell body) directions (Grafstein and Forman, 1980). The rate of transport is from

1.0 to 5.0 $\mu\text{m}/\text{sec}$. Slow axonal transport carries soluble proteins such as tubulin and other cytoskeletal building blocks through the axon at rates of 0.02 $\mu\text{m}/\text{sec}$ (McEwen and Grafstein, 1968).

Fast axonal transport is an active process. It requires chemical energy in the form of ATP (Ochs, 1971; Adams, 1982) and is dependent on MTs. Conditions which interfere with oxidative metabolism, such as the lack of oxygen, inhibit axonal transport (Ochs and Hollingsworth, 1971). Likewise, compounds such as colchicine or nocodazole which depolymerize MTs also inhibit transport (Karlsson and Sjöstrand, 1969; Paulson and McClure, 1975; Hammond and Smith, 1977; Wang and Goldman, 1978). These findings led to speculation that a force generating ATPase which interacts both with MTs and vesicle membranes is responsible for vesicle transport (Ochs, 1971; Grafstein and Forman, 1980; Weiss, 1986).

The dynamic movements of axonal transport have been studied with light microscopy of living cells (Smith, 1971; Kirkpatrick et al., 1972; Cooper and Smith, 1974; Forman et al., 1977). Mitochondria and other large undefined vesicles move along the longitudinal axis of the axon in a saltatory fashion. The vesicles vary in terms of speed, distance traveled, direction, and duration of pauses in between movements, but in general their overall rate of transport is similar to that of fast axonal transport (Forman et al., 1977). Similar movements have been described in other cell types (Rebhun, 1972) suggesting similar mechanisms for transport in these cells.

Despite these highly informative observations there are inherent limitations with the use of conventional light microscopy. Only the largest cellular vesicles and organelles, such as mitochondria, can be

visualized and the transport filaments themselves are not visible. Therefore, the electron microscope has been used to study the components of transport. Results from these EM studies demonstrated the parallel arrangement of MTs and neurofilaments along the longitudinal axis of the axon (Kreutzberg and Gross, 1977). In electron micrographs of thin sectioned cells the close association between MTs and membranous vesicles is evident (Bird, 1976). Occasionally, cross bridging elements have been reported between the MT and the vesicles (Jalfors and Smith, 1969; Smith et al., 1970; Raine et al., 1971; Burton and Fernandez, 1973; Smith et al., 1975; Miller and Lasek, 1985). Langford et al. (1987) also noted projections on isolated axoplasmic vesicles which resembled MT-vesicle cross bridges. Miller and Lasek (1985) speculated that these cross bridges represent the force generating ATPase responsible for vesicle transport. However, these observations have been questioned by reports that such bridges could be created artifactually (Ris, 1985; Kondo, 1985).

The above observations reveal several shortcomings of past studies of axonal transport which are also true of most motile systems studied. The light microscope has the advantage that it can provide information on dynamic events in living or reactivated systems, but it is seldom able to image the components involved in transport such as MTs or small vesicles and is totally incapable of imaging the force producing motors. On the other hand, the electron microscope can be used to visualize these transport components, however, it can only provide a static image and cannot reveal ongoing dynamic motile events. Additionally, fixation artifacts often plague sample preparation for electron microscopy (Crang

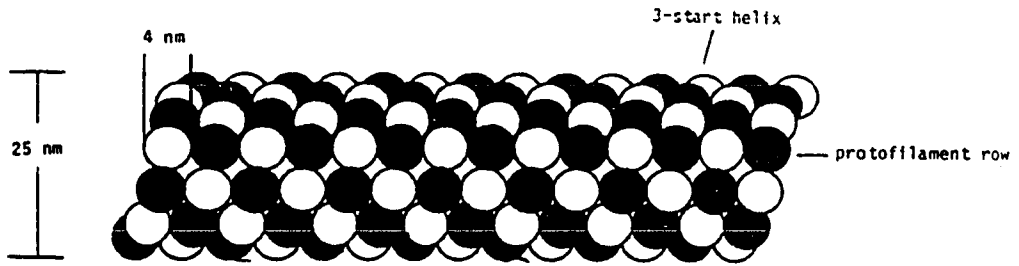
and Klomparens, 1988). Chemical fixation requires a few seconds to act during which dynamic cellular processes will continue. Instantaneous fixation of structure is not possible.

Before reviewing models of the mechanism of vesicle transport, it will be useful to highlight the properties of the two components involved in this transport; MTs and vesicles. Microtubules are tubular filamentous polymers composed of tubulin subunits and capable of binding to microtubule-associated proteins (MAPs)(Dustin, 1978). Neuronal tissue has been the source for most biochemical studies of MTs and MAPs due to their abundance in this tissue (Weisenberg, 1972). The MT polymer is composed of equal amounts of 55 kD alpha and beta tubulin subunits associated together as dimers (Shelanski and Taylor, 1967). These tubulin dimers are arranged into linear arrays of protofilaments with 13 protofilaments forming the wall of a 25 nm diameter MT (Dustin, 1978; Figure 1). The length of a MT varies depending on its cellular function. In neurons, MTs are believed to be as long as the axon itself which can be up to 10 meters in length in the whale (Dustin, 1978).

The MAPs promote the assembly of tubulin subunits into MTs in vitro and most likely stabilize the MTs in vivo (Sloboda et al., 1976). In mammalian brain there are two principle classes of MAPs; the high molecular weight MAPs and tau MAPs. The high molecular weight MAPs are comprised of MAPs 1A, 1A', 1B, 1C, 2A, and 2B (Vallee et al., 1984; Wiche, 1989). The tau MAPs represent a group of four polypeptides with molecular weights ranging from 55 kD to 62 kD (Weingarten et al., 1975; Cleveland et al., 1977). Other cells and tissues also contain MAPs. Some of these MAPs are very similar to the neuronal MAPs (Parysek et al., 1984; Huber et

Figure 1 - Schematic drawing of a microtubule. Alternating alpha (shaded) and beta tubulin subunits are arranged in rows to form a protofilament. Thirteen protofilaments make up the microtubule which is 25 nm in diameter. The arrangement of tubulin subunits, which measure approximately 4 nm in diameter, also form a three-start, left handed helix. (Redrawn from Shpetner and Vallee, 1989).

1



al., 1985; Neely and Boekelheide, 1988), while other MAPs appear to be unique (Vallee and Bloom, 1983). Most MAPs are observed in thin sections (Dentler et al., 1975) or in dried and metal shadowed preparations (Voter and Erikson, 1982) as slender filaments projecting from the microtubular surface. This finding suggests that MAPs may cross bridge MTs and vesicles in axons.

Early studies showed that an ATPase activity was associated with MTs. This activity would be consistent with a force producing molecule responsible for vesicle motility. However, Murphy et al. (1983) showed this reported ATPase activity to be an impurity and that neither MAP 1 nor MAP 2 had any ATPase activity. Thus, a function for MAPs (except for MAP 1C of bovine brain) in MT-based vesicle transport has not been established.

MTs arise from microtubule organizing centers which are usually located centrally near the nucleus within individual mammalian cells (Tucker, 1984). Electron-opaque amorphous satellites that surround centrioles are examples of microtubule organizing centers (Tucker, 1984). MTs are dynamically unstable in that their length fluctuates (Kirschner, 1989). Individual MTs grow slowly and continuously at their distal ends if the tubulin monomer and GTP concentrations are favorable. If neither of these conditions is optimal, the MT will shorten rapidly then begin to grow slowly again. The MTs are stabilized by MAPs and/or a "GTP cap" at their distal ends. These features as well as the arrangement of dimers give MTs an intrinsic polarity. The distal or fast growing end is termed the "plus" end, and the MT origin is termed the "minus" end.

The polarity of pre-existing cellular MTs can be determined morphologically by using a hook decoration procedure (Heideman and McIntosh, 1980). The curvature of the hooks in cross sectioned MTs indicates the plus and minus ends of the MTs. Using this procedure, Burton and Paige (1981) and Heidemann et al. (1981) determined the MTs in the axon are all oriented with their minus ends at the cell body, and their plus ends at the synapse. These observations suggest that the MTs provide a semi-rigid, non-elastic, polar filament which is suitably arranged to serve as a track for vesicle motility. They are also suitably organized to provide a structural role in defining the cell shape (Bershadsky and Vasiliev, 1988).

In contrast to the homogeneous properties of MTs from various sources, the vesicles transported along MTs can be quite heterogeneous in nature. Synaptic vesicles of nerve axons (Marchbanks and Israel, 1972), pigment granules of fish chromatophores (McNiven and Porter, 1984; Obika, 1986), and endosomes and lysosomes of tissue culture cells (Matteoni and Kries, 1987) are but a few examples of the variety of vesicles transported along MTs. Also, the morphology and organization of the endoplasmic reticulum (Teresaki et al., 1986) and the Golgi apparatus (Sandoval et al., 1984) are dependent upon MTs. These vesicles differ from one another in their sizes, compositions, and cellular functions. However, they do share two common properties: 1) they are transported along MTs and 2) they all have a membrane at their outer boundary.

The common association of vesicles with MTs and their transport along these MTs suggests a specific recognition between the membrane and the MT. Given the heterogeneity of the transported vesicles, a common receptor in

the vesicular membrane could account for their recognition and transport. Evidence for tubulin in membranes (Stephens, 1983; Stephens, 1986) would support a cross bridge model with a tubulin/MT binding site at each end of the force generating molecule. However, this is entirely speculative. The precise nature of this recognition and transport will require a greater understanding of the molecular components involved.

II. Technological Developments

Quick-Freeze, Deep-Etch Technique

In 1979 Heuser and co-workers developed the quick-freeze, deep-etch (QF-DE) technique to study the fusion of synaptic vesicles at the synaptic cleft (Heuser et al., 1979). This technique features ultra-rapid freezing with cooling rates approaching 10^6 degrees per second. The quick freezing not only halts cellular processes instantly, but also vitrifies the cellular water without the formation of damaging ice crystals. Thus, near-native ultrastructural details are preserved without the use of chemical fixatives or cryoprotectants. The rapidity of fixation yields ultrastructural details as close to their native state as is currently possible to obtain (Sitte et al., 1987).

The rapid freezing is achieved by compressing the sample against a highly polished copper block cooled to liquid nitrogen (-196° C) or liquid helium (-269° C) temperatures (Heuser et al., 1979). Excellent freezing is produced in a 20 μ m thick layer adjacent to the contact plane with the copper block. The sample is transferred to a freeze etch apparatus and fractured within the 20 μ m thick layer. Deep etching is possible because

non-etchable cryoprotectants have not been used. The deep etching exposes cellular structures such as the true membrane surfaces and the cytoskeletal structures that will be buried under the ice crystals if conventional freeze-fracture techniques are used (Hirokawa, 1986a). Following etching, the samples are rotary replicated with platinum and carbon and viewed in a transmission electron microscope. A tilting stage enables stereo pairs to be photographed. These stereo images permit the observation of cellular structures in three dimensions at high resolution (Heuser, 1981).

The QF-DE technique yields abundant information on cellular ultrastructure, especially concerning the cytoskeleton. Hirokawa has utilized this technique to study the three dimensional architecture of the nerve axon and its mechanism of intracellular vesicle transport. In his studies Hirokawa noted the fine cross bridges between MTs, neurofilaments, and membranous vesicles (Hirokawa, 1982; Hirokawa et al., 1985; Hirokawa and Yorifushi, 1986; Hirokawa, 1986b; Hirokawa et al., 1988b; Hirokawa et al., 1989). Unlike those seen in thin section electron micrographs, the cross bridges observed with this technique are numerous and very distinct. Likewise, Schnapp and Reese (1982) revealed the intricacies of the axoplasmic structure using this technique. All of these studies confirm the association and linkage of membranous organelles to MTs.

Combining immunocytochemistry with the QF-DE technique, Hirokawa has been able to identify certain cross linking structures such as MAP 1A (Shiumura and Hirokawa, 1987) and MAP 2 (Hirokawa et al., 1988a). In addition, the QF-DE technique or low angle rotary shadowing has enabled the direct observation of isolated molecules such as MAP 1 (Hirokawa,

1989), MAP 2 (Hirokawa, 1988), tau (Hirokawa et al., 1988b), dynein (Goodenough and Heuser, 1984), and kinesin (Hirokawa et al., 1989).

The high resolution of the QF-DE technique allows the observation of individual macromolecules (Heuser, 1983). In fact the arrangement of tubulin subunits within a MT has been revealed (Heuser and Kirschner, 1980). Temporal resolution is also precise. Although this technique can only produce a static image, the extremely rapid freezing rates allow the dynamic events existing immediately prior to, or during, freezing to be instantaneously stopped so that the resulting image is a more faithful representation of the dynamic structure than is possible to obtain by other techniques.

Video Enhanced Contrast Microscopy

Video enhanced contrast microscopy (VECM) has revolutionized light microscopy just as the QF-DE technique revolutionized electron microscopy. In 1981 Robert Allen interfaced a high resolution video camera to a light microscope equipped with differential interference contrast (DIC) optics and observed the contrast enhancement capabilities (Allen et al., 1981). By manually optimizing the gain and black level of the video camera, details in the image which are not visible by direct observation through the oculars are revealed. Also, the video camera can handle high light intensities which are overwhelming to the eyes (Schnapp, 1986). With the DIC optics the higher light intensity accentuates the differences in contrast. Thus high intensity illuminators and objective lenses with a high numerical aperture are used to maximize the optical system. In this way very low contrast images can be enhanced to highlight the desired

structural details. For example, single MTs in solution can be visualized with this technique (Allen et al., 1981; Schnapp, 1986). This capability is impressive given that the diameter of a MT is only 25 nm, ten times smaller than the resolution of the best light microscope. As a result of the diffraction of light, the MTs will appear to be 200-nm-wide filaments on the video monitor (Schnapp, 1986).

These imaging capabilities can be further expanded with the use of a digital image processing system (Allen et al., 1981). The two applicable processing functions are frame averaging and background subtraction. Frame averaging of stationary objects allows for the "addition" of multiple video frames so that subtle details are highlighted or enhanced. Continuous background subtraction eliminates the interference of out-of-focus structures which often obscures a particular image. Also, the effects of uneven illumination and lens imperfections can be minimized. A key feature of this computer processing is that the manipulations are performed at sufficiently rapid speeds to permit the image on the screen to be seen in real time (Allen et al., 1981). Thus, fully enhanced images of dynamic in vivo processes are obtained.

VECM has had a dramatic impact on MT-based vesicle motility studies. Hayden et al. (1983) were the first to observe MTs in a living cell and to view vesicles moving along these single MTs. This finding was expanded to show that vesicle transport could occur in both directions along a single MT (Hayden and Allen, 1984). Kachar et al. (1987) noted the dynamic shape changes of vesicles as they move along MTs. They pointed out that moving vesicles take on a teardrop shape with a flattened edge adjacent to the MT

and hypothesized that the flattened edge maximizes the contact between the vesicle and the MT. Also, the tear drop shape may be influenced by pulling the vesicle through the viscous cytoplasm (Kachar et al., 1987).

VECM is useful in studying fast axonal transport (Allen et al., 1982; Brady et al., 1982; Brady et al., 1985). In addition to confirming earlier observations of the saltatory motility of the large vesicles, two additional findings were noted. First, small (50 nm) motile vesicles have been detected for the first time. The transport of these vesicles is smooth and continuous (Allen et al., 1982) unlike the saltatory motions previously described for large vesicles (Cooper and Smith, 1974; Forman et al., 1977). Second, by using extruded axoplasm to provide a completely permeable system to which perturbations can be made, the effects of inhibitors have been directly determined. For example, the requirement for ATP for motility was confirmed (Brady et al., 1985). . Apyrase, which breaks down ATP to AMP, inhibits all transport. Addition of exogenous ATP restores transport. These and similar findings are bringing us closer to an understanding of the molecular basis for axonal transport.

III. Microtubule-based Motors

Kinesin

In 1985 Vale and co-workers made the interesting discovery that directed vesicle movements can occur along cytoplasmic filaments that had been separated from the extruded axoplasm of the squid giant axon (Vale et al., 1985c). These movements are ATP dependent and are inhibited by the ATP analog, AMP-PNP (Vale et al., 1985d; Brady et al., 1985). In the

presence of AMP-PNP the vesicles were observed to "freeze" along the filaments, suggesting that these vesicles are firmly bound to the filaments (Vale et al., 1985d; Lasek and Brady, 1985). Utilizing VECM and the QF-DE technique, Schnapp et al. (1985) determined these cytoplasmic filaments to be single MTs. These data support the hypothesis that interaction between vesicles and MTs is the basis for fast axonal transport.

Using AMP-PNP and a MT-affinity purification scheme, a soluble motility factor was isolated from the squid axoplasm (Vale et al., 1985d). This protein is capable of moving MTs across glass, and moving vesicles and carboxylated beads along single MTs (Vale et al., 1985d). The motile factor was named kinesin and represents the first candidate for a force generating molecule responsible for MT-based vesicular motile events of which fast axonal transport is the immediate example (Vale et al., 1985a).

Soon after its discovery in squid axons, kinesin was isolated from mammalian brain (Vale et al., 1985a), sea urchin eggs (Scholey et al., 1985) and Drosophila (Saxton et al., 1988), and was identified in mammalian tissue culture cells (Neighbors et al., 1988; Pfister et al., 1989). The widespread distribution of kinesin suggests a possible universal involvement of this molecule in cellular microtubular-based motile events such as vesicle transport and mitosis.

Kinesin isolated from bovine brain is a protein of 379 kD comprised of two 124 kD heavy chains and two 64 kD light chains (Bloom et al., 1988). It possesses an ATPase activity that is Mg^{2+} dependent and stimulated by MTs (Kuznetsov and Gelfand, 1986). The basal activity

varies with the tissue source as does the amount of stimulation by polymerized MTs (Hollenbeck, 1988). Soluble tubulin does not stimulate the kinesin ATPase activity. Kinesin is capable of hydrolyzing a wide range of nucleotides which include ATP, GTP, TTP, UTP, CTP, and ITP (Cohn et al., 1989). The ATPase activity is inhibited by 5 mM N-ethylmaleimide (Porter et al., 1987) or 100 μ M vanadate (Vale et al., 1985d).

The force generating properties of kinesin have been characterized using an in vitro motility assay (Vale et al., 1985d). In this assay kinesin is adsorbed to a coverslip and in the presence of ATP, single MTs bind and glide across the kinesin-coated surface. Alternatively, motile properties are examined by observing kinesin-coated latex beads or vesicles moving along stationary MTs (Vale et al., 1985d). Trypsinized vesicles and liposomes are not transported along the MTs, suggesting a membrane receptor (protein) is required for recognition and transport (Vale et al., 1985d).

Kinesin promotes MT gliding at rates ranging from 0.5 to 0.9 μ m/sec (Vale et al., 1985d; Porter et al., 1987; Cohn et al., 1987; Saxton et al., 1988). In the presence of Mg^{2+} , all the nucleotides listed above support gliding motility to some extent (Cohn et al., 1989). N-ethylmaleimide, vanadate, AMP-PNP, and chelators of Mg^{2+} act as non-competitive inhibitors to kinesin driven MT gliding (Cohn et al., 1989).

Force generation for kinesin is directed toward the plus ends of the MTs. Kinesin-coated beads move distally along MTs nucleated on isolated centrosomes (Vale et al., 1985d). In addition, demembranated and salt extracted Chlamydomonas axonemes, which fray at their plus ends, are

translocated across kinesin-coated coverslips with their frayed ends trailing (Paschal and Vallee, 1987).

Kinesin-coated bead movements can be determined with nanometer scale precision using a computer program to track bead movements along single MTs. The beads move in discrete 4 nm steps along the MT (Gelles et al., 1988). This distance corresponds to the spacing of individual tubulin monomers along the MT (Dustin, 1978; and Figure 1). There is little to no side-to-side movement indicating motility occurs along a single protofilament (Gelles et al., 1988).

Morphologically, kinesin resembles a small myosin molecule. Two 10-nm globular heads are connected by a single thin stalk to a fan shaped tail (Hirokawa et al., 1989). The overall length of the molecule is 80 nm with a flexible hinge region in the center of the stalk. The globular heads have been identified as the 120 kD heavy chains which contain the ATPase activity as well as the MT binding domains (Yang et al., 1989). The 64 kD light chains have been localized in the fan shaped tail and presumably serve as the vesicle binding domain (Hirokawa et al., 1989).

The function of kinesin has not yet been unequivocally determined. In reconstituted vesicle transport systems kinesin, by itself, is unable to support vesicle motility along MTs (Schroer et al., 1988). In addition to kinesin other undefined components of the cytosol are required to promote vesicle motility. Although the exact role kinesin plays in motility is unclear, it is hypothesized to play roles in anterograde axonal transport (Vale et al., 1985a), mitosis (Scholey et al., 1985), expansion of the endoplasmic reticulum (Vale and Hotani, 1988; Dabora and Sheetz, 1988b), and receptor-mediated endocytosis (Vale, 1987).

Localization at the light microscopic level supports the proposed functions (Scholey et al., 1985; Neighbors et al., 1988, Pfister et al., 1989). In the sea urchin egg, kinesin is localized in the mitotic spindle. In cultured cells kinesin displays a punctate pattern which is abolished when the cells are pre-treated with Triton X-100. These data suggest that kinesin is associated with vesicles primarily.

The function of kinesin is currently being addressed by functional inhibition and molecular genetic methods. Monoclonal antibodies which inhibit in vitro motility have been produced (Ingold et al., 1988). These antibodies may prove useful for in vivo inhibition studies. In Drosophila the gene for the kinesin heavy chain has been identified, cloned and sequenced (Yang et al., 1989). In conjunction with this work, kinesin deficient Drosophila mutants are being developed to further elucidate the function of this novel MT-based motor (Saxton and Raff, 1988).

Cytoplasmic Dynein

Not long after the discovery of kinesin, Paschal et al. (1987) showed that calf brain MAP 1C is a MT-based motor distinct from kinesin. MAP 1C possesses a MT-stimulated ATPase activity and can translocate MTs in an in vitro motility assay.

Several properties distinguish MAP 1C from kinesin. The most profound difference is the direction of transport. MAP 1C translocates demembranated and salt extracted Chlamydomonas axonemes with the frayed or plus-end leading, indicating a minus-end directed transport (Paschal and Vallee, 1987). In the axon this would correspond to retrograde axonal transport, opposite to that of kinesin. The average gliding velocity for

MAP 1C is 1.25 $\mu\text{m}/\text{sec}$, nearly twice that of kinesin (Paschal et al., 1987).

The ATPase of MAP 1C resembles kinesin in that virtually all nucleotides are hydrolyzed by this enzyme (Shpetner et al., 1988). However, the rate of hydrolysis for GTP, CTP, and TTP exceeds that of ATP by as much as 10 fold. But, unlike kinesin, only ATP is capable of supporting MT gliding (Shpetner et al., 1988). The ATPase activity is strongly inhibited by 5 to 10 μM vanadate and 1 mM N-ethylmaleimide (Shpetner et al., 1988). This is another distinguishing feature of this MT-based motor, making it distinct from kinesin.

MAP 1C appears to be a much larger molecule than kinesin. The predominant MAP 1C polypeptide is >350 kD on SDS-PAGE and has a sedimentation coefficient of 20S (Paschal et al., 1987). The sedimentation coefficients of the other high molecular weight MAPs are only 3-5S (Paschal et al., 1987), and the S value for kinesin is only 9.6S (Bloom et al., 1988). These properties of MAP 1C are surprisingly similar to those of axonemal dyneins, the ATPases responsible for ciliary or flagellar bending (Gibbons, 1981). Further examination has revealed the comigration of MAP 1C with Chlamydomonas axonemal dynein (Paschal et al., 1987). An additional comparison has been made using vanadate photocleavage, which cleaves dynein heavy chains at their ATP binding site (Gibbons et al., 1987). Vanadate cleavage of MAP 1C produces two cleavage fragments of -185 and 225 kD (Paschal et al., 1987). Thus, MAP 1C shows striking similarities to axonemal dyneins.

Scanning transmission electron microscopic (STEM) analysis of MAP 1C reveals a two headed dynein morphology (Vallee et al., 1988). This

finding verifies MAP 1C as cytoplasmic dynein, the long sought analog of ciliary and flagellar dynein. From STEM analysis the average mass of the cytoplasmic dynein is calculated to be 1.26×10^6 daltons (Vallee et al., 1988). Combined with data from gel densitometry, the composition of this cytoplasmic dynein molecule was shown to consist of two 410 kD heavy chains, three 74 kD subunits, and one each of 59, 57, 55, and 53 kD subunits (Vallee et al., 1988).

Despite the similarities between brain cytoplasmic dynein and the axonemal dyneins of sea urchin and Chlamydomonas flagella, important differences exist. The polypeptide composition of the intermediate and light chains is markedly different for each dynein species (Bell et al., 1979; Pfister et al., 1982; Paschal et al., 1987). Presumably, this difference is manifested in the different functional roles for the two species. Vallee et al. (1989) suggested that the unique subunit composition of cytoplasmic dynein is particularly suited for binding to organelles rather than MTs. Also, the ATPase properties for the two dyneins are different. Axonemal dyneins are only capable of hydrolyzing ATP (Gibbons, 1966), while cytoplasmic dyneins exhibit a broad range of substrate specificity (Shpetner et al., 1988).

Like kinesin, cytoplasmic dynein can be isolated from a number of tissue sources. In addition to neuronal tissue, cytoplasmic dynein has been isolated from rat liver (Collins and Vallee, 1989) and rat testes (Neely and Boekelheide, 1988), HeLa cells (Pfarr and McIntosh, 1988), chick embryo fibroblasts (Schroer et al., 1989) and sea urchin eggs (Pratt, 1981). A dynein-like ATPase very similar to the cytoplasmic dynein has also been isolated from nematodes (Lye et al., 1987).

Likewise, a dynein-like ATPase has been isolated from Reticulomyxa which supports bidirectional motility of latex beads on MTs (Euteneuer et al., 1988).

The functional activity of cytoplasmic dynein has been studied using vanadate photocleavage and an in vitro motility assay (Schroer et al., 1989; Schnapp and Reese, 1989). Chick embryo fibroblast cytosol, which contains cytoplasmic dynein, is capable of promoting minus-end directed vesicle motility along single MTs. Vanadate photocleavage of the cytosol results in the loss of all minus-end directed vesicle movement. The addition of purified cytoplasmic dynein restores the vesicle motility. This finding strongly suggests that cytoplasmic dynein is the motor for minus-end directed vesicle transport. However, as for kinesin, other undetermined and uncharacterized soluble factors are required for motility. Purified cytoplasmic dynein alone is unable to support motility in a reconstitution system using purified vesicles and MTs (Schroer et al., 1989).

IV. Paramecium as a model system

The ciliate Paramecium, a "primitive" eukaryote, offers an attractive system for the study of vesicle transport. The digestive system has been well characterized and provides a clear picture of membrane transport, flow and recycling (for reviews see Allen, 1984; Fok and Allen, 1988). The digestive vacuoles proceed through a four step cycle which includes formation, acidification, digestion, and defecation (Fok et al., 1982).

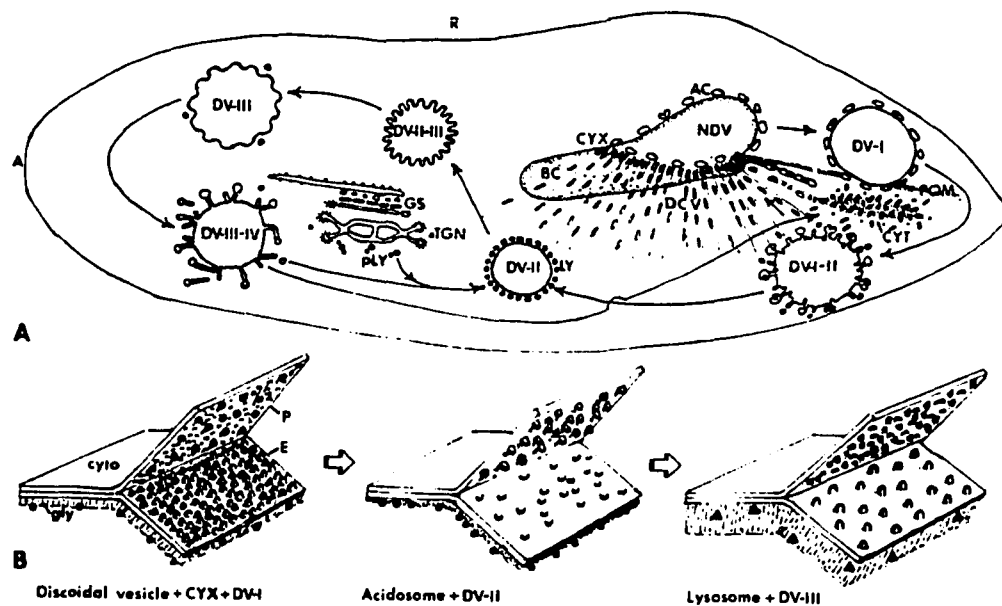
Three separate pools of vesicles contribute membrane at precise times to three of the digestive vacuole stages (Allen, 1984). In addition, monoclonal antibodies have been raised to each of the three vesicular pools and are being utilized to further characterize these membranes (Fok et al., 1986). One population of vesicles, the discoidal vesicles, were observed to be closely associated with MTs in electron micrographs and were reported to be transported along MTs (Allen, 1974; Allen and Fok, 1980) although this transport was not directly visualized.

Besides the above features Paramecium is an excellent cellular system to study MT-based vesicle transport, because of its large size (50 x 200 μm), ease of cultivation (Fok and Allen, 1979) and handling, and it offers, through its well defined digestive system, a unique opportunity to understand processes such as MT-motor-vesicle recognition. A detailed description and a schematic diagram (Figure 2) of this model system is presented to facilitate a better understanding of vesicle and vacuole movements in this cell.

In 1974 Allen described an elaborate cytoskeletal architecture near the oral apparatus of Paramecium which presumably facilitates the transport of discoidal vesicles toward the cytopharynx (Allen, 1974). The oral apparatus consists in part of approximately 40 ribbons of MTs, with each ribbon consisting of 10 to 12 MTs lying side by side. These ribbons are arranged at 1 μm intervals along the left edge of the cytopharynx from which they extend several μm into the cytoplasm (Allen, 1974). Discoidal vesicles are in close association with these microtubular ribbons (MTR). These vesicles maintain a constant 40-nm spacing from the MTR and are predominantly on one side of the ribbon (Allen, 1974). Occasionally,

Figure 2 - Schematic drawings of membrane flow and modifications in the phagosome-lysosome system of Paramecium. A. View of Paramecium from the dorsal surface. The anterior end (A) is to the left and the right side (R) is at the top. The buccal cavity (BC) is in a mid ventral location and is continuous with the cytopharynx (CYX) where nascent phagosomes (NDV) form. Ribbons of microtubules fan out from the cytopharynx directing discoidal vesicles (DCV) to this region. Acidosomes (AC) bind to the NDV as it forms and travel with the phagosome (DV-I) as it moves along the postoral bundles of microtubules (POM) toward the cell's posterior pole. Fusion of the acidosomes and retrieval of DV-I membrane results in a smaller and acidified DV-II which binds to lysosomes (LY). Fusion of lysosomes with the DV-II leads to a DV-III or phagolysosome. After digestion lysosome components are retrieved, mix with primary lysosomes (pLY) which bud from the Golgi stack (GS) and/or the trans Golgi network (TGN) and eventually bind to another DV-II. The spent vacuole (DV-IV), from which lysosome membrane components and acid phosphatase are removed, passes to the cytoproct (CYT) where it is defecated. Spent vacuole membrane is retrieved as tubular vesicles of which at least some become discoidal vesicles. B. Membrane modification can be seen in the freeze fracture appearance of the membrane especially on the E-fracture face (E) but also on the P-fracture face (P). Another modification occurs in the appearance of the glycocalyx (gly) lining the luminal side of vesicle and vacuole membranes. The cytosolic (cyto) side of the membranes has not been studied, but must bear recognition factors. In addition, different populations of vesicles have different antigenic binding sites which are indicated here as circles, squares and rectangles on the luminal sides of the membranes. The exact location of these antigenic sites is not actually known. Additional details can be found in the text. (From Allen et al., 1988).

2



A

B

cross bridges between the MTs and vesicles are observed and their constant 40-nm spacing even with buckled ribbons suggested a firm linkage between the two structures (Allen, 1975).

Pulse chase experiments utilizing horseradish peroxidase subsequently verified that these vesicles are being transported along the MTR (Allen and Fok, 1980). At the cytoproct, the digestive vacuole contents are defecated and the membrane of the vacuole is retrieved in the form of tubules (Allen and Wolf, 1974). The tubules are then transformed into discoidal vesicles as they associate with the MTR. At the open cytoproct, these tubules pick up horseradish peroxidase from the medium. With time, the labelled discoidal vesicles appear at the cytopharynx. Thus, the membrane of the digestive vacuole is retrieved as discoidal vesicles and transported back to the cytopharynx along MTR to form additional digestive vacuoles.

The discoidal vesicle transport is just one of the steps in the digestive vacuole cycle. The digestive cycle begins when a digestive vacuole is formed at the cytopharynx by the fusion of discoidal vesicles with the cytopharyngeal membrane (Allen, 1974). As the vacuole grows, a second population of acidic vesicles, the acidosomes, bind to the nascent vacuole (Allen and Fok, 1983a-c). An unknown stimulus triggers the release of the vacuole from the cytopharynx. The vacuole, now termed a stage I digestive vacuole (DV-I)(Fok et al., 1982) moves rapidly to the posterior end of the cell. The subsequent fusion of acidosomes with the vacuole causes the vacuolar pH to drop from 7 to 3 in a matter of minutes (Fok et al., 1982). As the vacuolar pH drops the vacuole condenses in size as membrane tubules are retrieved yielding a stage II DV (Allen and

Staelin, 1981). The lysosomes now recognize the acidified and condensed vacuoles and bind to them. Lysosomal fusion with the DV-II results in a DV-III which is the digestion phase of the cycle (Fok et al., 1984). The lysosomal enzymes hydrolyze the engulfed vacuolar contents. Following digestion, at least some part of the lysosomal membrane is retrieved from the vacuole (Allen and Fok, 1984), which is now termed a DV-IV. The DV-IV is defecation competent (Fok et al., 1982) and can fuse with the cytoproct to release the undigestible vacuolar contents (Allen and Wolf, 1974). The spent vacuolar membrane is retrieved and recycled to the cytopharynx as described above. This entire digestive process requires as little as twenty minutes for completion.

In the course of studying this sequence of events, much knowledge has been gained as to the nature and function of each of the vesicular pools that give rise to the DV membranes. Each pool of vesicles has a characteristic morphology, evident in both thin section and conventional freeze fracture electron microscopy (Allen, 1984). Also, the cellular distribution of each pool is known. For example, the discoidal vesicles and acidosomes are predominantly located near the oral region. Recently, monoclonal antibodies specific for each vesicular pool and corresponding digestive vacuole stage have been obtained. These antibodies have been used to localize the epitopes on the vacuolar and vesicular membranes both at the light (Fok et al., 1986) and EM (Allen et al., 1986) levels. These antibodies are currently being utilized for the isolation and characterization of the membranes of the digestive system. Thus, this system offers the unique opportunity to study the transport of several partially defined vesicle pools.

MT-based motility in Paramecium also occurs along the postoral fibers. These fibers are bundles of MTs which originate from the right side of the oral region and extend to the posterior end of the cell (Jurand and Selman, 1969; Cohen et al., 1982). The nascent vacuole travels along these fibers immediately following the pinching off of the vacuole from the cytopharynx. While this transport process has long been recognized (Mast, 1947), the basis for this movement is not well characterized. Cohen et al. (1984) note the rate of transport is extremely rapid ($\sim 15 \mu\text{m}/\text{sec}$) and postulate that actin microfilaments may be involved in the transport process.

Other vesicles in Paramecium display saltatory motility in vivo. Aufderheide (1977, 1978) found that mitochondria and trichocysts (secretory organelles) display saltatory motility in immobilized cells. These organelles are frequently found adjacent to MTs in electron micrographs and Plattner et al. (1982) proposed that trichocysts move along MTs to their docking sites in the cell cortex.

MATERIALS AND METHODS

Materials

Paramecium multimicronucleatum was cultured in an axenic medium (Table 2 in Appendix) according to Fok and Allen (1979) and harvested at mid logarithmic phase of growth. Stationary phase cultures reached cell densities of $\sim 8,000$ cells per ml. Taxol was a generous gift of Dr. Matthew Suffness, National Cancer Institute, Bethesda, MD. Sea urchin dynein was generously provided by Dr. Ian Gibbons. Phosphocellulose-purified tubulin, Drosophila kinesin, and 3 anti-kinesin antibodies were provided by Dr. Bill Saxton, Dept. of Biology, Indiana University, Bloomington, IN. Two additional anti-kinesin antibodies were provided by Dr. Jonathan Scholey, National Jewish Center for Immunology and Respiratory Medicine, Denver, CO. Electrophoresis reagents were obtained from Bio-Rad Laboratories (Richmond, CA). Unless noted, all other reagents were obtained from Sigma Chemical Co. (St. Louis, MO). All buffer and media formulations used in this study can be found in Tables 2 - 8 in the Appendix.

Methods

I. Video Microscopy

DIC microscopy - Free swimming paramecia were immobilized by gentle compression between a slide and coverslip as excess fluid was being withdrawn with filter paper strips (Whatman #1, Hillsboro, OR) while observing the cells under low power. Intracellular vesicle transport was

monitored using either a Zeiss Axioplan or Zeiss Universal microscope equipped with differential interference contrast (DIC) optics (Thornwood, NY). The optical and video trains were as follows: Axioplan microscope (located in the Department of Biology, Indiana University, Bloomington, IN) - a 100 watt mercury arc lamp, heat reflecting and absorbing filters, a 546 nm interference filter, a 1.4 numerical aperture (N.A.) condensor, a 100X/1.3 N.A. Plan-neofluar objective, a 2X optivar, a Dage 68 video camera (Michigan City, IN) with Newvicon tube, Panasonic WV-5410 monitor (Secaucus, NJ) and Panasonic AG6300 1/2 inch video recorder; the Universal microscope was equipped as was the Axioplan except for a 100 watt halogen lamp, a 40X/.75 N.A. or 100X/1.25 N.A. Planachromat objective, a 16X or 8x projection lens (instead of optivar), a Dage 67M camera and a Panasonic WV-5470 monitor. Image enhancement of recorded images, when required, was performed on a Kontron IBAS II image analysis system (Zeiss, Thornwood, NY). Single video frames were normalized and a low pass filtered image was subtracted from the original image to correct for uneven illumination. The contrast of the resultant image was then digitally enhanced. Photographs were taken directly from the monitor with a 35 mm camera using a macro lens and Kodak Panatomic-X film (Rochester, NY). A 50 lines/inch ronchi ruling (Edmund Scientific Co., Barrington, NJ) was used in front of the camera lens to filter out the video scan lines.

Neutral Red Labelling - Acidic compartments were labelled by adding neutral red (0.05 mg/ml) to the cell culture. After one min the labelled cells were pelleted in a clinical centrifuge and resuspended in fresh axenic medium. These cells were immobilized, observed with brightfield illumination and recorded on videotape.

II. Electron Microscopy

Quick-Freeze, Deep-Etch Technique - Cells were rapidly frozen according to Allen et al. (1989). Briefly, living paramecia were pelleted using a clinical centrifuge at full speed for 1 min. A small drop of the pellet was placed on a thin copper hat mounted on a foam cushion. This assembly was transferred to the MM80 head of a Reichert-Jung KF80 rapid freezing device (Cambridge Instruments, Buffalo, New York). The sample was impact frozen against a highly polished copper block cooled by liquid nitrogen to -195° C. The frozen sample was stored in liquid nitrogen until use.

Freeze fracturing and etching was performed in a Balzers 401 freeze-etch apparatus (Hudson, NH) as previously described (Hirokawa, 1986a; Allen et al., 1989). The quick-frozen sample was fractured within 20 μ m of the frozen surface to insure minimal ice crystal damage. The temperature of the cold table was raised to -95° C for 4 - 6 min to allow for the sublimation of ice from the freshly cleaved surface. A 2-nm thick layer of platinum shadow was rotary replicated at an angle of 24° and this was followed by a 15-nm carbon backing coat shadowed at an angle of 80° . The replica was removed and cleaned first on bleach, and then chromic acid and this was followed by rinsing in DDW before picking up the replicas on Formvar-coated slot grids (Ted Pella, Redding, CA). The replicas were examined at 80 kV in a Zeiss 10A electron microscope (Thornwood, NY). Micrographs were printed in reverse contrast so that raised areas appear white against a black background.

Microtubule Polarity - The hook decoration procedure of Heidemann and McIntosh (1980) was used. Briefly, cells were incubated in a hook decoration buffer (Table 3 in Appendix) for 20 min. Following incubation, cells were fixed for 30 min with 2% glutaraldehyde (Ladd Research Industries, Inc., Burlington, VT) in 0.5 M PEM (Table 3 in Appendix) containing 1% tannic acid (Fisher Scientific Co., Springfield, NJ). The fixed cells were washed twice with 0.5 M PEM buffer, twice with DDW, then dehydrated through a series of increasing percentages of ethanol. Spurr's resin (Electron Microscopy Sciences, Fort Washington, PA) was used as the embedding medium and cured at 60° C for 2 days. Cells were mounted and sectioned either transversely or longitudinally using a glass knife on a Reichert-Jung Ultracut E ultramicrotome. Sections were picked up on Formvar-coated slot grids, stained with aqueous uranyl acetate and lead citrate (Reynolds, 1963) then examined at 80 kV in the Zeiss 10A. Care was taken to follow orientation of the sections throughout the process to insure proper polarity determination.

Thin Section Electron Microscopy - Cells were fixed with 0.25% glutaraldehyde in phosphate buffer, and embedded in Lowicryl K4M resin (Polysciences, Inc., Warrington, PA) according to the manufacturer's instructions. The cells were sectioned, stained and observed as outlined above.

III. Biochemical Isolations and Related Procedures

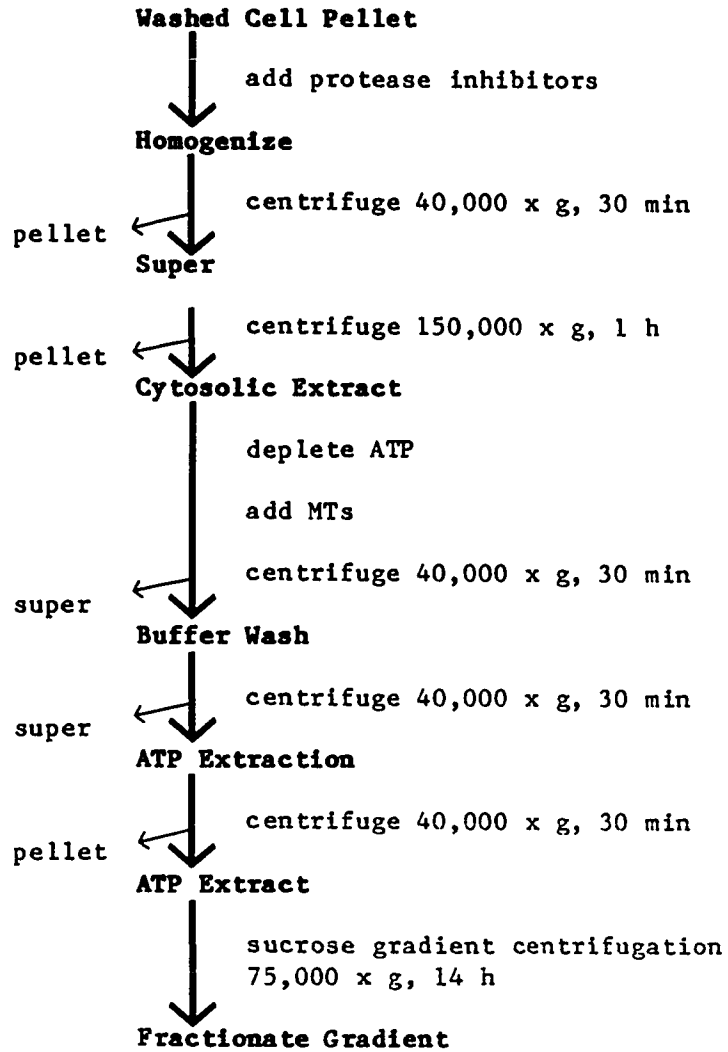
Bovine Brain Microtubules - The taxol isolation procedure of Vallee (1982, 1986) was used. Briefly, bovine brain white matter was homogenized

in 1 volume of PEM buffer (Table 4 in Appendix) using a teflon-in-glass homogenizer on a drill press at low speed. The homogenate was centrifuged at 40,000 x g for 30 min in a Beckman J2-21M centrifuge using a JA20 rotor (Beckman Instruments, Palo Alto, CA). The supernatant was recovered and centrifuged again at 150,000 x g for 1 h in a Beckman L2-65B centrifuge with a TY-65 rotor. The resulting supernate (cytosolic extract) was recovered and its volume was measured. Taxol and GTP were added at concentrations of 20 μ M and 1mM, respectively, and the extract was warmed to 37° C for 30 min to polymerize the MTs. The MTs were pelleted at 40,000 x g for 30 min through a 10% sucrose cushion in PEM buffer. The MTs were resuspended with PEM to one fifth the volume of the original cytosolic extract then washed once with PEM and twice with 10 mM MgATP and 0.36 M NaCl in PEM buffer to release the bound MAPs and motors. The resultant pellet was virtually pure tubulin free of contaminating proteins. The pellet was resuspended to one tenth of the original volume of the cytosolic extract with PEM buffer containing 10 μ M taxol, frozen in liquid nitrogen and stored at -80° C.

Cytoplasmic Dynein (see Figure 3) - 5 or 10 L of cells were harvested using a cream separator and concentrated to a pellet using a clinical centrifuge. After washing twice with cold PEM buffer the cell pellet was resuspended in an equal volume of PEM buffer containing protease inhibitors (0.1 mg/ml soybean trypsin inhibitor, 2 mM phenylmethylsulfonyl fluoride, and 1 mM dithiothreitol). Unless otherwise noted, all subsequent manipulations were performed at 4° C. Cells were homogenized to approximately 80% breakage using a ball bearing homogenizer

Figure 3 - Purification scheme for cytoplasmic dynein from Paramecium. See text for additional details.

3



(Berni-tech Engineering, Saratoga, CA) and a cytosolic extract was obtained as above. Hexokinase (36 units/ml) and glucose (9 mM) were added and incubated for 15 min at room temperature to deplete endogenous ATP. MAP-free bovine brain MTs and taxol were added to 0.3 mg/ml and 20 μ M, respectively, and incubated on ice for 25 min to allow the dynein to bind to the MTs. An additional five min incubation at 37° C was carried out to insure the complete polymerization of the MTs. The MT/dynein pellet obtained by centrifugation at 40,000 x g for 30 min was washed once with PEM buffer and was resuspended to one fifth of the volume of the original cytosolic extract with PEM containing 10 μ M taxol. The dynein was extracted from the MTs by the addition of 10 mM MgATP in PEM. Following a 20 min incubation at room temperature the MTs were pelleted as above. Cytoplasmic dynein was recovered in the supernate and concentrated in a Centricon 30 microconcentrator (Amicon Corp., Danvers, MA). The concentrated ATP-sensitive extract was layered on a 6 ml linear sucrose gradient (5 - 20%) in dynein buffer (Table 5 in Appendix) and centrifuged for 14 h at 75,000 x g in a Beckman SW50.1 rotor. The gradient was fractionated from the bottom, and 0.4 ml fractions were collected.

Axonemal Dynein - Cells were harvested and pelleted as described above for the isolation of cytoplasmic dynein. Cells were washed with cold Dryl's solution (Table 6 in Appendix) to induce trichocyst firing (trichocysts are potential contaminants)(Adoutte et al., 1980). The cell pellet was resuspended in 5 pellet volumes of Dryl's solution. An equal volume of STEN (Table 7 in Appendix) was added and incubated for 10 min on ice. Deciliation was initiated with the addition of 10 mM CaCl₂

and 30 mM KCl, and allowed to continue for an additional 15 min. The extent of deciliation was monitored by darkfield microscopy. The cell bodies were pelleted at half speed in a clinical centrifuge. The supernate containing cilia was recovered and centrifuged at 27,000 x g for 20 min. The cilia were washed twice in dynein buffer then resuspended to the original cell pellet volume. Demembration was accomplished by incubating in cold 1% Triton X-100 for 30 min. The axonemes were washed twice with dynein buffer to remove the membrane fraction. The resultant pellet was resuspended with 0.5 volume of high salt extraction buffer (0.6 M NaCl in dynein buffer) and incubated for 15 min on ice. The axonemes were pelleted at 40,000 x g for 30 min and the dynein was recovered in the supernate and concentrated in a Centricon 30. The concentrated dynein extract was layered on a linear sucrose gradient (5 - 25%) in dynein buffer and centrifuged for 12 h at 75,000 x g and fractionated.

Ion Exchange Chromatography - Cytoplasmic dynein obtained from peak sucrose gradient fractions were pooled and dialyzed against column equilibration buffer (CEB, Table 8 in Appendix). The dialyzate was layered over a 1 ml DEAE-Sephacel column equilibrated with CEB. The column was washed with CEB until the absorbance of the eluate returned to the baseline (approximately 20 ml of CEB). Elution of cytoplasmic dynein was accomplished with 10 ml of CEB supplemented with 200 mM KCl. Fractions of 1.5 ml were collected. Protein concentrations were monitored using an LKB column chromatography system (Pharmacia LKB Biotechnology Inc., Pleasant Hill, CA).

Vanadate Photocleavage - The procedure of Gibbons et al. (1987) was used. Briefly, vanadate and MgATP both at 150 μ M were added to the sucrose gradient purified dynein. Controls contained MgATP but no vanadate. The samples and controls were irradiated for 1 h on ice with a 365 nm UV light from a distance of approximately 5 cm.

In Vitro Motility Assay - 16 μ l aliquots of either a crude ATP extract or sucrose gradient purified cytoplasmic dynein were adsorbed to a glass coverslip for 15 min in a moist chamber. 2 μ l of taxol-stabilized MTs composed of phosphocellulose-purified tubulin (0.2 mg/ml, containing 20 μ M taxol and 1 mM GTP) and 2 μ l of 50 mM MgATP were added and the coverslip was inverted onto a glass slide and sealed with valap (1:1:1 vaseline, lanolin, paraffin). Motile properties were observed with the DIC optics of an Axioplan microscope and recorded on videotape.

Drosophila kinesin was used as a positive control for MT gliding motility. (Note: this assay was performed with Dr. Bill Saxton at Indiana University).

Other Biochemical Procedures - Protein determination was performed using the Bio-Rad protein assay. SDS-PAGE was performed according to Laemmli (1970) under denaturing and reducing conditions. The gels were stained with either Coomassie Brilliant Blue R-250 or the silver staining procedure of Merril et al., (1981). The malachite green method for the detection of inorganic phosphate (Lanzetta et al., 1979) was used for the ATPase and CTPase assays. Sedimentation coefficients were determined as described by Martin and Ames (1961).

IV. Ultrastructural Analysis of Isolated Proteins

Negative Stain - A carbon film was evaporated onto freshly cleaved mica. The carbon film was floated onto purified dynein samples diluted to ~ 10 $\mu\text{g/ml}$ with dynein buffer. The film was transferred to a drop of aqueous uranyl acetate (1%) and picked up on uncoated mesh grids (Ted Pella, Redding, CA). The grids were then allowed to air dry and viewed in the Zeiss 10A electron microscope at 80 kV.

Low Angle Rotary Shadowing - Dynein samples from the sucrose gradients were mixed with glycerol to a final concentration of 50% glycerol (v/v). A 10 μl sample was sprayed onto a freshly cleaved mica surface from a simple device consisting of an air can with a flexible hose and a 200 μl pipette tip. The samples were then mounted under vacuum on the Balzers rotary stage. After the droplets had dried (~ 10 min) they were rotary replicated with a 1-nm platinum coat from an angle of 7° . A 15-nm carbon film was shadowed from an angle of 80° . The replicas were removed, floated on DDW, picked up on uncoated mesh grids and viewed in the Zeiss 10A electron microscope at 80 kV.

RESULTS

I. Vesicle transport along the MTR

DIC microscopy

Video enhanced contrast microscopy of immobilized Paramecium allowed the direct observation of vesicle transport along the cytopharyngeal microtubular ribbons. Transport was most easily seen when the cells were lying on either their left or ventral sides. In this orientation the MTR radiated out perpendicular to the cytopharynx so that the edges of the MTR were visible and looked more like a single MT (Figure 4). Other identifiable cellular structures were present which helped to determine the correct orientation of the cell (Figure 5). The nascent digestive vacuole was discernable in most cases, although it was often in a different focal plane than the MTR. The edge of the nascent vacuole took on a beaded appearance due to the presence of bound acidosomes which covered the vacuole (Figure 6).

The best observations of vesicle transport were made immediately following compression of the cells. Vesicle transport along the MTR was only visible for a few μm adjacent to the cytopharynx. Vesicle transport was smooth, continuous and seemingly never-ending. All vesicles travelled at approximately the same rate, which was determined to be 5.8 ± 0.9 $\mu\text{m}/\text{sec}$ (Figure 7). In no instance did a vesicle "pass" another, or stop and reverse directions.

Vesicle transport was primarily unidirectional towards the cytopharynx (Figure 7). In addition, transport continued right up to the

Figure 4 - VECM micrograph of the microtubular ribbons. The MTR (between arrowheads) radiate from the cytopharynx (cyx) and extend 20 μm into the cytoplasm. Only the edges of the MTR are visible which makes them appear as single MTs. This cell was treated with N-ethylmaleimide, which highlighted the visibility of the MTR. BC = buccal cavity, A = anterior, P = posterior. Bar = 2.0 μm .

Figure 5 - Low magnification VECM micrograph of identifiable cellular structures in Paramecium. The beating cilia in the buccal cavity (BC) are indicative of cellular viability. The morphology of the oral apparatus indicates anterior (A) and posterior (P) poles of the cell. The bracketed area represents the optimum area for vesicle transport visualization along the MTR. Other recognizable structures include the nucleus (N), trichocysts (T), mitochondria (M), and digestive vacuoles (DV). Bar = 5.0 μm .

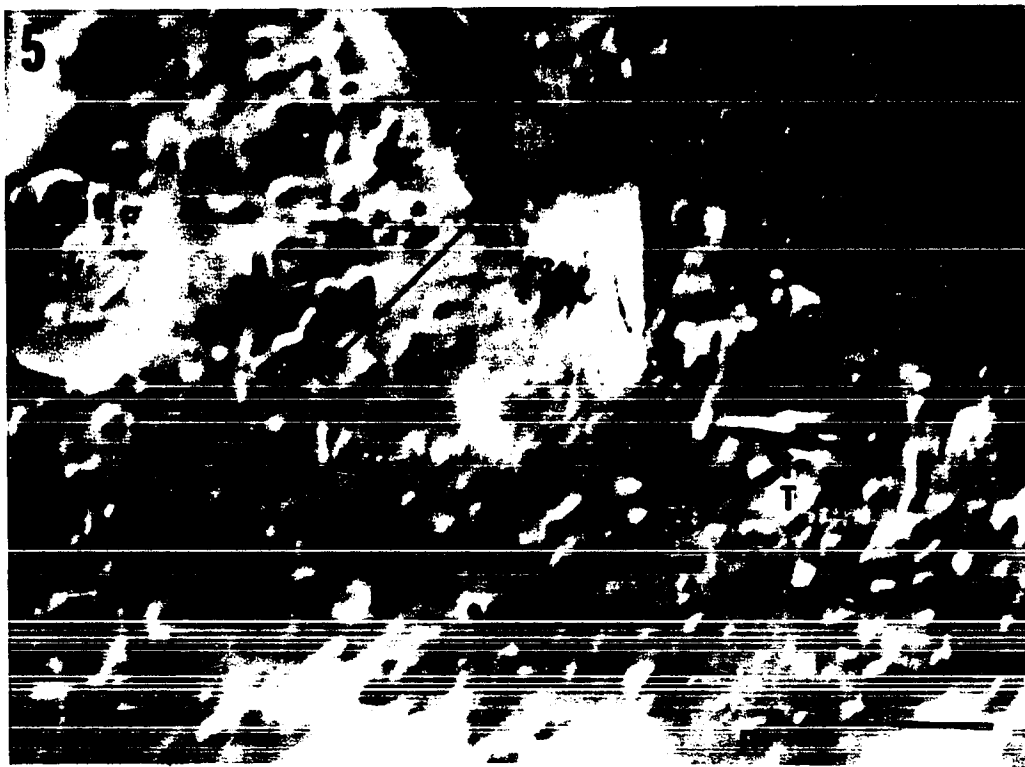
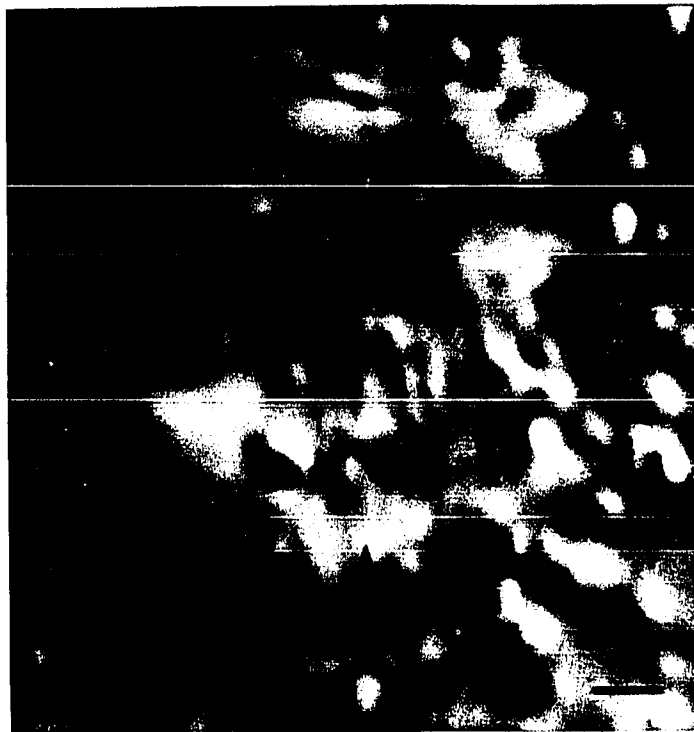
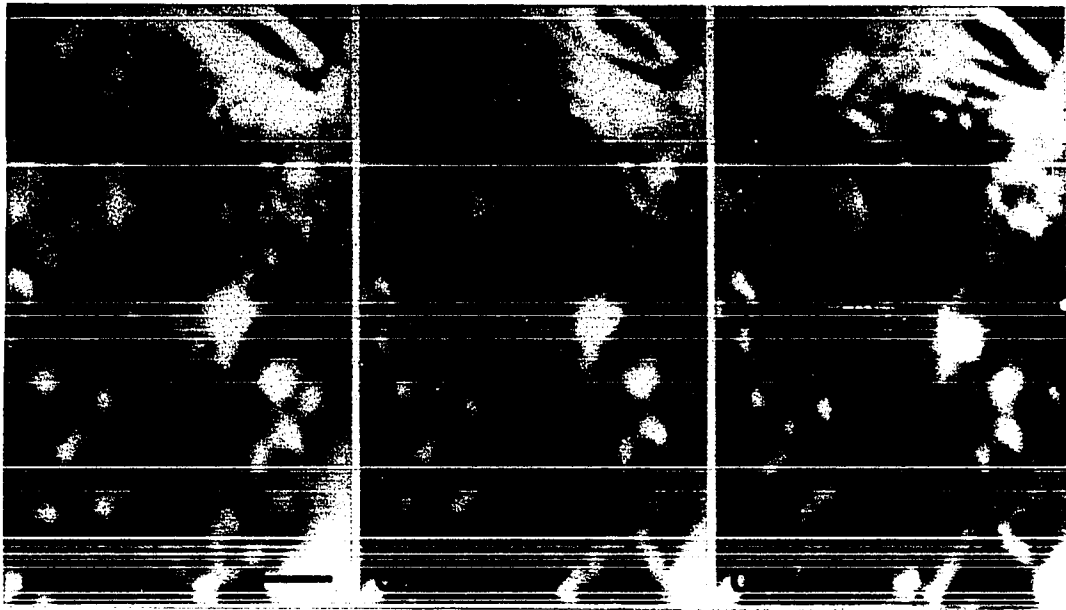
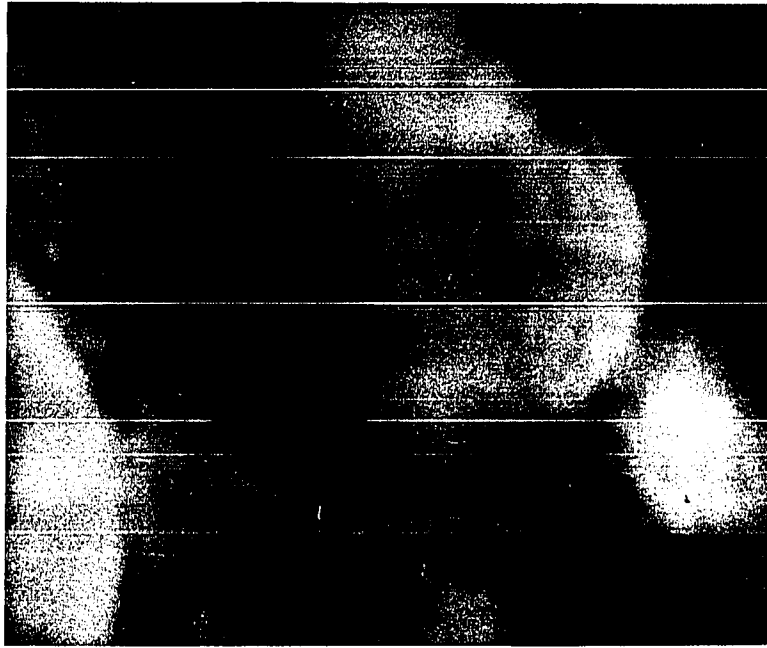


Figure 6 - Beaded appearance of the nascent vacuole. The nascent digestive vacuole (NDV) grows at the posterior end of the oral apparatus. The edge of the nascent vacuole assumes a beaded appearance due to the presence of bound acidosomes which associate with the nascent vacuole. Once the nascent vacuole has pinched off from the oral apparatus, the acidosomes will fuse with the vacuole. This fusion will result in the acidification of the digestive vacuole lumen (Allen and Fok, 1983a). Bar = 2.5 μm .

Figure 7a-c - Vesicle transport toward the cytopharynx. The three sequential video frames illustrate two vesicles (a and b) as they move up to the cytopharynx (cyx) along a MTR (between arrowheads). In 7c, vesicle "a" has disappeared and only vesicle "b" is still visible. Note that both vesicles are on the anterior side of the MTR. The rate of vesicle transport is approximately 6 $\mu\text{m}/\text{sec}$. Time between frames (in seconds) is noted. A = anterior, P = posterior. Bar = 2.0 μm .



cytopharynx membrane at which time the vesicles "disappeared" (Figure 7), but there was no apparent build-up of vesicles in this area despite the unidirectional transport. Occasionally, vesicles moved away from the cytopharynx (Figure 8), but this movement was rare. The rate of this outward-directed transport was 5.8 ± 0.9 $\mu\text{m}/\text{sec}$ and was also smooth and continuous.

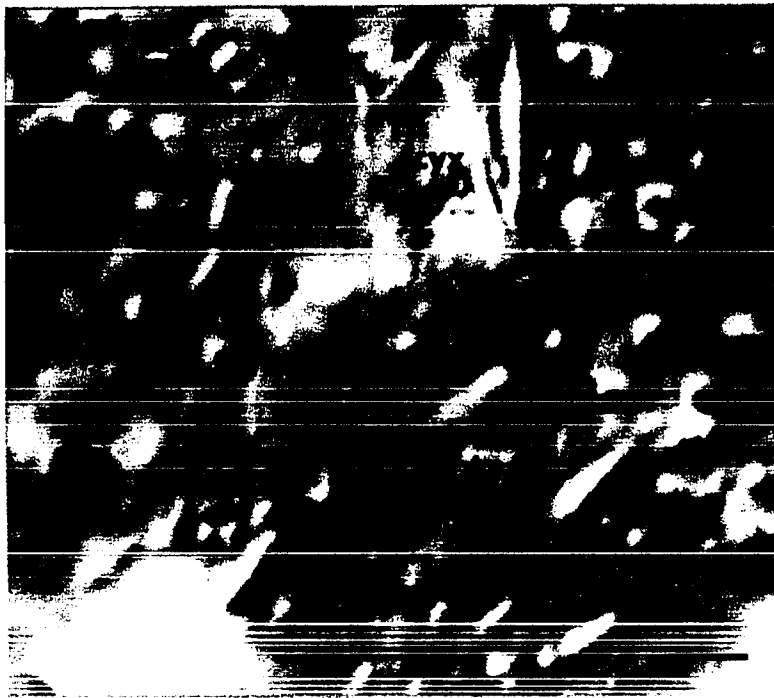
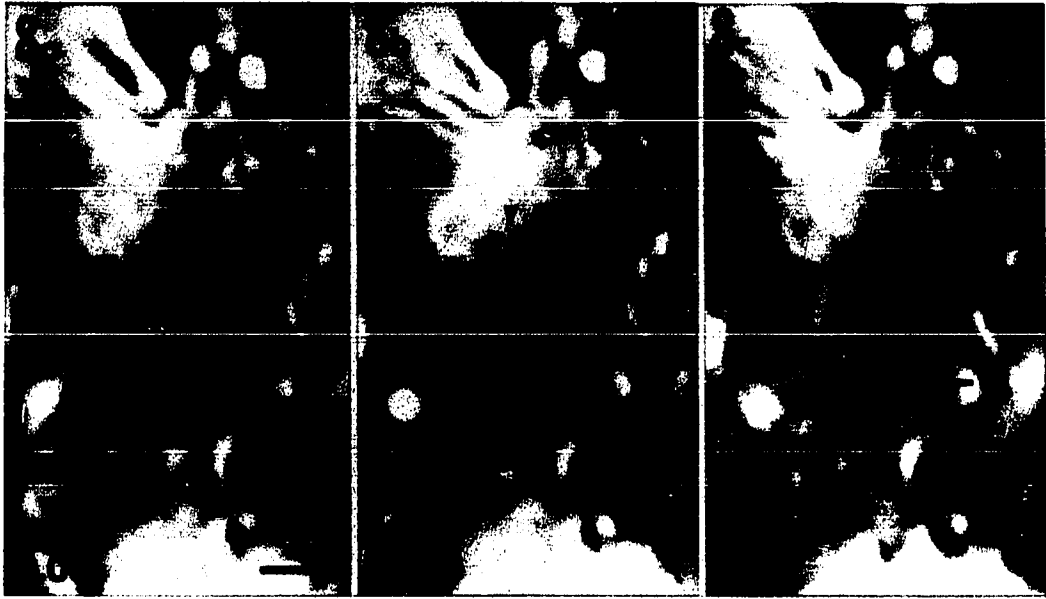
An interesting pattern of transport was observed when both the moving vesicles and the adjacent MTR were visible. Vesicles moving toward the cytopharynx appeared to travel along the anterior side of the MTR (Figure 7). In contrast, vesicle movement away from the cytopharynx appeared to occur along the posterior side of the MTR (Figure 8).

Two groups of vesicles were transported along the MTR (Figure 9). The first group of vesicles was small and flattened with dimensions of 0.1 μm by 0.6 μm . These flat vesicles were barely discernable and appeared as moving bumps on the surface of the MTR. The second group of vesicles was spherical with diameters ranging from 0.5 to 1.2 μm . These vesicles were quite prominent and served as the general indicator for vesicle transport. Other recognizable organelles such as mitochondria, trichocysts and crystals were visible in this area, but they were not transported along the MTR. Thus, two subsets of vesicles were selectively transported on the MTR.

Attempts were made to specifically inhibit this vesicle transport. However, the cells were very sensitive to perturbation and an appropriate buffer system to study vesicle transport inhibition and reactivation was not found. Therefore, discriminating between the non-specific effects of the permeabilizing buffer and the inhibitory reagent used

Figure 8a-c - Vesicle transport away from the cytopharynx. The three sequential video frames illustrate a vesicle (arrow) as it moves away from the cytopharynx (cyx) along a MTR (between arrowheads). Note that this vesicle is on the posterior side of the MTR. The rate of outward transport is approximately 6 $\mu\text{m}/\text{sec}$. Time between frames (in seconds) is noted. A = anterior, P = posterior. Bar = 2.0 μm .

Figure 9 - VECM morphology of vesicles transported along the MTR. Vesicles transported along the MTR were of only two morphologies. One vesicle type is small and flattened with dimensions of 0.1 x 0.6 μm . These small vesicles were barely visible (arrowheads) as they moved along the MTR toward the cytopharynx (cyx). The other vesicle type is easily seen as a large spherical vesicle (arrow). These large vesicles ranged from 0.5 - 1.2 μm in diameter. Because the large vesicles were easily seen, they were used as the indicator for vesicle transport along the MTR. Bar = 2.5 μm .



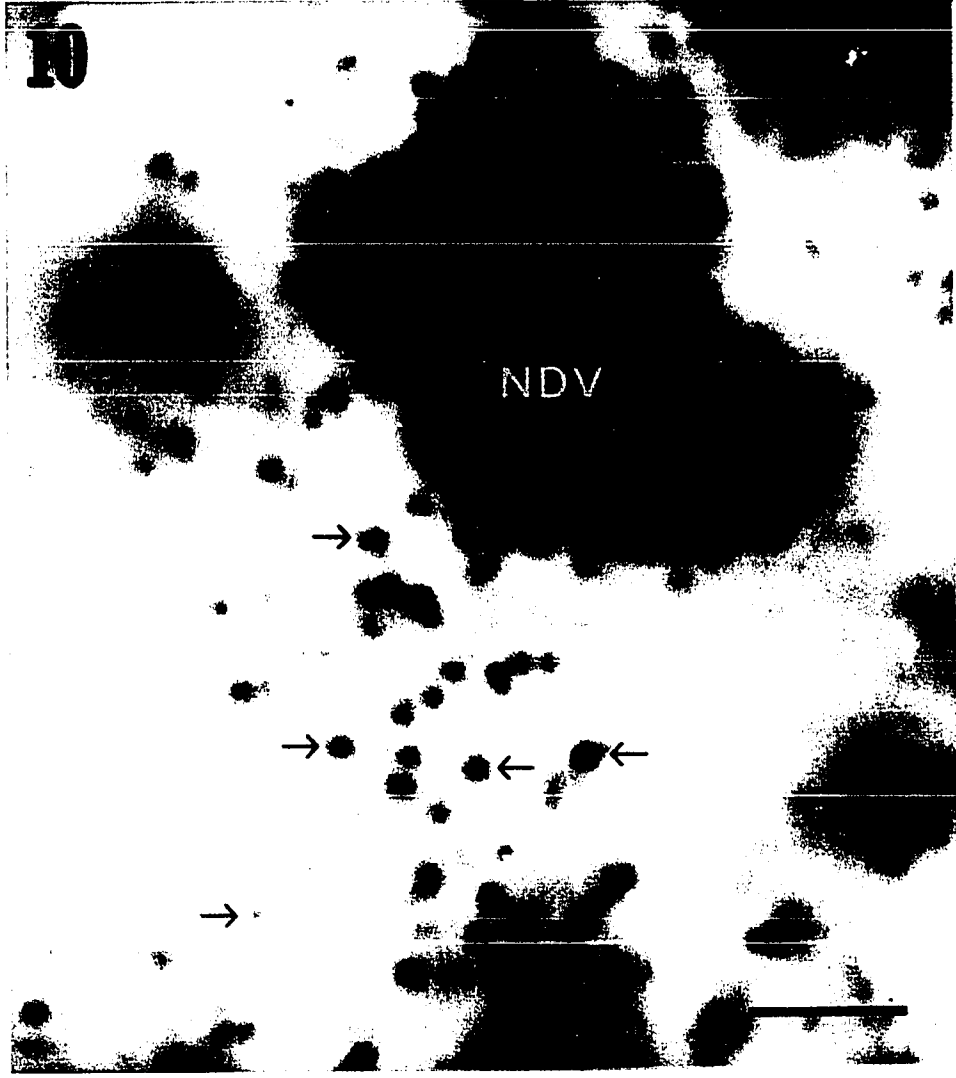
(N-ethylmaleimide or vanadate) was not possible. Thus, the results obtained were inconclusive.

Neutral red labelling

In an attempt to identify the acidosomes, which accumulate neutral red (Allen and Fok, 1983c), living cells were pulsed with neutral red and vesicle transport was observed. Unlike DIC microscopy, the broad focal plane of brightfield illumination enabled the detection of vesicle transport over long distances and in virtually any cellular orientation. Vesicle transport toward the cytopharynx was detectable for as long as 20 - 30 μm . However, neither the small flat vesicles nor microtubular ribbons were detectable using this technique.

The acidosomes were unmistakably labelled as large red vesicles (Figure 10). The sizes of these labelled vesicles were identical to the large spherical vesicles seen with DIC microscopy. The acidosomes were transported from the cytoplasm to the cytopharynx, apparently along the MTR. Acidosome transport toward the cytopharynx took on two forms. Within a few μm of the cytopharynx the transport was smooth and continuous as described previously for DIC microscopy. But at more distal locations, the transport was sometimes disrupted by short pauses, after which transport would resume. In a few instances, at these distal locations, the acidosomes did not move again and sometimes even reversed directions. Neutral red labelling also revealed a greater percentage of acidosomes moving distally than was seen with DIC microscopy, but the net flow of the acidosomes observed with this technique, as before, was toward the cytopharynx.

Figure 10 - Neutral red labelling of acidosomes. Neutral red is a weak base and accumulates inside acidic compartments such as acidosomes. The acidosomes (arrows) are labelled and easily distinguished by video microscopy using brightfield illumination. Acidosomes which have accumulated around a nascent digestive vacuole (NDV) appear as a large black mass. The transport of the acidosomes is easily visualized, even at low magnifications. Note that the MTR are not visible with this technique. Bar = 5.0 μm .



Upon reaching their destination at the cytopharynx, transport stopped as the acidosomes accumulated around the nascent digestive vacuole (Figure 10). Occasionally, single acidosomes could be seen to attach to the nascent vacuole and begin vibrating wildly as the oral cilia beat upon the nascent vacuole membrane.

Quick-freeze, deep-etch

To obtain a faithful representation at the ultrastructural level of the components involved in vesicle transport along the MTR, the QF-DE technique was used. This technique enabled the observation of cellular ultrastructure in its near-native condition. The granular appearance of the cytoplasm indicated that the cells were well preserved, particularly in shallow fractures through the cell cortex. Although slightly deeper fractures were required to expose the oral region, the structural preservation in these fractures was still quite adequate. The MT protofilament substructure was not as well preserved in these deeper fractures, but other cellular details such as vesicle morphologies were clearly defined.

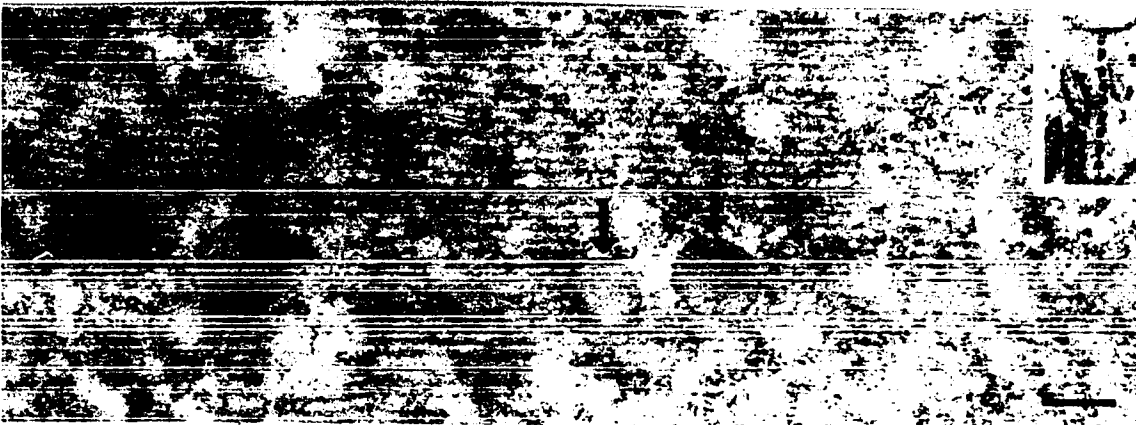
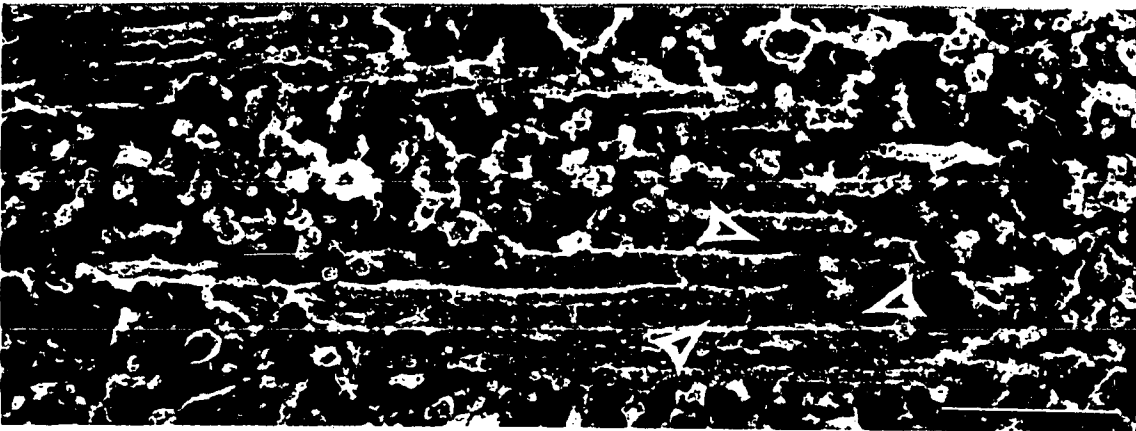
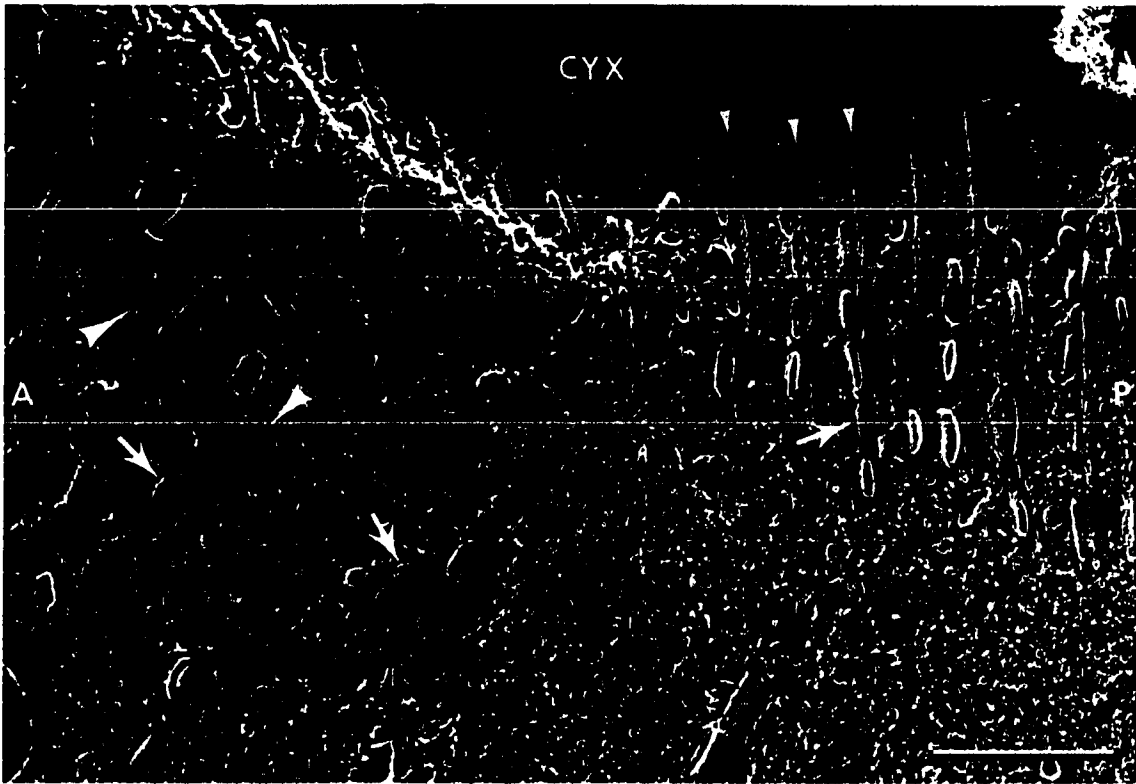
Fractures through the oral region revealed structures such as the MTR, the cytopharynx membrane, and discoidal vesicles (Figure 11). The MTR were verified as parallel MTs lying side by side to form a planar ribbon (Figures 12, 13). The individual MTs of the MTR were separated by a center-to-center spacing of 43 ± 3 nm. These MTs were extensively cross-linked by fine crossbridges with a somewhat regular spacing of 36 ± 8 nm (Figure 12). The planar sheet of the MTR was best illustrated in conventional thin sections (Figure 13). The MTR were attached to the

Figure 11 - QF-DE fracture through the oral region. The MTR (arrowheads) extend away from the cytopharynx membrane (cyx), and are also found free in the cytoplasm. Discoidal vesicles (arrows) are aligned in single file along the anterior side of the MTR. Acidosomes are excluded from this area where the MTR lie adjacent to the cytopharynx membrane. A = anterior, P = posterior. Bar = 1.0 μ m.

Figure 12 - High magnification of the MTR illustrating the cross-links (arrowheads) between the individual microtubules. The center-to-center spacing between MTs is 43 ± 3 nm. The individual cross-links are spaced 36 ± 8 nm apart in a somewhat regular pattern. Bar = 0.2 μ m.

Figure 13 - Thin section micrograph illustrating planar sheet of the MTR. Several ribbons have joined together in this section which was several μ m from the cytopharynx membrane. The planar nature of this ribbon restricts vesicle transport to either one side of the ribbon or the other. Several discoidal vesicles also in planar view (arrows) are present along the MTR. Bar = 0.25 μ m.

Inset - Cross section of a single MTR. Again, transport of vesicles along the MTR is restricted to one side or the other. Discoidal vesicles are present on the anterior side of this MTR. Same magnification as Figure 13.



cytopharynx membrane by short linkers (Figure 14). The E face of the cytopharynx membrane contained numerous, densely packed intramembrane particles (Figure 14).

The discoidal vesicles appeared as flattened vesicles with diameters ranging from 0.2 to 0.4 μm . Their E fracture face contained numerous intramembrane particles and was identical in appearance to the cytopharynx membrane (Figure 14). The discoidal vesicles were lined up single file along the MTR. As with DIC microscopy, they were predominately on the anterior side of the MTR (Figures 11, 14), and maintained a constant spacing of 30 to 40 nm from the MTR. At high magnifications, cross bridges were especially evident between the discoidal vesicles and the MTR (Figure 14).

The acidosomes were numerous in the oral region, but they were excluded from the MTR directly adjacent to the cytopharynx membrane (Figure 11). Instead the acidosomes accumulated around the nascent digestive vacuole (Figure 15) and appeared to be firmly bound to the nascent vacuole by short, thin cross-linkers (Figure 16). Beside their accumulation around the nascent DV, the acidosomes were found next to the MTR or free in the cytoplasm.

The acidosome morphology was quite distinct which made them easily recognizable (Figures 17-20). The acidosome E face was smooth and virtually free of intramembrane particles, but had small holes or indentations where the large particles of the P face were pulled out of the membrane (Figure 17). The P face was decorated with large intramembrane particles (Figure 18). The QF-DE technique illustrated a unique luminal etching pattern for the acidosome which is best described

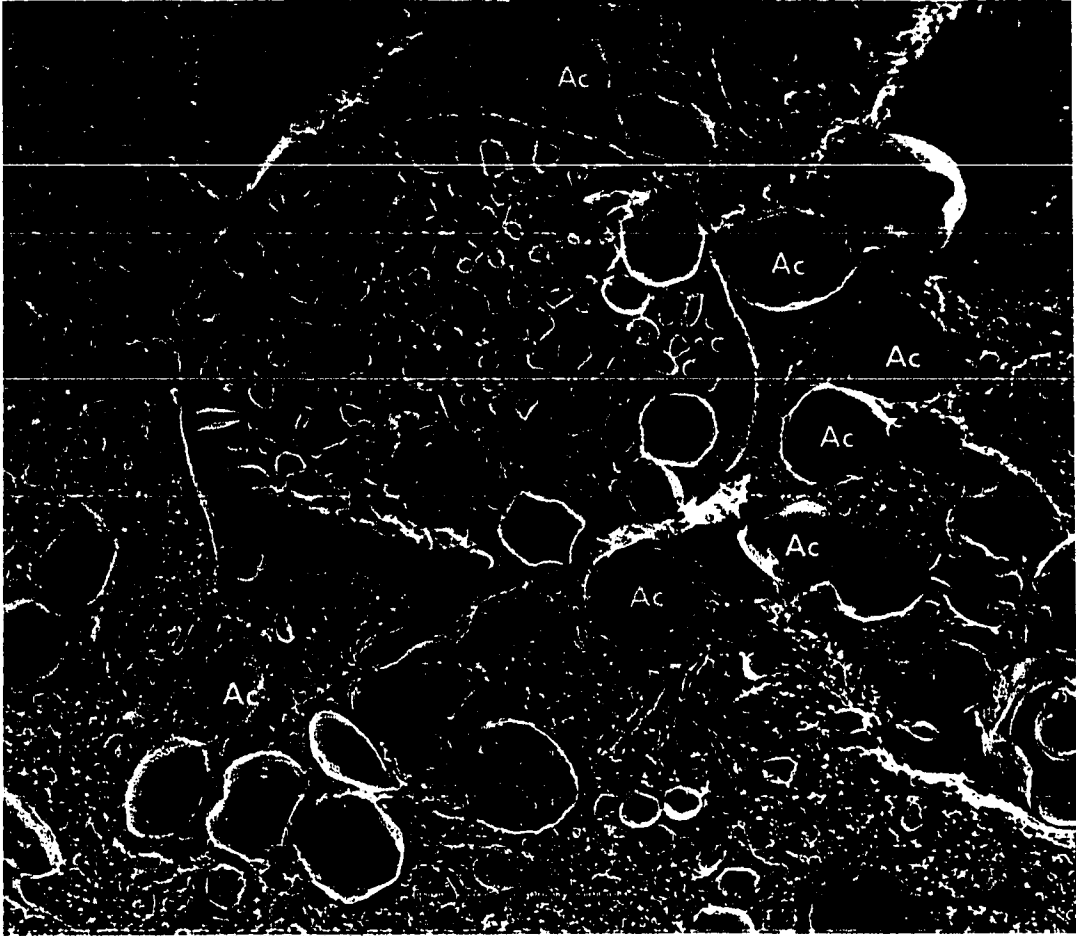
Figure 14 - High magnification of the MTR adjacent to the cytopharynx. The discoidal vesicles (arrows) are clearly aligned along only the anterior side of the MTR. Cross-bridges are evident between the vesicles and the MTR (bent arrows). In this QF-DE cross fracture, only the edge of the MTR is visible, and appears as a single MT. The MTR are attached to the cytopharynx membrane (cyx) by short thin linkers (arrowheads). Note the similar appearance of the discoidal vesicle membrane (large arrow) to that of the cytopharynx membrane. Bar = 0.25 μ m.

CYX



Figure 15 - QF-DE fracture of acidosomes (Ac) surrounding a nascent digestive vacuole (NDV). Bar = 1.0 μm .

Figure 16 - High magnification of an acidosome (Ac) that appears firmly bound to the nascent digestive vacuole (NDV) by short linkers (arrowheads). Note the flatness of the acidosome membrane adjacent to the nascent vacuole membrane. This appearance suggests an attempt to maximize contact between the two membranes. The particulate appearance of the nascent vacuole membrane E face is apparent (arrow). Bar = 0.25 μm .



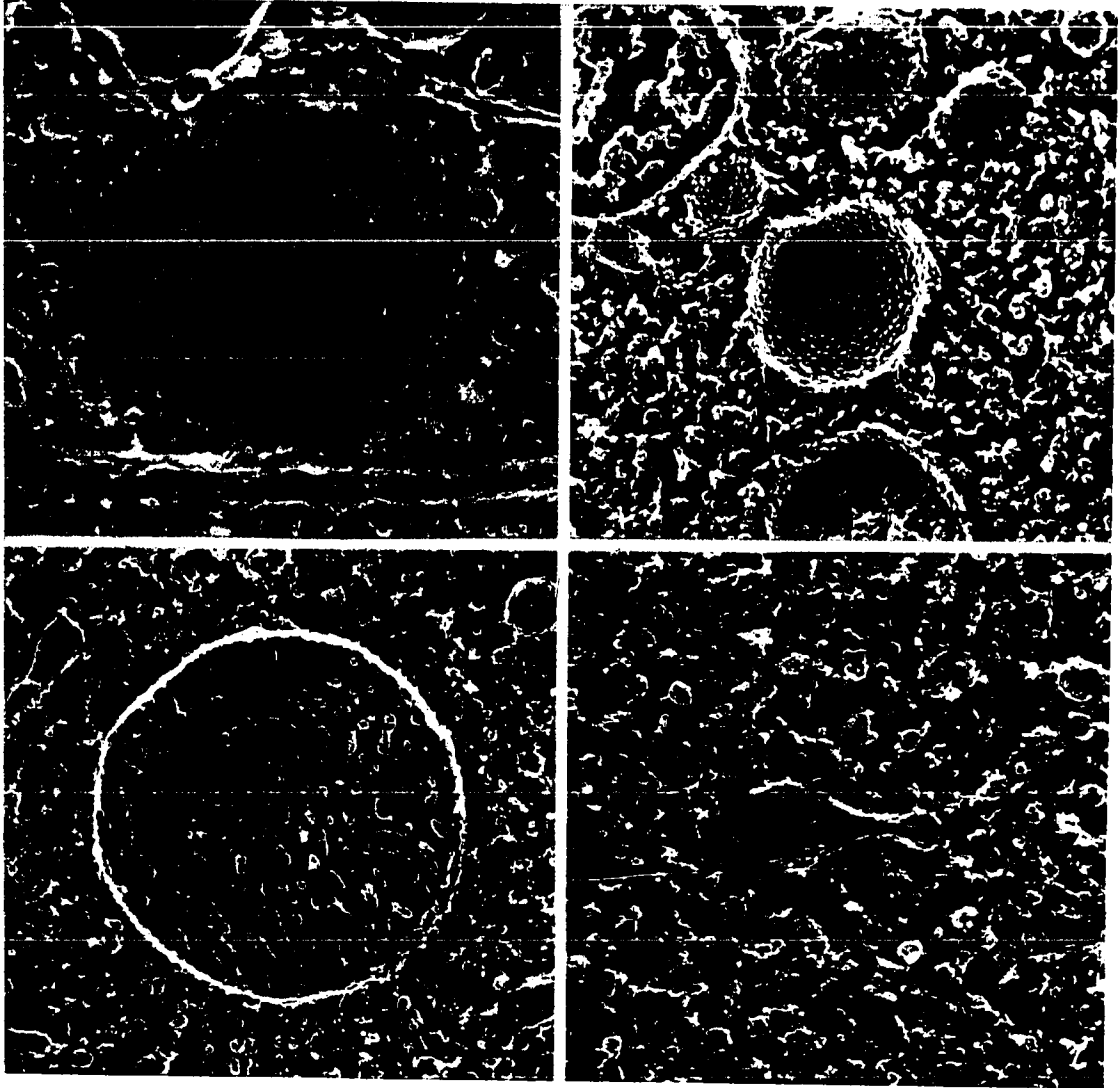
Figures 17 to 20 - QF-DE acidosome morphologies

Figure 17 - E fracture face of an acidosome along the MTR (arrows). The E face is virtually free of intramembrane particles. However, small holes or depressions are evident on the E face where the large particles of the P face have been pulled from this leaflet. Bar = 0.25 μ m.

Figure 18 - P fracture face of the acidosome. Note the large loosely packed intramembrane particles. Bar = 0.25 μ m.

Figure 19 - Cross fracture of an acidosome illustrating the unique labyrinthine appearance of the lumen. This feature is beneficial in positively identifying acidosomes throughout the cytoplasm. Also, the occasional membrane invaginations into the acidosome is apparent. The P fracture face (Pf) of such an invagination is present in the lumen of this cross fractured acidosome. Bar = 0.25 μ m.

Figure 20 - A very small acidosome which illustrates the wide range of sizes for the acidosomes. The unique luminal etching pattern identifies this small odd-shaped vesicle as an acidosome. Bar = 0.25 μ m.



as labyrinthine (Figure 19). This distinct etching pattern has provided a marker for the identification of acidosomes throughout the cytoplasm and in cellular fractions. The sizes of acidosomes varied greatly ranging from 0.15 μm up to nearly 1 μm in diameter (Figure 20). Profiles of these acidic vesicles were usually round, but invaginations of the surface into the vesicle lumen were frequently seen (Figure 19).

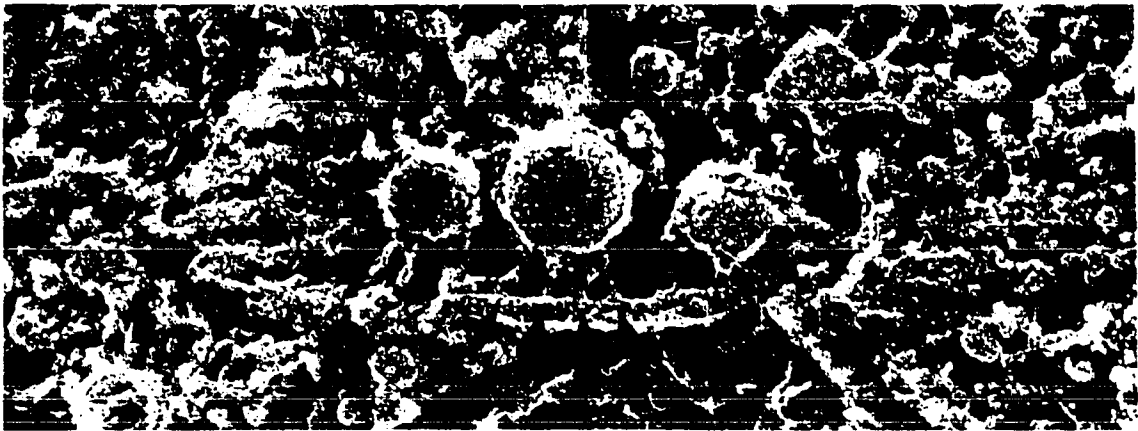
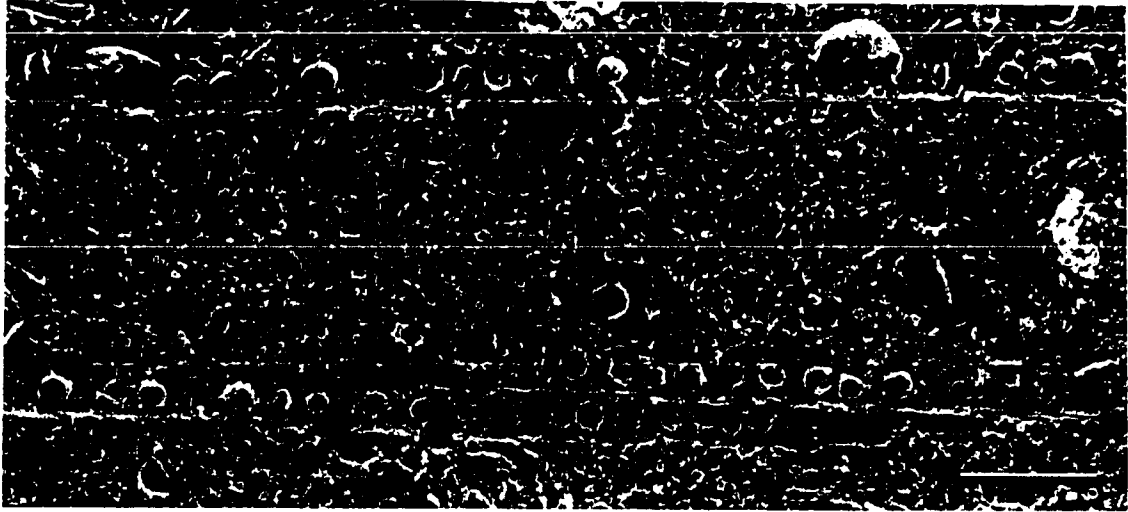
A third population of previously unidentified small vesicles was discovered using the QF-DE technique. These vesicles measured 100 nm in diameter and were found to be intermixed with discoidal vesicles and acidosomes on the anterior side of the MTR (Figure 21). The E face of these 100 nm vesicles was smooth and nearly identical in appearance to the acidosome E face. Because of their small size they were never found in cross fracture so their lumens were not exposed. These vesicles also maintained a constant 30 to 40 nm spacing from the MTR and cross bridges were very prominent in most cases (Figure 22).

Microtubule polarity

To determine the polarity of the MTs of the MTR and thus the direction of vesicle transport, the cytoplasmic MTs of Paramecium were decorated with curved hooks. The soluble cytoplasm of the cell was entirely washed out and only the cytoskeletal structures and an occasional trichocyst remained. The percentage of MTs with hooks was low, however enough MTs were decorated to make accurate polarity determinations. The polarity of the MTs was determined using the "right hand rule." This was achieved by curving the fingers of your right hand in the same direction as the hooks on the decorated MT. The extended right thumb pointed toward the minus-end of the MT.

Figure 21 - 100 nm vesicles. A previously unidentified population of 100 nm vesicles is present along the anterior side of the MTR. These small vesicles are intermixed with discoidal vesicles (arrows) and acidosomes along the MTR. As with the discoidal vesicles, these 100 nm vesicles maintain a constant 30 - 40 nm distance from the MTR. Bar = 0.5 μ m.

Figure 22 - High magnification of 100 nm vesicles. At high magnifications, cross bridges (arrows) are evident between the 100 nm vesicles and the MTR. Bar = 100 nm.



The MTR did not form hooks readily. However, when present the hooks on these MTs were clockwise indicating their minus-end was at the oral region (Figure 23). Other MTs in this area which originated at the oral region also had clockwise hooks (Figures 24). Thus, the origin or minus-ends of the MTR were at the oral region and the plus-ends were located distally. This orientation corresponded to a predominantly minus-end directed transport for the vesicles moving along the MTR toward the cytopharynx.

II. Postoral fiber transport

DIC microscopy and neutral red labelling

Transport along the postoral fibers (microtubular bundles) was clearly different from the transport along the MTR. Digestive vacuoles pinched off from the cytopharynx and glided down the postoral fibers (Figure 25). Massive transport of a heterogeneous population of vesicles would follow for a few seconds, then all transport would stop. There seemed to be a distinct on/off switching mechanism for this transport.

Unlike the MTR transport, the postoral fiber transport was non-specific with regard to vesicle type. Trichocysts, mitochondria, crystals, and other small vesicles were rapidly transported toward the posterior end of the cell. This transport occurred only in close association with the postoral fibers (Figures 26, 27) and continued for one or two seconds following vacuole formation. These characteristics suggested a directed transport and not a "vacuum" effect brought on by the passage of the large digestive vacuole through the viscous cytoplasm.

Figures 23 and 24a-c - Polarity determination of the MTR.

Figure 23 - Cross section of the MTR (between arrows) near their origins and viewed from their distal ends toward their origin in the filamentous reticulum. The percentage of hook formation on these MTs was very low. Only two clockwise hooks (arrowheads) were found to decorate the MTR in this field. BC = buccal cavity. Bar = 0.2 μ m.

Figures 24a-c - Successive serial sections of a single MT in the proximity of the MTR. This microtubule (arrow), which displays a clockwise hook, appears to originate near a mass of amorphous material (AM). This amorphous material resembles the filamentous reticulum (FR) from which the postoral fibers and MTR appear to originate. Bar = 0.2 μ m.

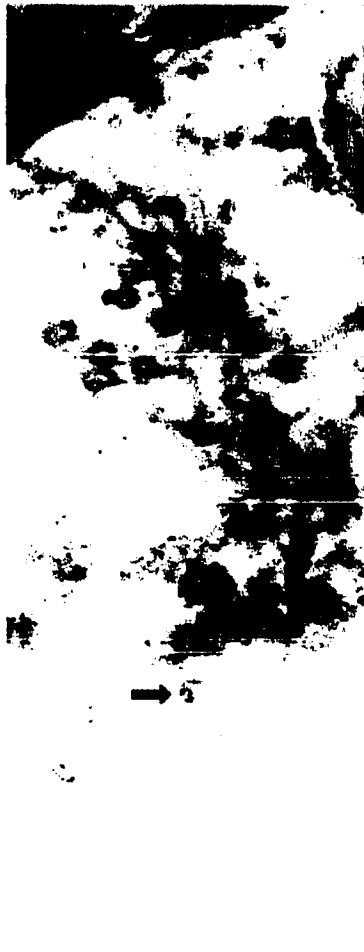
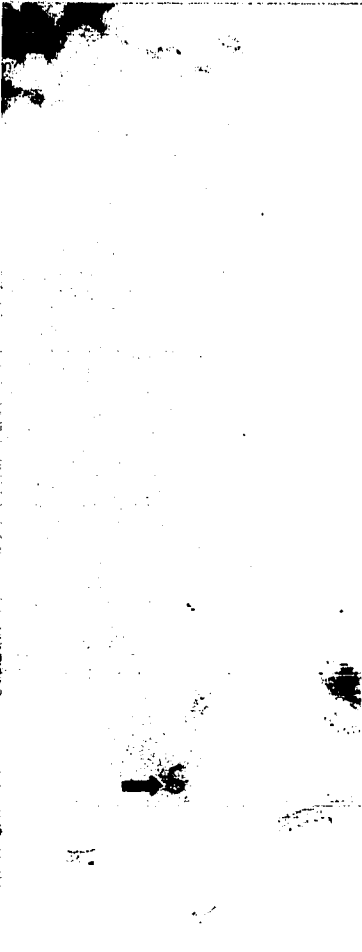
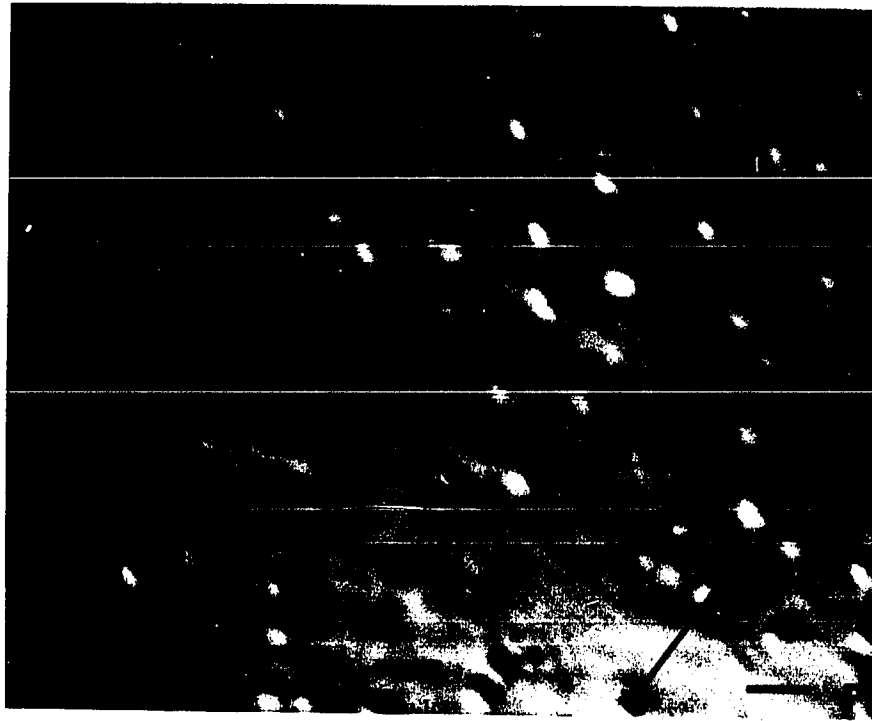


Figure 25a-c - Digestive vacuole release from the oral apparatus. The three sequential video frames illustrate the formation of a digestive vacuole and the initial transport along the postoral fibers. In 25a, the spherical nascent digestive vacuole (NDV) is growing at the posterior end of the buccal cavity (BC). In 25b, the vacuole elongates as it begins transport along the postoral fibers (not visible) toward the cells posterior end. In 25c, only a thin, trailing membrane extension (brackets) remains connected to the oral apparatus. The vacuole will next completely separate from the oral apparatus and glide down the postoral fibers. Time between frames (in seconds) is noted. Bar = 5.0 μm .



Figure 26 - VECM micrograph of the postoral fibers. The postoral fibers (between brackets) consist of several bundles of MTs that extend from the oral apparatus to the posterior end of the cell. The postoral fibers serve as a track to guide the newly formed digestive vacuole to the cell's posterior end. A = anterior, P = posterior. Bar = 2.0 μm .

Figure 27a-c - Postoral fiber transport. The three sequential micrographs illustrate the transport of a crystal (arrow) along the postoral fibers (not visible). The rate of transport is a very rapid 20 $\mu\text{m}/\text{sec}$. Time between frames (in seconds) is indicated. A = anterior, P = posterior. Bar = 2.0 μm .



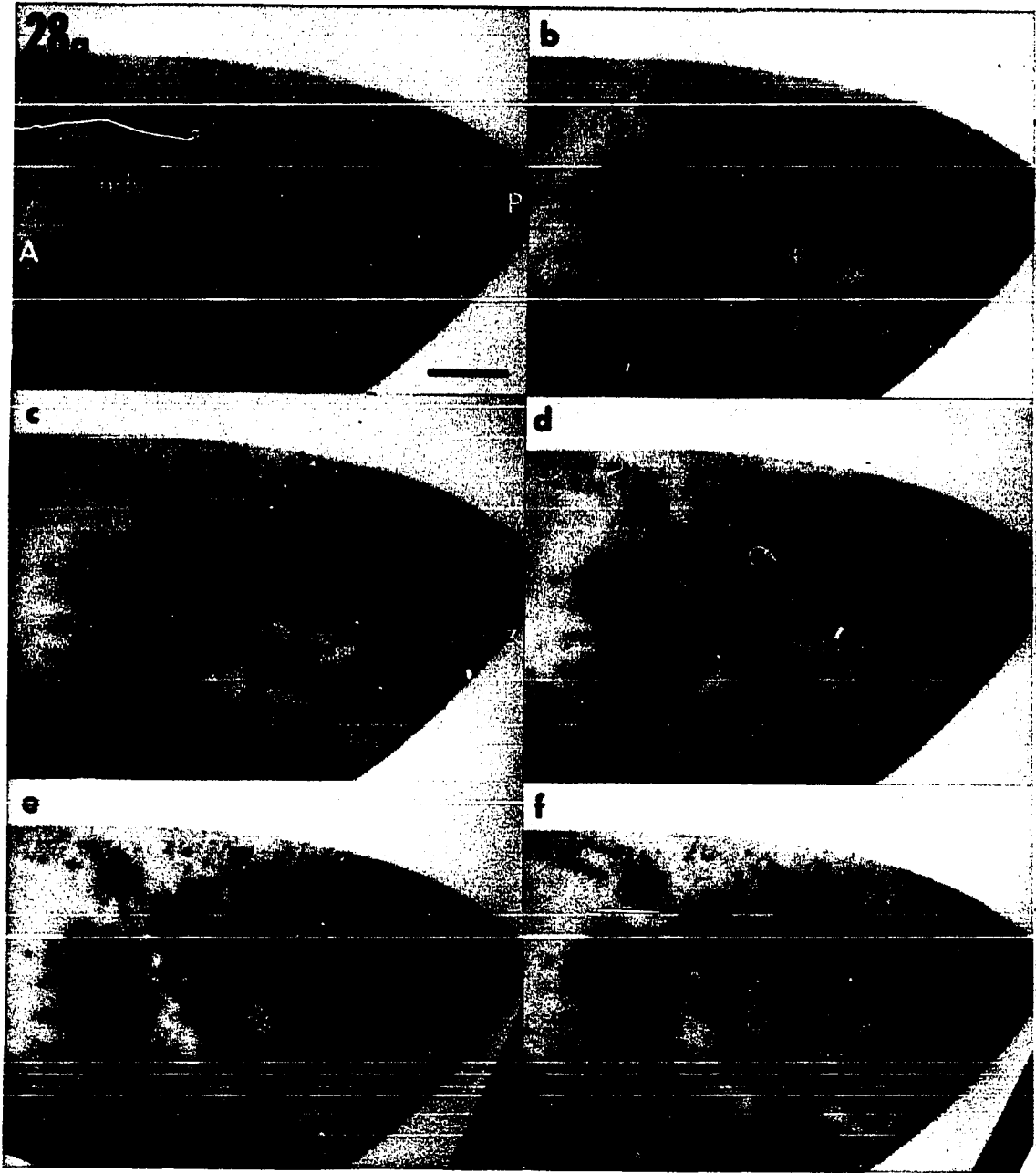
Also, following release of the vacuole from the post oral fibers, the ends of the postoral fibers would whip back and forth in the posterior end of the cell. However, this may have been an artifact of immobilization.

Postoral transport was exclusively unidirectional from the cytopharynx to the posterior end of the cell. Transport was primarily smooth and continuous, but occasionally vesicles would stop for a moment then move again. The rate of transport was very rapid ($\sim 20 \mu\text{m}/\text{sec}$) and over a large distance ($\sim 30 - 40 \mu\text{m}$).

Digestive vacuole release and transport was especially evident with neutral red labelling (Figure 28), which permitted some insight into the mechanism of vacuole formation. Vacuole release began as the membrane adjacent to the postoral fibers began to slide toward the cell's posterior end. The entire food vacuole would rotate and elongate with thin extensions along the postoral fibers at the leading and trailing edges of the vacuole. The vacuole was separated from the cytopharynx only after the vacuole was several μm down the postoral fibers. The separation of the vacuole from the cytopharynx appeared to be elastic in that the connection between the vacuole and cytopharynx became extremely thin and seemed to be pulled apart. There was no evidence for a constriction of the anterior end of the nascent digestive vacuole prior to transport down the postoral fibers.

The vacuole movement along the postoral fibers was not a simple sliding or rolling motion. Instead, the vacuole became elongated maximizing its contact with the postoral fibers. The large rounded bulk of the vacuole did not appear to move readily through the cytoplasm while the edge in contact with the postoral fibers continued to move at a rapid

Figure 28a-f - Digestive vacuole transport and rotation. These six video frames of a neutral red labelled cell highlight the transport and rotation of a digestive vacuole down the postoral fibers. The nascent digestive vacuole (ndv) in 28a will elongate and rotate as it moves along the postoral fibers to the posterior end of the cell. A white dot on the vacuole may be used as a reference point to follow the vacuole rotation through approximately 270°. The curved arrow in 28d indicates the direction of rotation. Time between frames (in seconds) is indicated. A = anterior, P = posterior. Bar = 10.0 μm .



pace. This motion was especially evident after the vacuole had apparently been released from the ends of the post oral fibers. The membranous extension that trailed the vacuole remained bound to and continued to be transported along the postoral fibers. The net result of these movements was the rotation of the vacuole through approximately 360° in a backwards spinning fashion as it moved along the postoral fibers.

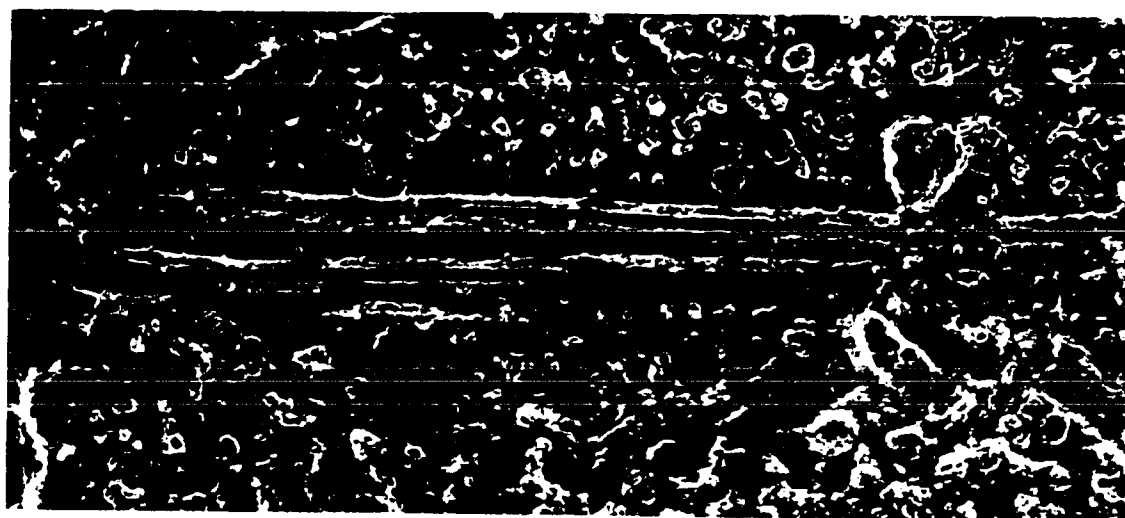
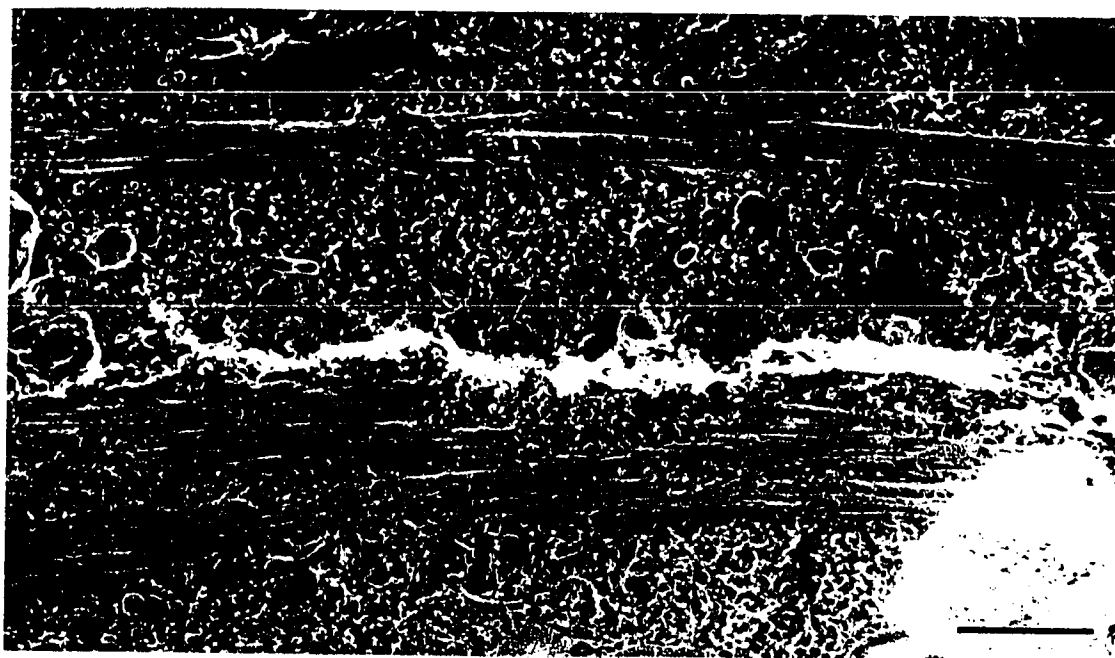
Quick-freeze, deep-etch and microtubule polarity

The ultrastructural features of the postoral fibers were visualized using the QF-DE technique. The postoral fibers were found to extend from the oral region toward the posterior end of the cell (Figure 29). The postoral fibers consisted of several bundles of parallel MTs. The individual MTs were occasionally cross-linked to one another, but in some areas the microtubules were virtually smooth and not cross-linked (Figure 30). There were no regularly arranged vesicles associated with these MT bundles unlike the MTR which has the three populations of vesicles linked to them by cross bridges. Neither the nascent digestive vacuole nor a transporting digestive vacuole were encountered adjacent to the postoral fibers.

In determining the polarity of the MTs, the postoral fibers were found to display clockwise hooks when viewing toward the oral region from a distal location (Figure 31). At the oral region, several MTs of the postoral fibers also displayed clockwise hooks (Figure 32). Thus, the minus-ends of the postoral fibers were at the oral region and the distal ends of the postoral fibers represented the plus-ends. Therefore, transport along the postoral fibers was exclusively a plus-end directed transport.

Figure 29 - QF-DE fracture of the postoral fibers. These bundles of MTs (arrows) extend from the right side of the oral region to the posterior end of the cell. The new digestive vacuole travels along these fibers en route to the posterior end of the cell. Unlike the MTR, these MTs are arranged in thick three dimensional arrays and are essentially free of bound vesicles. Also, the cross-linking between individual MTs is not as apparent as with the MTR. A = anterior, P = posterior. Bar = 0.5 μ m.

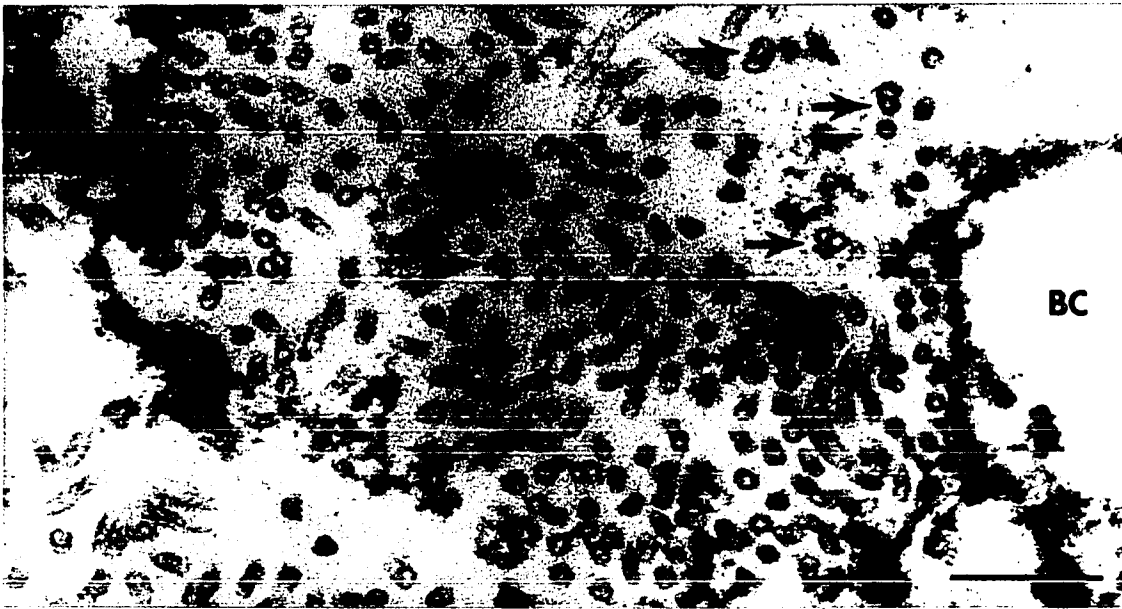
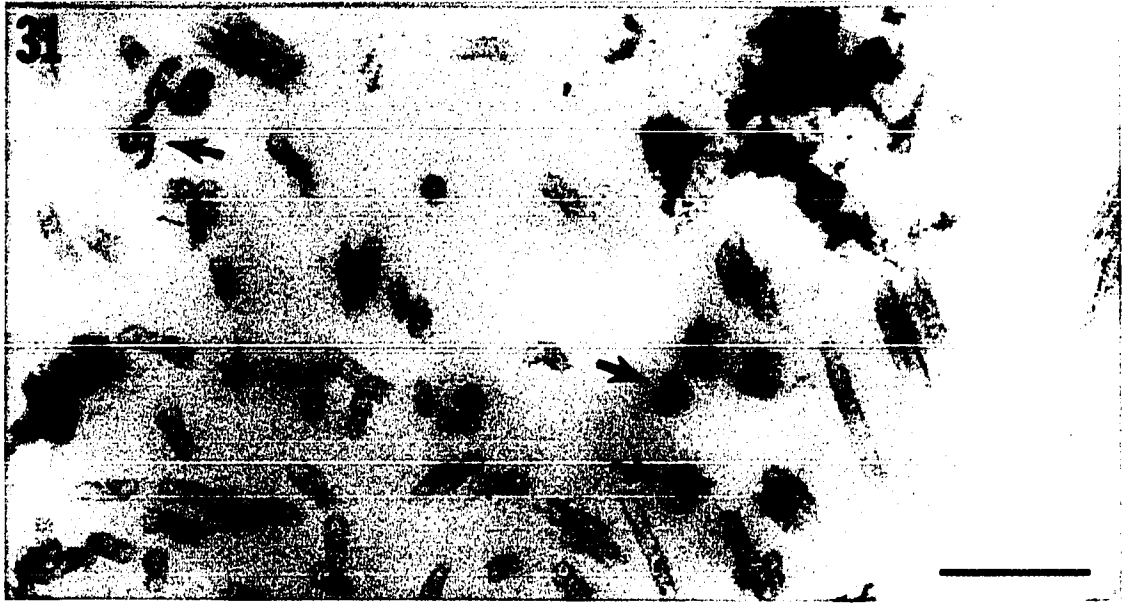
Figure 30 - High magnification of a segment of the postoral fibers. These parallel MTs bear randomly spaced cross-linkers and few associated vesicles. Also, the spacing between the individual MTs is variable. Bar = 0.2 μ m.



Figures 31 and 32 - Polarity determination of the postoral fibers

Figure 31 - Cross section of the postoral fibers distal to, and viewed from their distal ends toward the oral region. A few of the MTs display clockwise hooks (arrows). Bar = 0.2 μ m.

Figure 32 - Cross section of the postoral fibers near their origin at the oral region. Here the microtubules are more densely packed, but only a few contain clockwise hooks (arrows). BC = buccal cavity. Bar = 0.2 μ m.



III. Cytoplasmic dynein isolation

The existence of MT-based vesicle transport suggested the presence of a MT-based motor(s) in Paramecium. A purification scheme was modified from published procedures (Vale et al., 1985d; Euteneuer et al., 1988; Schnapp and Reese, 1989) in order to isolate any MT-based motor from the cytosol of Paramecium. Utilizing a MT-affinity purification scheme (Figure 3), a high molecular weight (>350 kD), nucleotide-sensitive binding protein was isolated from a Paramecium cytosolic extract (Figure 33). The isolation of this protein was strictly dependent upon the depletion of endogenous ATP from the cytosolic extract and the addition of exogenous MTs. (Paramecium MTs cannot be easily isolated using either the taxol or temperature-cycle assembly methods which necessitated the use of the brain MTs as the affinity matrix.)

On SDS-PAGE the protein had the same relative mobility as sea urchin flagellar dynein and bovine brain cytoplasmic dynein (Figure 34). Vanadate photocleavage produced two cleavage fragments of approximately 165 kD and 200 kD verifying the protein as a dynein-like molecule (Figure 35). Comparison with thyroglobulin (an 18S sedimentation coefficient standard) on 5 - 20 % sucrose gradients indicated a sedimentation coefficient of approximately 16S for the cytoplasmic dynein (Figure 36).

A 120 kD polypeptide present in the ATP extract (Figure 33) comigrated with the dynein heavy chains on both sucrose gradients (Figure 37) and through ion exchange chromatography (data not shown). Western blots of this polypeptide failed to cross react with 5 different anti-kinesin antibodies suggesting the protein was not a kinesin-related

Figure 33 - Purification procedure for cytoplasmic dynein. MAP-free, bovine brain MTs (lane 2) are mixed with an ATP depleted, high speed cytosolic extract from Paramecium (lane 3). The MTs and bound proteins are pelleted by centrifugation, washed once with buffer, and resuspended to one fifth of the original cytosolic extract volume (lane 4). The MTs are extracted with MgATP and centrifuged. The ATP extract (lane 5) contains cytoplasmic dynein (arrowheads), a 120 kD polypeptide (*), residual tubulin, and a varying amount of other contaminating polypeptides. The final MT pellet (lane 6) does not contain the additional high molecular weight polypeptide that was present prior to ATP extraction (lane 4). T = tubulin, molecular weight standards (lane 1) are indicated by their relative molecular weights in kD. 7% SDS-PAGE, coomassie stained.

Figure 34 - Relative mobilities of sea urchin dynein, Paramecium cytoplasmic dynein, and brain cytoplasmic dynein (MAP 1C). The cytoplasmic dynein from Paramecium (lane 2) has the same R_f as both sea urchin flagellar dynein (lane 1) and brain dynein (lane 3). DHC = dynein heavy chains, T = tubulin. 7.5% SDS-PAGE, coomassie stained.

Figure 35 - Vanadate cleavage of Paramecium cytoplasmic dynein. Two cleavage fragments of 200 kD and 165 kD (arrows) were produced upon UV irradiation in the presence of ATP and vanadate (lane 2). The cytoplasmic dynein control sample (lane 1), which lacked vanadate, was not cleaved. This verifies the Paramecium cytoplasmic dynein as a true dynein-like molecule. 7% SDS-PAGE, coomassie stained.

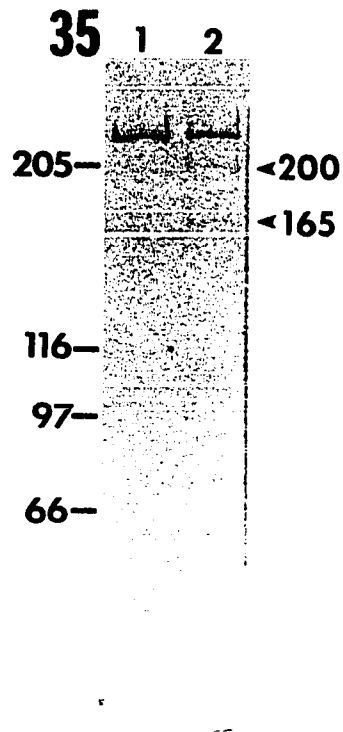
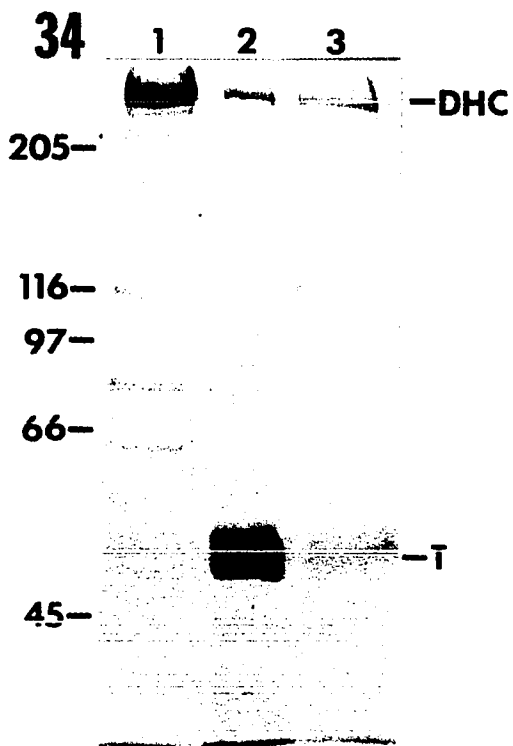
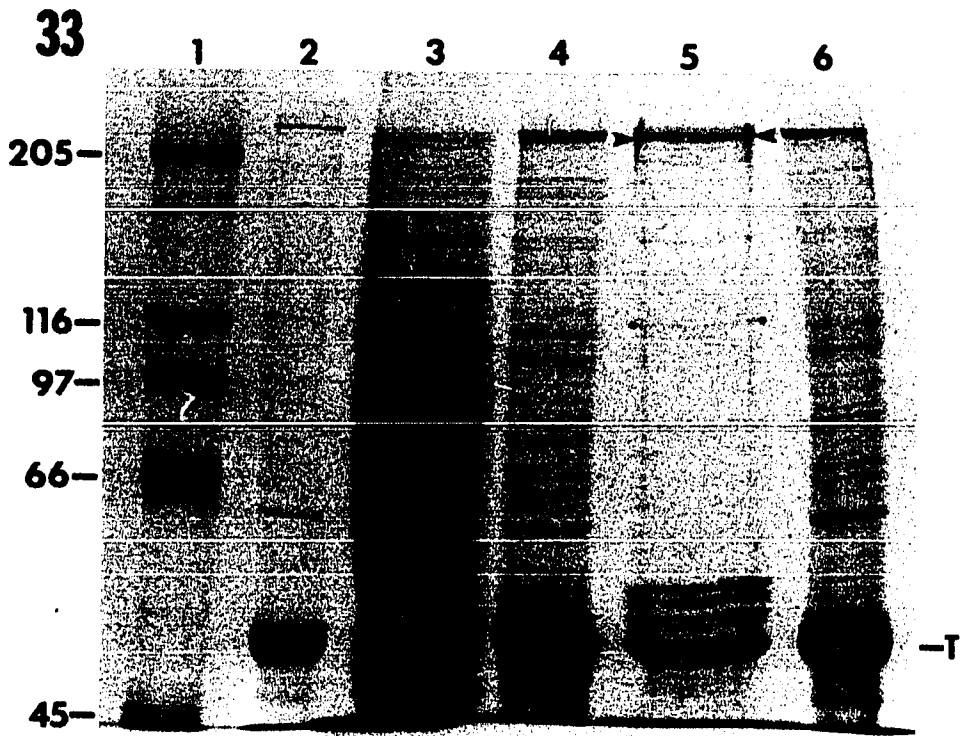
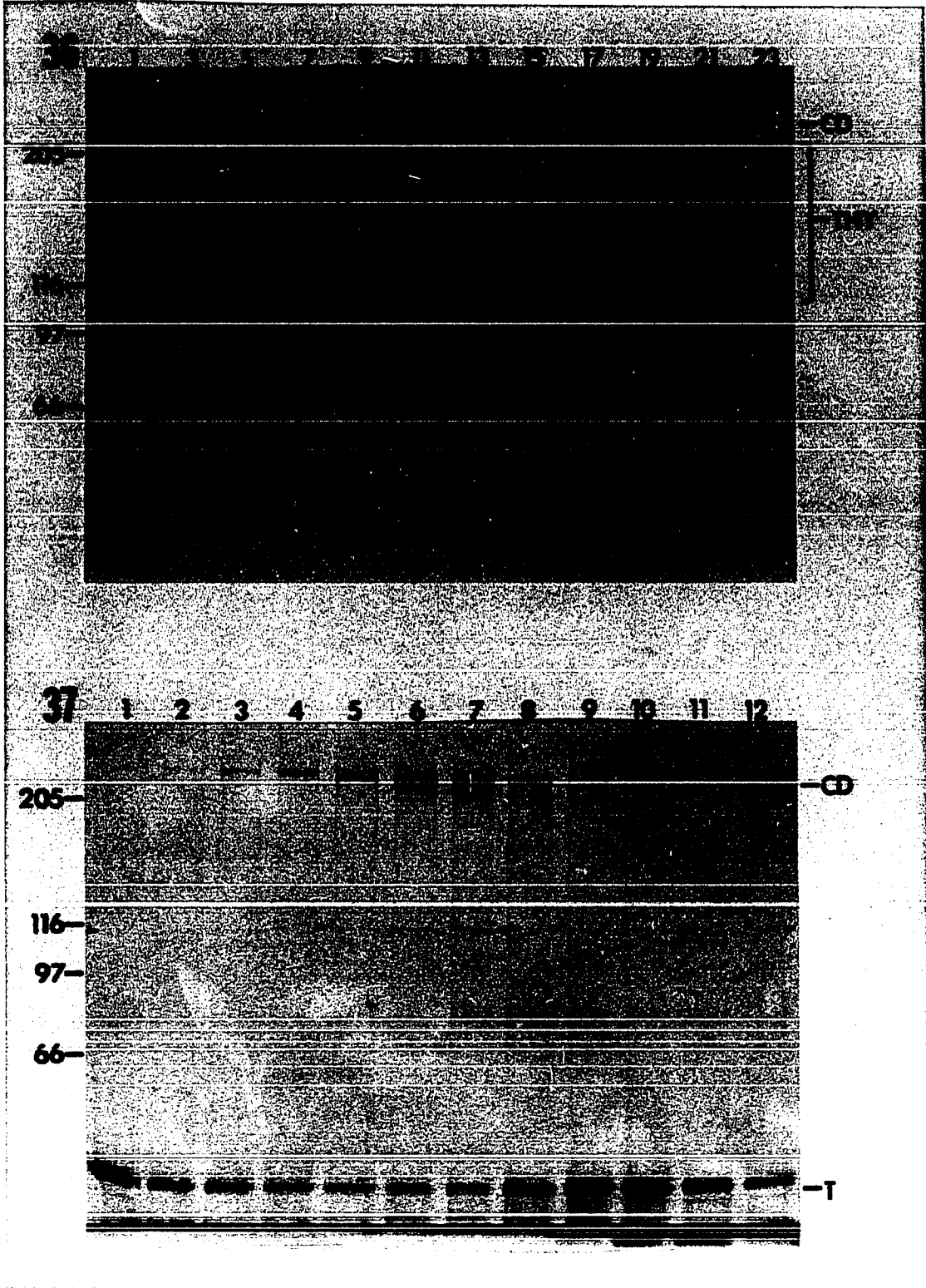


Figure 36 - S value determination for cytoplasmic dynein. In comparison with thyroglobulin (18S) the Paramecium cytoplasmic dynein was found to have a sedimentation coefficient of approximately 16S. Fractions from the 5 - 20% sucrose gradient (24, 0.2 ml for this particular gradient) are indicated above each lane (1 = bottom, 23 = top). The thyroglobulin appears as several bands on the gel. CD = cytoplasmic dynein, Thy = thyroglobulin. 7% SDS-PAGE, coomassie stained.

Figure 37 - Sucrose gradient purification of Paramecium cytoplasmic dynein. The fraction numbers from the bottom (#1) of the tube are indicated. A faint 120 kD polypeptide (between arrowheads, and also figure 31, lane 5) cosediments with the cytoplasmic dynein heavy chain. Tubulin contamination across the gel varies from preparation to preparation. CD = cytoplasmic dynein, T = tubulin. 7% SDS-PAGE, silver stained.



species (data not shown). Thus, this polypeptide was most likely an intermediate chain of the dynein molecule.

The ATPase and CTPase activities of the sucrose gradient purified protein were determined (Table 1). Both the ATP extract and sucrose gradient purified samples were tested in their ability to couple ATP hydrolysis to force generation using an in vitro motility assay. Both the ATP extract and the sucrose gradient fractions promoted the binding of MTs to the coverslip (Figures 38, 39, 40). The gradient fractions also supported bending and kinking motions indicative of force generating properties (Figure 39) as well as MT gliding (Figure 40). The rate of MT gliding was approximately 1.2 $\mu\text{m/s}$.

Visualization of the isolated protein by negative stain or low angle rotary shadowing revealed a two headed "v" shaped molecule (Figure 41). The globular heads measured 15.2 ± 1.6 nm and were connected to an amorphous base by thin stems. The overall width and height of the negatively stained molecules ranged from 28 - 57 nm wide by 35 - 40 nm high. The prominence of the base and stems varied considerably. Low angle rotary shadowing yielded the same overall morphology, but with slightly larger dimensions due to the platinum coating (Figure 41).

Comparison to Axonemal Dyneins

Because paramecia are ciliates and have dyneins in their cilia, the Paramecium cytoplasmic and axonemal dyneins were compared by several different criteria to insure the cytoplasmic dynein was not an axonemal precursor. Salt extraction of Paramecium axonemes and purification on sucrose gradients yielded two dynein species (Figure 42). The two dyneins

TABLE 1 - ATPase and CTPase activities of cytoplasmic and axonemal dyneins^a

	ATPase	CTPase	CTPase/ATPase
Cytoplasmic Dynein ^b	347 ± 80 (8) ^c	474 ± 24 (2)	1.4
22S Axonemal Dynein	286 ± 96 (4)	206 ± 58 (2)	0.7
12S Axonemal Dynein	250 ± 42 (2)	163 ± 42 (2)	0.7

^aspecific activities were presented as nmol/min/mg protein

^bthe specific activity of cytoplasmic dynein was stimulated 4 fold by taxol stabilized MTs at a final concentration of 0.2 mg/ml and inhibited 57% by 20 μM vanadate

^cparenthesis refer to number of experiments

Figure 38 - MT attachment to coverslip surface. An ATP-sensitive extract (Figure 33, lane 5) adsorbed to a coverslip induces the binding of single MTs (composed of phosphocellulose-purified tubulin) to the coverslip surface. These MTs were not gliding across the coverslip surface despite the presence of 10 mM MgATP. Bar = 2.0 μ m.

Figure 39a-b - Bending or kinking of a MT. An aliquot of sucrose gradient purified cytoplasmic dynein (Figure 37, lane 6) induced bending and kinking movements on single MTs indicative of force production. In 39a, a single MT is attached to the coverslip surface. In 39b, the same MT as seen in its bent or kinked conformation. A stationary particle (arrow) may be used as a reference point. Bar = 2.0 μ m.

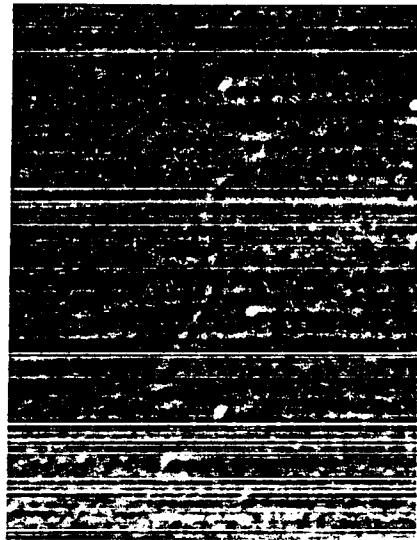
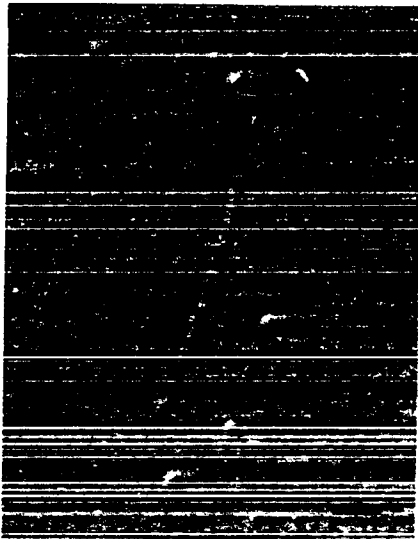
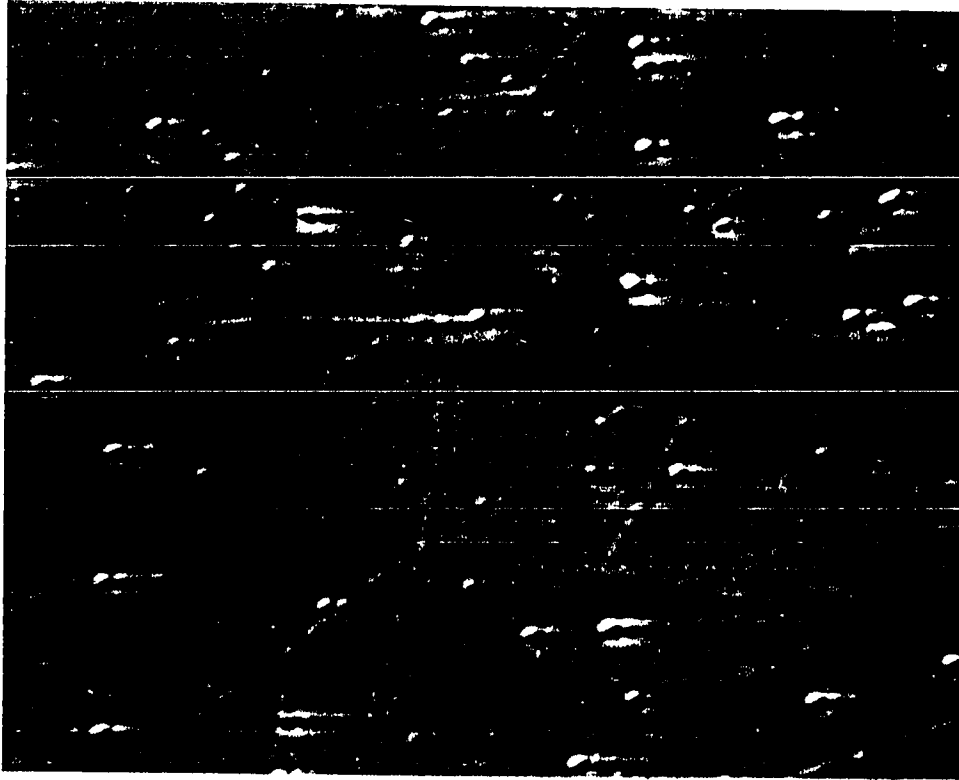


Figure 40a-d - MT gliding. The sequential video frames illustrate a MT gliding across a glass coverslip coated with sucrose gradient purified cytoplasmic dynein (Figure 39, lane 6). A stationary particle (arrowhead) is used as a reference point for gliding motility. The end of the MT (arrow) moves up to and past the stationary particle as the MT glides in the direction of the open arrow. The rate of gliding is $1.2 \mu\text{m}/\text{sec}$. Time between frames (in seconds) is indicated. Bar = $2.5 \mu\text{m}$.

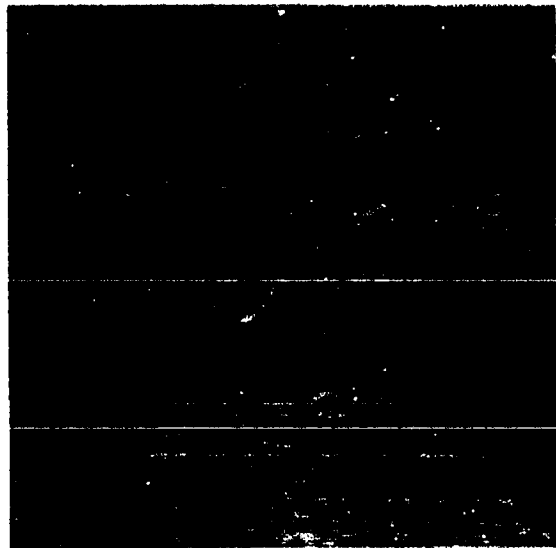
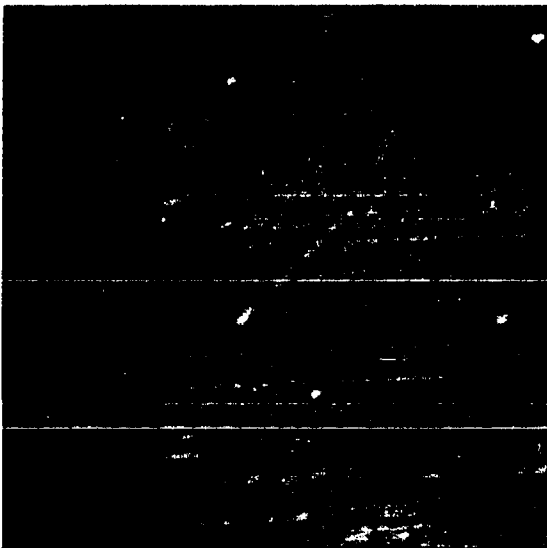
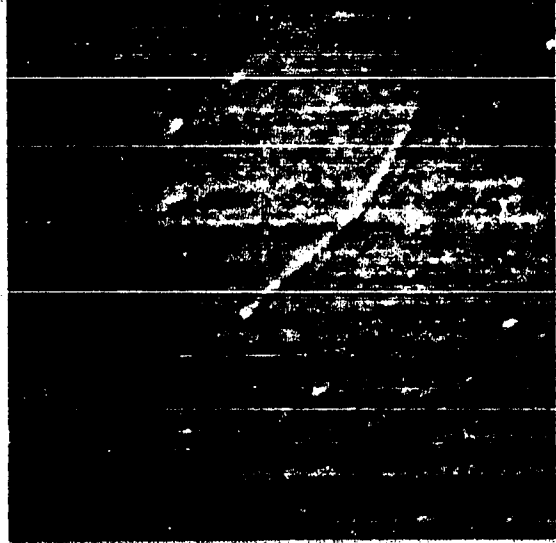
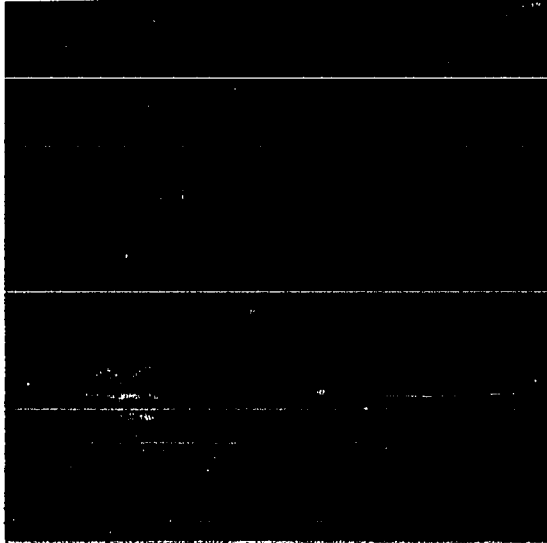
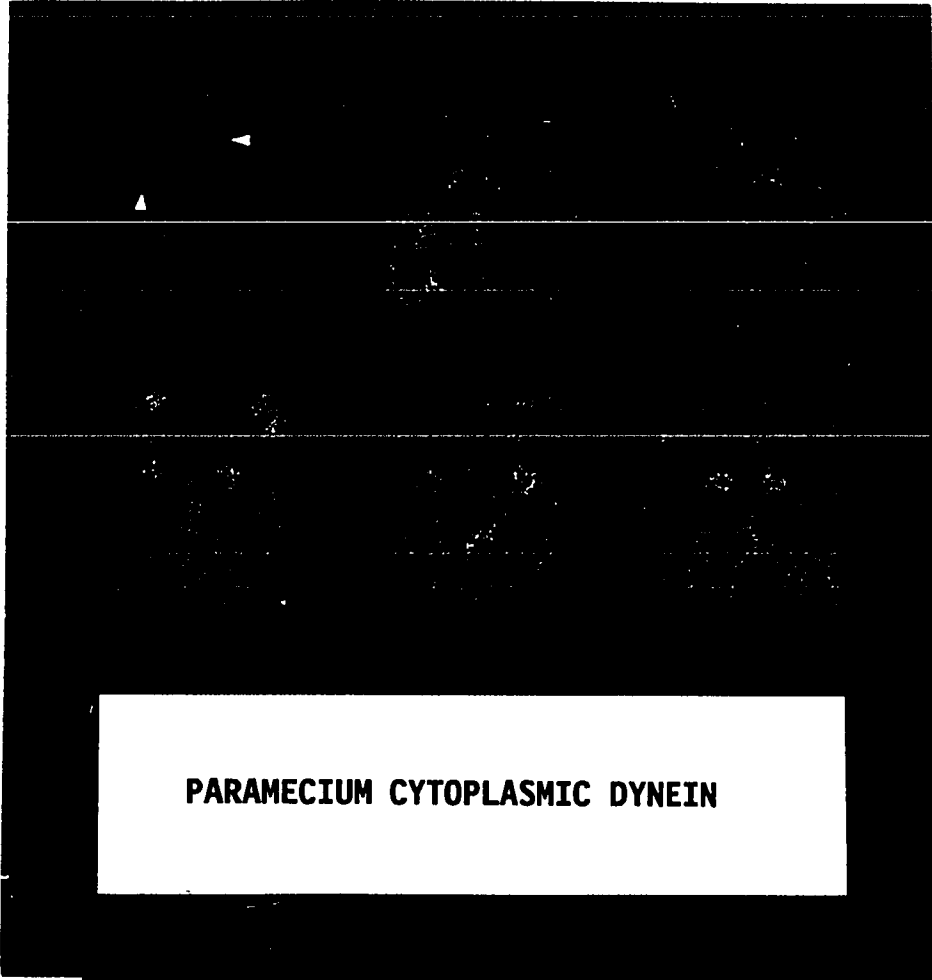


Figure 41 - Ultrastructural analysis of cytoplasmic dynein from Paramecium.

The top six panels were negatively stained preparations of sucrose gradient purified dyneins. Two 15-nm globular heads, which correspond to the dynein heavy chains, are connected by thin stems to an amorphous base. Occasionally, small projections (arrowheads in upper right panel) protrude from the globular heads. Bar = 10 nm.

The bottom four panels were low-angle, rotary-shadowed preparations. The morphology is basically the same as seen with negative staining. However, with this technique, the structures of the base and projections from the globular heads (arrowheads) are more prominent. Bar = 10 nm.



PARAMECIUM CYTOPLASMIC DYNEIN

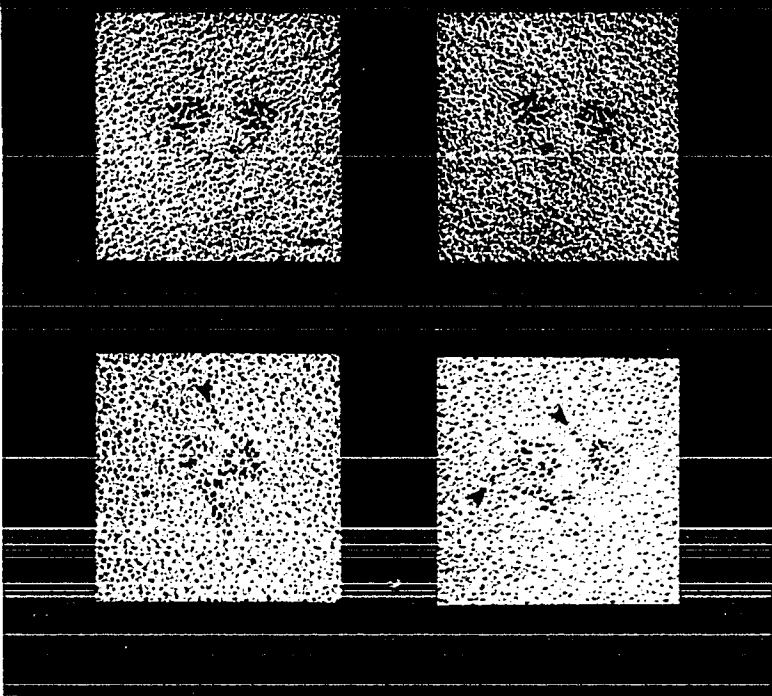
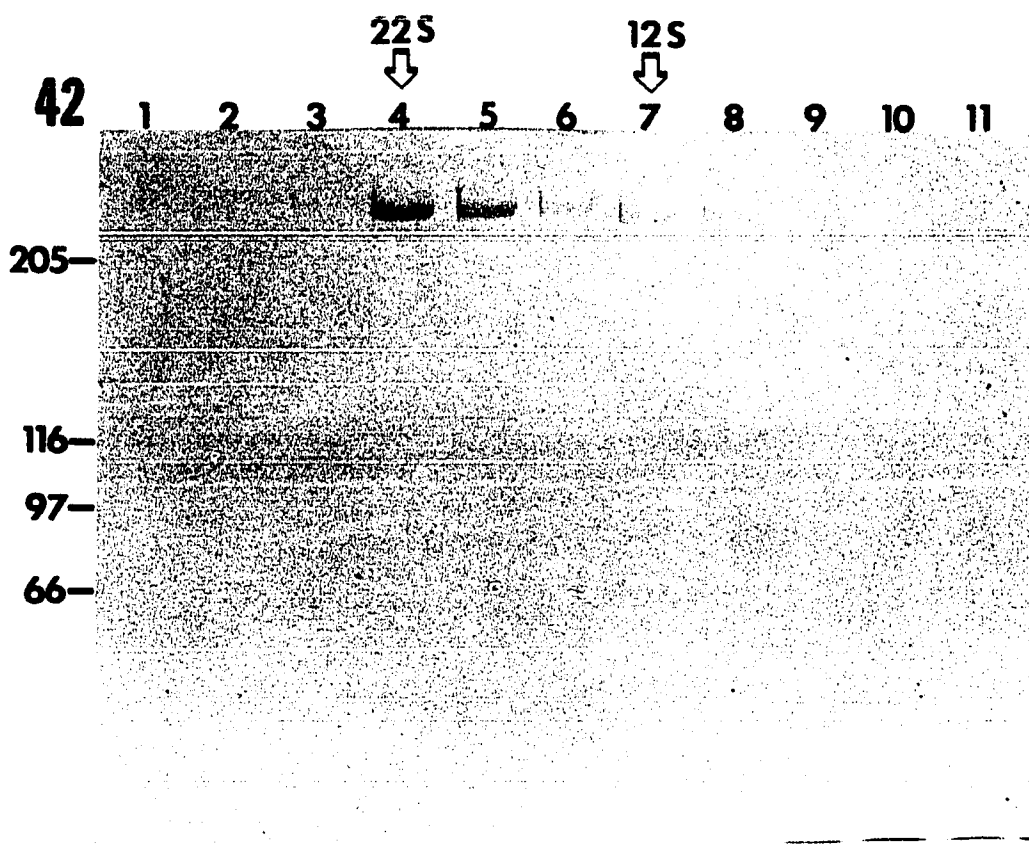


Figure 42 - Purification of Paramecium axonemal dyneins. Two dynein species were resolved by sucrose gradient centrifugation of axonemal high salt extracts. A 22S dynein is found in fraction 4, and a minor 12S species is found in fraction 7. The fraction numbers from the bottom of the tube are indicated. 7% SDS-PAGE, coomassie stained.



had sedimentation coefficients of 22S and 12S, respectively.

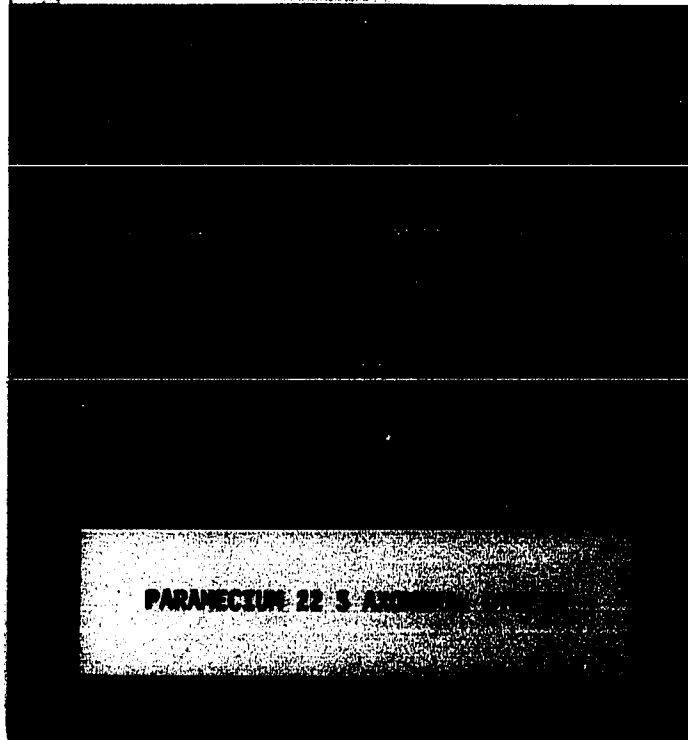
Ultrastructural analysis revealed a three headed molecule for the 22S dynein and a single headed molecule for the 12S (Figure 43).

Comparison of polypeptide composition and vanadate cleavage patterns of the three dynein species revealed striking differences (Figure 44). The 22S dynein had three intermediate chains of 84, 77 and 71 kD. The 12S dynein had two intermediate chains of 110 and 105 kD. Vanadate cleavage of these two dyneins revealed six and two cleavage fragments for the 22S and 12S dyneins, respectively.

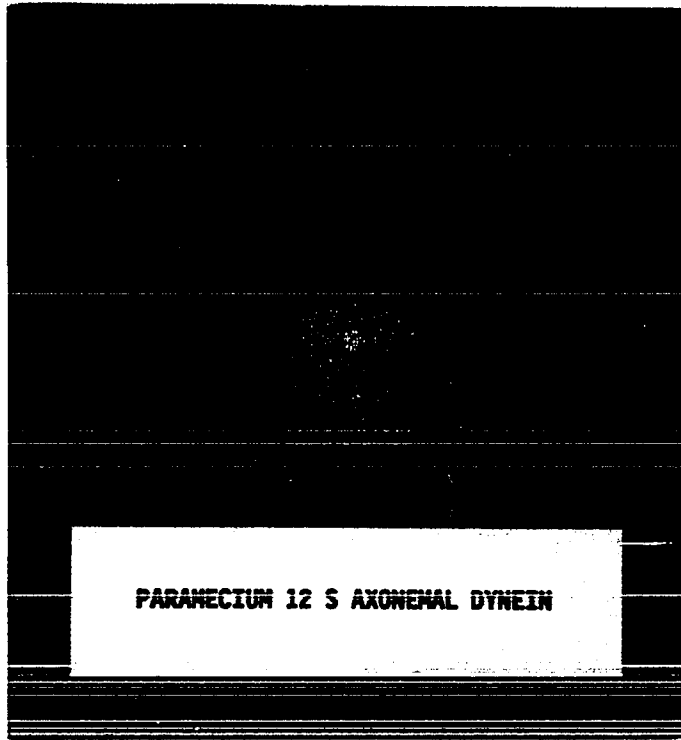
In addition, the purification schemes for the two dyneins (cytoplasmic vs. axonemal) were very different. In no instance was axonemal dynein isolated using the cytoplasmic dynein protocol nor was cytoplasmic dynein isolated using the axonemal dynein isolation protocol. Thus, each preparation was relatively pure and free of contamination by the alternative dynein species.

Figure 43 - Ultrastructural analysis of axonemal dyneins from Paramecium. The peak fractions of both 22S (Figure 42, lane 4) and 12S (Figure 42, lane 7) were negatively stained and examined. The 22S dynein was found to be a three headed molecule (top six panels), while the 12S dynein was a single headed molecule (bottom six panels). Bar = 10 nm.

43



PARAMECIUM 22 S AXONEMAL DYNEIN



PARAMECIUM 12 S AXONEMAL DYNEIN

Figure 44a-b - Comparison of vanadate cleavage patterns and intermediate chain composition for the three dynein species. 44b is a schematic diagram of 44a. 7% SDS-PAGE, silver stained.

Intermediate chain comparison:

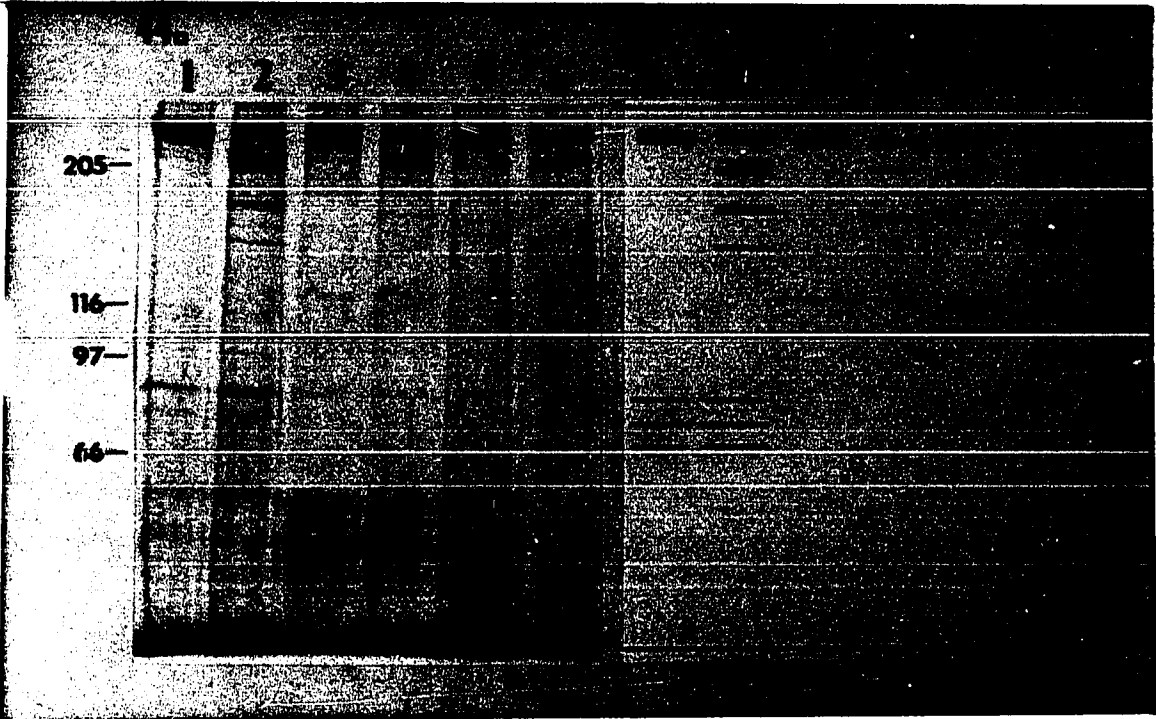
<u>Dynein species</u>	<u>Intermediate chains</u>
Lanes 1,2 = 22S axonemal dynein	84, 77, 71 kD
Lanes 3,4 = cytoplasmic dynein	120 kD
Lanes 5,6 = 12S axonemal dynein	110, 105 kD

Vanadate cleavage pattern comparison:

Lanes 1,3,5 are controls. Lanes 2,4,6 are cleaved samples

<u>Dynein species</u>	<u>Cleavage fragments</u>
Lane 2 = 22S axonemal dynein	220, 200(2) ^a , 180(2), 150 kD
Lane 4 = cytoplasmic dynein	200(2), 165(2) kD
Lane 6 = 12S axonemal dynein	200(2) kD

^anumber of fragments



DISCUSSION

In this thesis, I have examined the MT-based vesicle transport in Paramecium using VECM and the QF-DE technique. I have also isolated a cytoplasmic dynein which is a strong candidate for the vesicle motor, as demonstrated in other systems. This study also demonstrates that MT-based vesicle transport in a primitive eukaryote such as Paramecium is similar to the MT-based vesicle transport in higher organisms. In addition, there are a number of distinguishing features of this system which makes it a useful model system for studying MT-based vesicle transport. The data also expand our knowledge of the events involved with digestive vacuole formation.

Only two groups of vesicles could be observed by VECM to be transported along the MTR in Paramecium. The small flattened vesicles correspond to discoidal vesicles based on their morphology and location along the MTR. The larger spherical vesicles are identified as acidosomes by their ability to accumulate neutral red and their subsequent accumulation around the nascent digestive vacuole. This is the first indication that acidosomes are translocated in a MT-dependent manner. One function for each of these vesicle populations in Paramecium has been established (Allen, 1974; Allen and Fok, 1983a-c), and their transport in the manner described supports these functional roles. Because these vesicles are selectively transported along the MTR while other vesicle populations are not, a specific recognition between these vesicles and the MTR is suggested. The nature of this recognition is unknown, but seems somewhat unique because, in other systems, a multitude of vesicles are reported to be transported along the same MT (Allen et al., 1982).

The QF-DE analysis identified a third population of 100 nm vesicles that are most likely too small to be recognized using our VECM system with living Paramecium. The function of these vesicles is unknown. The morphology of their E face and their association with the MTR suggest they may be acidosome precursor vesicles which coalesce to form the large acidosomes. As the origin of the acidosomes remains unknown it is tempting to attribute the role of these 100 nm vesicles to be acidosome precursors. However, the 100 nm vesicles may merely be small transport or shuttle vesicles returning recycled membrane to the nascent vacuole.

The unique luminal etching pattern exhibited by the acidosomes following the QF-DE technique provides a distinguishing marker for these acidic vesicles. Acidosomes in many shapes and sizes are found throughout the cytoplasm. Thus, acidosomes are not confined to the oral region, although the oral region is where they are most abundant. Unfortunately, the small 100 nm vesicles are not found in cross fracture. Therefore their lumens are not exposed and whether they are acidosome precursors or not awaits further investigation.

The characteristics of the vesicle transport along the MTR were unexpected. The rate, the smooth nature, and the sidedness of transport are all unique observations for in vivo systems, especially concerning the large size of the vesicles transported. The rate of vesicle transport along the MTR (5.8 $\mu\text{m}/\text{sec}$) is faster than both axonal transport (directly visualized either in vivo (2.5 $\mu\text{m}/\text{sec}$, Allen et al., 1982) or in vitro (2.2 $\mu\text{m}/\text{sec}$, Vale et al., 1985c) and considerably faster than the speed of transport in tissue culture cells (0.4 $\mu\text{m}/\text{sec}$, Dabora and Sheetz, 1988).

Only Reticulomyxa, a freshwater amoeba, has similar or higher rates of vesicle transport (up to 20 $\mu\text{m}/\text{sec}$, Koonce et al., 1986).

The smooth nature of transport along the MTR is also in contrast to most systems. Vesicle transport in living cells or tissue is classically described as saltatory or exhibiting frequent stops, starts, reversals in direction and changes in velocity (Dabora and Sheetz, 1988). This is especially true when referring to the larger transported vesicles. However, in the extruded axon and other in vitro systems, the nature of vesicle transport is described as smooth and continuous (Brady et al., 1985, Dabora and Sheetz, 1988). These authors attribute the smooth movements to the lack of an extensive cytoplasmic matrix. In Paramecium the transport of acidosomes, which can be characterized as large vesicles, is smooth, especially within 5 - 10 μm of the cytopharynx. Neutral red labelling reveals a more saltatory nature of transport in areas distal to the cytopharynx, which becomes increasingly smooth closer to the cytopharynx. Also, despite the predominant unidirectional motility there is no apparent build-up of vesicles at the cytopharynx, at least in the same plane as vesicle transport.

The most interesting phenomenon of vesicle transport along the MTR is the sidedness with respect to the direction of transport. This observation was initially suggested by Allen (1974). To reiterate, vesicles (both discoidal vesicles and acidosomes) moving toward the cytopharynx do so along the anterior side of the MTR. Vesicles which occasionally move away from the cytopharynx do so along the posterior side of the MTR. A mechanistic explanation for this observation is as yet unclear.

The three characteristics of transport (rate, smooth nature, and sidedness) can be partially explained by the elaborate nature of the MTR itself. Because the MTR are planar sheets of MTs lying side by side, a particular vesicle does not have access to 360° of the MT as it might with a single MT. Thus, vesicle transport along these ribbons is restricted to either one side of the ribbon or the other, which partially explains the sidedness of transport. Approximately 40 of these MTRs extend perpendicular to the cytopharynx and radiate approximately 20 μM into the cytoplasm, creating 40 or so barrier-free "channels" for vesicle transport to the cytopharynx. Consequently, vesicle transport, at least near the proximal ends of the MTR, is not hindered by a meshwork of cytoskeletal elements or other large organellar obstructions lying in the path of transport. This could contribute to the smooth nature and rapid rate at which transport may proceed.

An alternative hypothesis for the smooth nature and rapid rate of vesicle translocation is related to the contact of each vesicle with the MTR. Because the MTR is a sheet of MTs, each vesicle is in contact with up to twelve MTs rather than just a single MT as is found in most other systems. Therefore, there may be a larger number of motor molecules propelling the discoidal vesicles and acidosomes in Paramecium. The more motors that are involved, the greater the chance of at least one motor being in contact with a MT at all times which could give rise to a smoother transport of vesicles. Also, the higher number of motors per vesicle might support a more rapid translocation rate. Vale and Toyoshima (1989) show the rate of MT gliding increases by increasing the concentration of dynein molecules adsorbed to the glass coverslip in an in

vitro assay. Thus, it might be expected that below a certain maximum number, the more dynein molecules involved with translocation, the higher the rate of transport.

The lack of vesicle build-up near the cytopharynx despite the unidirectional transport is also a consequence of the structures of the oral apparatus. The MTR at the cytopharynx bend sharply around a structure known as the cytostomal cord, and attach to the cytopharyngeal membrane (Allen, 1974). The discoidal vesicles travel around this bend and fuse with the cytopharyngeal membrane. This in turn provides the membrane for the expansion of the nascent vacuole membrane. As the nascent vacuole membrane grows, it is in close proximity to the bend of the MTR. Presumably as the moving acidosomes encounter this bend they come into contact with and bind to the nascent vacuole. The bound acidosomes are released from the MTR and move away from this area as the vacuole grows. This scenario is supported by three lines of evidence. First, acidosomes are not found directly adjacent to the cytopharynx from the bend to the proximal ends of the MTR (Figure 11). Second, the acidosomes appear firmly bound to the nascent vacuole membrane (Figure 16). Finally, acidosomes bound to the nascent vacuole are visualized in a different focal plane than for visualization of acidosome transport along the MTR (Figure 6). Schematic models for vesicle transport along the MTR are presented in Figures 45 to 47.

The digestive vacuole transport along the postoral fibers is also a MT-based transport, however its characteristics are quite different from

Figure 45 - "Channels" created by the MTR. This schematic cross section through the MTR illustrates the barrier-free channels (between dashed lines) through which acidosomes, discoidal vesicles and the 100 nm vesicles may pass unhindered. Mitochondria, trichocysts and other large organelles are excluded from these channels except where two ribbons have joined to form one wide ribbon. Also, note the numerous motors powering each vesicle, which may help promote the smooth and rapid transport.

45

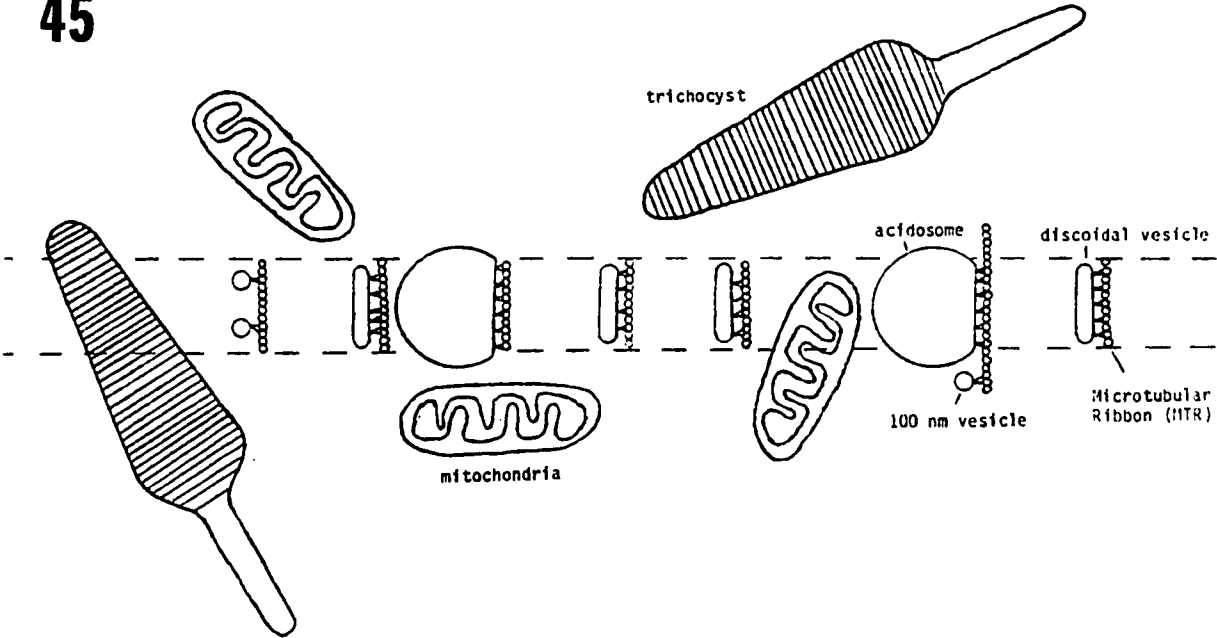


Figure 46 - Dorsal view of vesicle transport toward the oral region. The acidosomes and discoidal vesicles are found primarily on the anterior side of the MTR as they move toward the cytopharynx. The discoidal vesicles fuse with the cytopharynx membrane and provide the membrane for the growth of the nascent digestive vacuole. The acidosomes bind to the growing nascent digestive vacuole. Eventually, the vacuole will pinch off from the oral apparatus and move posteriorly along the postoral fibers.

46

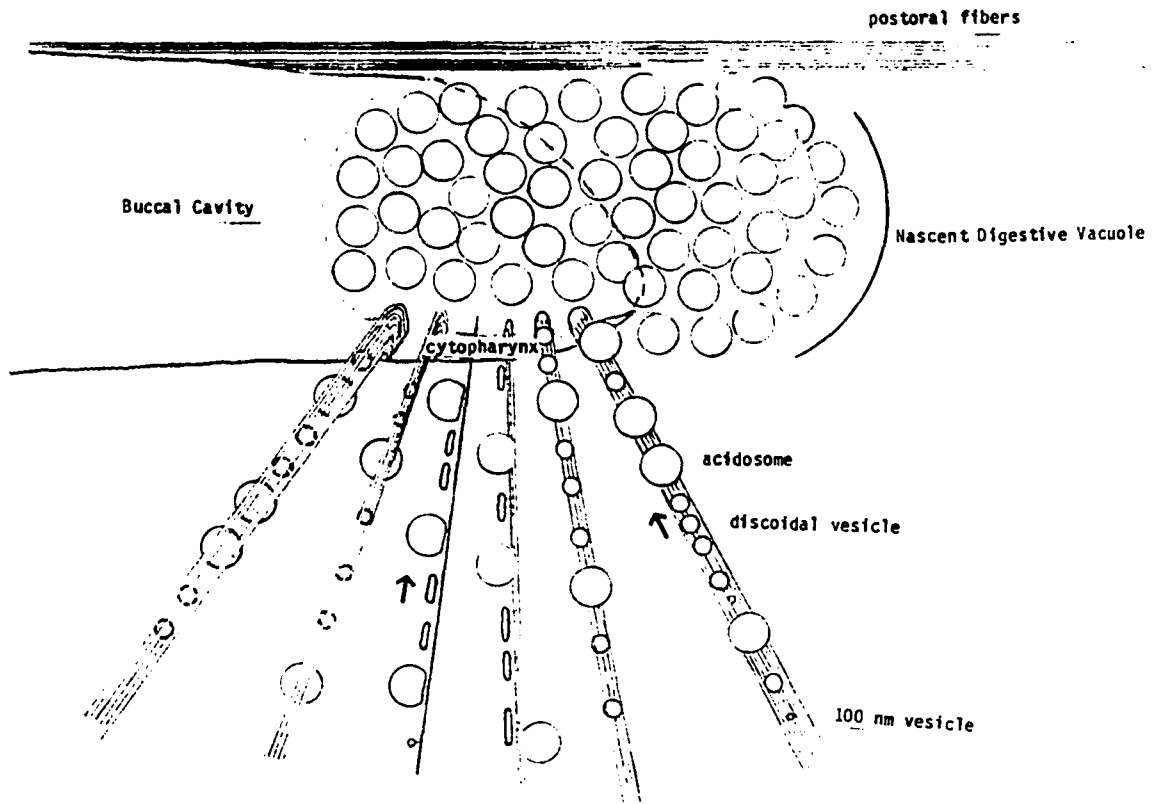
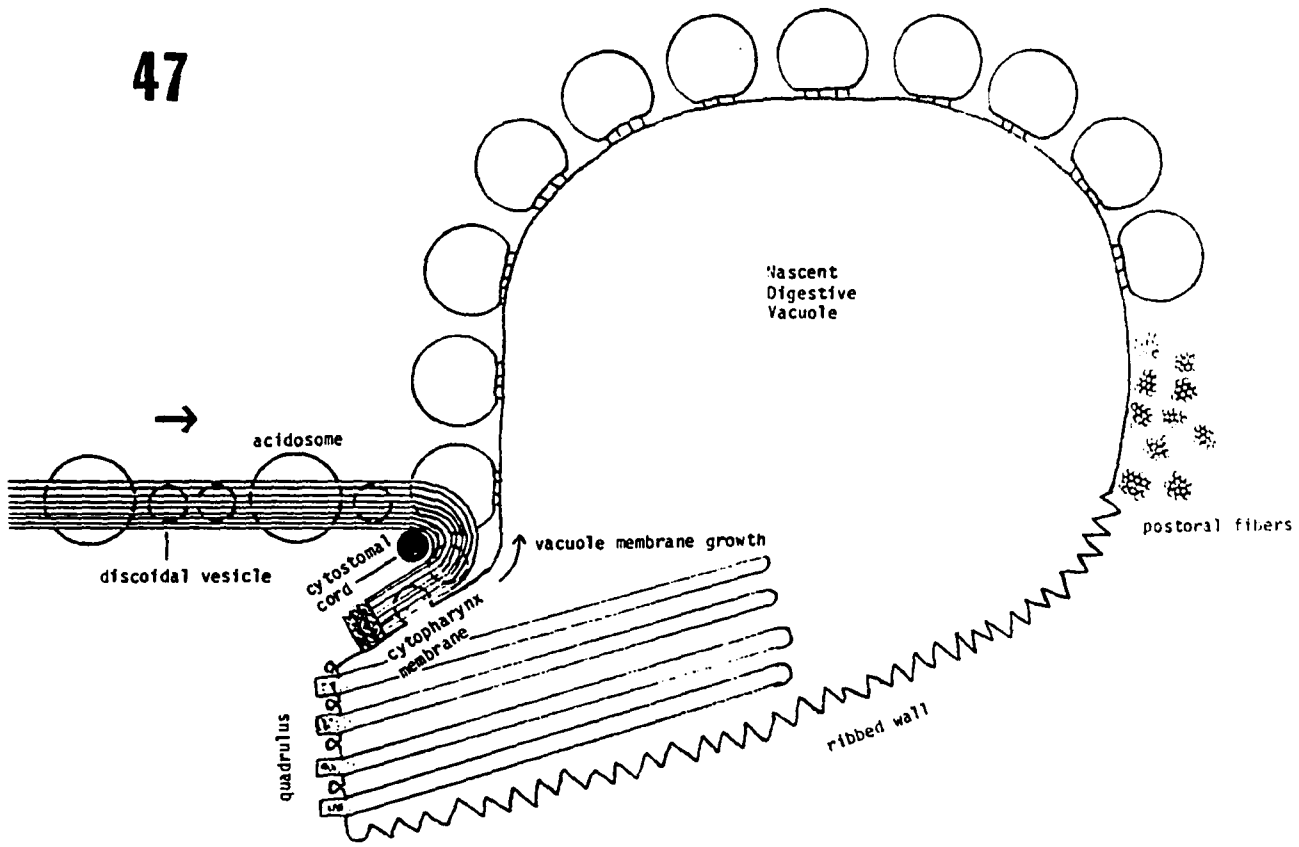


Figure 47 - Vesicle transport and associated vacuole growth. This cross section through the nascent digestive vacuole at the cytopharynx membrane highlights the structures of the oral apparatus. The discoidal vesicles move around the bend in the MTR and fuse with the cytopharynx membrane thus causing the growth and development of the nascent digestive vacuole. The acidosomes move up to and bind with the nascent vacuole. As the vacuole grows, the acidosomes are moved away from this location which allows more acidosomes to bind to the vacuole.

47



vesicle transport along the MTR. Two striking features of postoral transport are the on/off mechanism and the rate of vacuole transport.

The postoral fibers are composed of MTs that are immunologically related to other tubulins (Cohen et al., 1982), yet vesicle transport along these fibers only occurs during the few seconds following digestive vacuole formation. An unknown stimulus triggers the nascent vacuole to elongate along the postoral fibers, release from the cytopharynx and glide along the postoral fibers to the posterior end of the cell. A heterogeneous population of vesicles are transported along the postoral fibers following after the digestive vacuole. Soon after the passage of the vacuole all directed transport abruptly stops. This cycle repeats itself with each successive digestive vacuole produced.

Cohen et al. (1984) demonstrated the presence of filamentous actin adjacent to the postoral fibers only during the transport of a digestive vacuole along the postoral fibers. Also, cytochalasin B (an actin antagonist) inhibits digestive vacuole release and transport from the cytopharynx (Cohen et al., 1984; Allen and Fok, 1985). My data would also favor an actin/MT-based transport system which undergoes cycles of actin polymerization - digestive vacuole/vesicle transport - actin depolymerization and cessation of transport.

The rate of transport ($\approx 20 \mu\text{m}/\text{sec}$) is also unusual in comparison with other plus-end directed movements in other systems. This is especially true given the in vitro rate of kinesin driven movements ($0.5 \mu\text{m}/\text{sec}$, Cohn et al., 1989). Other plus-end directed MT-based motors may exist, but

they have not yet been isolated or described. Again, only the Reticulomyxa system supports such high rates of vesicle transport (Koonce et al., 1986).

The transport may, in part, be the mechanism for the vacuole release from the cytopharynx. Some authors suggest a sphincter-like mechanism for vacuole release, but no such structure has been demonstrated. The hypothesis suggested by this study in which the postoral fiber transport rate is much greater than the rate of vacuole growth would imply that the vacuole is simply pulled away from the cytopharynx. The elastic nature of the membranes themselves may act somewhat like a soap bubble forming and breaking free from a small ring. Likewise, the nascent vacuole is rapidly pulled away from the cytopharynx until the trailing membrane closes together and fuses with itself, thus being released from the cytopharynx.

The transport of discoidal vesicles and acidosomes along the MTR, and digestive vacuole growth, release and transport along the postoral fibers must be intricately tied together. Digestive vacuoles form from discoidal vesicles at approximately 1 per minute under optimal conditions (Fok et al., 1988). These authors estimated a minimum speed of 1.7 $\mu\text{m}/\text{sec}$ for discoidal vesicle transport, assuming there is a continuous and abundant supply of discoidal vesicles, to provide ample membrane to attain this vacuole formation rate. The direct observation of vesicle transport along the MTR reveals a rate nearly four times faster than this calculated minimum. Therefore, the rate of movement of discoidal vesicles appears not to be the limiting factor in vacuole formation.

With the multitude of MT-based movements in Paramecium, the presence of a MT-based motor powering such movements was sought. By capitalizing on the affinity of conventional MT-based motors for MTs in the absence of ATP, an isolation scheme was developed to isolate such a motor from the cytosol of Paramecium. Using this method I was able to isolate and characterize a cytoplasmic dynein. The physical, structural and chemical properties of this molecule are similar to those of the cytoplasmic dyneins isolated from brain tissue (Paschal et al., 1987), squid axons (Schnapp and Reese, 1989), testis (Neely and Boekelheide, 1988), and a dynein-like molecule from Reticulomyxa (Euteneuer et al., 1988).

The properties of this molecule--its heavy chains of >350 kD together with its intermediate chain polypeptide, its ATPase activity which is sensitive to low concentrations of vanadate, and the vanadate-mediated photocleavage of its heavy chains--are all classical dynein-like properties (Gibbons, 1989). The structural characterization, which reveals a two-headed dynein morphology, support the above properties and determination of the molecule as a true dynein. This two-headed structure is identical to the cytoplasmic dyneins of neuronal tissue (Vallee et al., 1988; Schnapp and Reese, 1989) and rat testis (Neely and Boekelheide, 1988).

Another characteristic property of cytoplasmic dyneins is their ability to hydrolyze the nucleotide CTP at a higher rate than the hydrolysis of ATP (Shpetner et al., 1988). Although the CTPase/ATPase ratio is not as high as with brain cytoplasmic dynein, the cytoplasmic dynein from Paramecium fulfills this criterion. In addition, this

cytoplasmic dynein is capable of ATP-coupled force production as demonstrated using an in vitro motility assay.

However, because paramecia are ciliates, it was necessary to demonstrate that the cytoplasmic dynein was not a ciliary precursor. Axonemal dyneins were isolated by salt extraction of demembrated cilia. The two dynein species which are isolated (22S & 12S) closely resemble the two axonemal dynein species found in Paramecium tetraurelia (Travis and Nelson, 1988). By five separate criteria (polypeptide composition, sedimentation coefficient, morphology, vanadate cleavage patterns, and CTPase/ATPase ratio) the cytoplasmic dynein shows significant differences from both the 22S and 12S axonemal dyneins of Paramecium. Therefore it is reasonable to conclude that the cytoplasmic dynein is not a ciliary precursor, but rather a distinct dynein species and may therefore participate in cytoplasmic MT-based motility.

Interestingly, axonemal dyneins are not isolated from the cytosol along with the cytoplasmic dynein. One would expect at least a small soluble pool of axonemal dynein precursors. However, even though axonemal dyneins were not found to be contaminants of the isolated cytoplasmic dynein, their absence doesn't necessarily mean that they do not exist in soluble form. Porter et al. (1988) found at least two isoforms of dyneins in the unfertilized sea urchin egg. One isoform has a high affinity for MTs in the absence of ATP, while the second isoform has a low affinity for MTs regardless of the presence or absence of ATP. The low-affinity isoform is immunologically related to axonemal dyneins, while the high-affinity isoform seems unique. The high affinity isoform also has an elevated CTPase/ATPase ratio (Grissom et al., 1989). These authors

hypothesize that the high affinity dynein is a cytoplasmic dynein and the low affinity dyneins are soluble axonemal precursors. Thus, axonemal dynein precursors may also exist in the cytosol of Paramecium, but are not isolated using the procedure for the cytoplasmic dynein isolation.

It is becoming clear that cytoplasmic dyneins play a major role in the MT-based transport of vesicular organelles. Vanadate photocleavage of cytosolic extracts from either cultured cells (Schroer et al., 1989) or squid axons (Schnapp and Reese, 1989) inhibits minus-end directed vesicle transport along MTs. The addition of chick brain cytoplasmic dynein is able to restore the minus-end directed transport in the cultured cell extracts. Also, cytoplasmic dynein has been localized on the surface of membranous organelles in the axon (Hirokawa et al., 1989). The Paramecium cytoplasmic dynein may, perhaps, perform similar vesicle transport functions such as the transport of the discoidal vesicles and acidosomes along the MTR.

Cytoplasmic dyneins are minus-end directed motors. The minus ends of the MTR are at the oral region, thus much of the transport along the MTR is minus-end directed and could be mediated by cytoplasmic dynein. The rapid rate of vesicle transport also favors a dynein-like motor as opposed to a kinesin-like motor. However, the bidirectional transport along the MTR would require either two distinct motors or a bidirectional motor as found in Reticulomyxa (Euteneuer et al., 1988).

Actually, the Reticulomyxa and Paramecium motility systems share many common features. Besides having bidirectional vesicle transport along MTs with rates higher than those found in other systems, only dynein-like molecules have been isolated from these two organisms using exogenous

bovine brain MTs as the affinity isolation matrix. The lack of a kinesin-like molecule, exclusively a plus-end directed motor, in either organism is interesting because both systems show bidirectional vesicle transport. The specific activities of their dynein-like motors are similar and these specific activities are inhibited to the same extent by 20 μ M vanadate (Euteneuer et al., 1988). Using in vitro assays, the Reticulomyxa motor displays bidirectional movements of latex beads on MTs, while the Paramecium motor promotes MT gliding. Unfortunately, the direction of MT gliding was not determined, nor was the latex bead assay performed for the Paramecium motor.

Although the rate of in vitro motility is not the same as the in vivo rate of vesicle transport, this does not exclude the cytoplasmic dynein as a favorable candidate for producing this movement. The conditions of the in vitro motility assays rarely mimic native in vivo conditions, thus most in vitro systems display reduced MT gliding rates when compared to in vivo vesicle transport rates (Vale et al., 1985d; Euteneuer et al., 1988). For example, the rate of bead movements in Reticulomyxa in an in vitro assay is only 3.6 μ m/sec compared to ~20 μ m/sec for in vivo vesicle transport rates.

Vallee et al. (1989) suggest that the different polypeptide composition of cytoplasmic dynein may reflect its functional activity. The intermediate chain polypeptides of brain cytoplasmic dynein may form the membrane/organelle binding site at the base of the molecule. Likewise, the intermediate chains of axonemal dyneins may be suited to bind to the A subfiber of the axonemal microtubular doublet. A similar situation may exist in Paramecium. The intermediate chain composition of

cytoplasmic dynein is markedly different from the axonemal dyneins. Perhaps this difference allows cytoplasmic dynein to bind to membranous vesicles such as discoidal vesicles or acidosomes. The dynein heavy chains would still be free to attach and propagate along a MT.

In summary, I have revealed the properties of vesicle transport along MTs in Paramecium, and isolated a cytoplasmic dynein which may power these vesicle movements. My findings have shown the oral region cytoskeleton to be a specialized structure for the transport of discoidal vesicles, acidosomes, and the 100 nm vesicles. Several properties which are unique to this system, such as the sidedness, the smooth nature and the high rate of transport, make Paramecium an excellent model system to study MT-based motility. In addition, several other features make Paramecium an excellent system to study the in vivo function of cytoplasmic dynein. The apparent lack of kinesin or other motors suggests that the cytoplasmic dynein powers all vesicle movements. Also, because the discoidal vesicles and acidosomes have been highly characterized and monoclonal antibodies have been raised against them, this system is ideal for determining the nature of the MT-motor-vesicle recognition, which has not been determined in any system.

Table 2 - Axenic Media Formulation

Component	mg per ml	ug per ml
Proteose peptone	10	
Trypticase	5	
Yeast RNA	1	
Phosphatidyl ethanolamine		200
Magnesium sulfate		500
Stigmasterol		5
Vitamins		
Calcium pantothenate		5
Nicotinamide		5
Pyridoxal HCl		5
Riboflavin		5
Pyridoxamine HCl		2.5
Folic Acid		25
Thiamine HCl		15
Biotin		0.00125
DL-Thioctic Acid		0.05

Table 3 - Hook Decoration Buffer

0.5 M PIPES, pH 6.6		0.5 M PEM
1.0 mM EGTA		
1.0 mM MgSO ₄		
2.0 mg/ml tubulin		
1.0 mM GTP		
2.5 % DMSO		
1.5 % Triton X-100		

Table 4 - PEM Buffer

0.1 M PIPES, pH 6.6
1.0 mM EGTA
1.0 mM MgSO ₄

Table 5 - Dynein Buffer

10 mM Tris, pH 7.2
100 mM NaC ₂ H ₃ O ₂
3 mM MgSO ₄
1 mM EGTA
1 mM DTT

Table 6 - Dryl's Solution

119

1 mM Na₂HPO₄
 1 mM NaH₂PO₄
 2 mM Na₃C₆H₅O₇
 1.5 mM CaCl₂

pH to 6.8

Table 7 - STEN

0.5 M Sucrose
 20 mM Tris, pH 7.5
 2 mM EDTA
 6 mM NaCl

Table 8 - Column Equilibration Buffer

10 mM Tris, pH 8.0
 4 mM MgCl₂
 0.1 mM EGTA
 60 mM KCl

Appendix table abbreviations and symbols

CaCl ₂	calcium chloride
DMSO	dimethyl sulfoxide
DTT	dithiothreitol
EDTA	ethylenediaminetetraacetic acid
EGTA	ethylene glycol-bis(β-aminoethyl ether) N,N,N',N',- tetraacetic acid
GTP	guanosine, 5'-triphosphate
KCl	potassium chloride
MgCl ₂	magnesium chloride
MgSO ₄	magnesium sulfate
NaCl	sodium chloride
NaC ₂ H ₃ O ₂	sodium acetate
Na ₃ C ₆ H ₅ O ₇	sodium citrate
Na ₂ HPO ₄	sodium phosphate dibasic
NaH ₂ PO ₄	sodium phosphate monobasic
PIPES	piperazine-N,N'-bis[2-ethanesulfonic acid]
Tris	tris(hydroxymethyl)aminomethane

- Adams, R. J. 1982. Organelle movement in axons depends on ATP. *Nature* (London) 297:327-329.
- Adoutte, A., R. Ramanathan, R. M. Lewis, R. R. Dute, K.-Y. Ling, C. Kung, and D. L. Nelson. 1980. Biochemical studies of the excitable membrane of Paramecium tetraurelia. III. Proteins of cilia and ciliary membranes. *J. Cell Biol.* 84:717-738.
- Allen, R. D. 1974. Food vacuole membrane growth with microtubule-associated membrane transport in Paramecium. *J. Cell Biol.* 63:904-922.
- Allen, R. D. 1975. Evidence for firm linkages between microtubules and membrane-bounded vesicles. *J. Cell Biol.* 64:497-503.
- Allen, R. D. 1984. Paramecium phagosome membrane: from oral region to cytoproct and back again. *J. Protozool.* 31:1-6.
- Allen, R. D., N. S. Allen, and J. L. Travis. 1981. Video-enhanced differential interference contrast (AVEC-DIC) microscopy: a new method capable of analyzing microtubule-related movement in the reticulopodial network of Allogromia laticollaris. *Cell Motil.* 1:291-302.
- Allen, R. D., and A. K. Fok. 1980. Membrane recycling and endocytosis in Paramecium confirmed by horseradish peroxidase pulse-chase studies. *J. Cell Sci.* 45:131-145.
- Allen, R. D., and A. K. Fok. 1983a. Phagosome fusion vesicles of Paramecium. I. Thin-section morphology. *Eur. J. Cell Biol.* 29:150-158.
- Allen, R. D., and A. K. Fok. 1983b. Phagosome fusion vesicles of Paramecium. II. Freeze-fracture evidence for membrane replacement. *Eur. J. Cell Biol.* 29:159-165.
- Allen, R. D., and A. K. Fok. 1983c. Nonlysosomal vesicles (acidosomes) are involved in phagosome acidification in Paramecium. *J. Cell Biol.* 97:566-570.
- Allen, R. D., and A. K. Fok. 1984. Retrieval of lysosomal membrane and acid phosphatase from phagolysosomes of Paramecium caudatum. *J. Cell Biol.* 99:1955-1959.
- Allen, R. D., J. Metzals, I. Tasaki, S. T. Brady, and S. P. Gilbert. 1982. Fast axonal transport in squid giant axon. *Science* 218:1127-1129.
- Allen, R. D., C. C. Schroeder, and A. K. Fok. 1988. Phagosome-lysosome membrane traffic in Paramecium. Proceedings of a workshop on protein traffic, ILRAD, Nairobi, Kenya (in press).

- Allen, R. D., C. C. Schroeder, and A. K. Fok. 1989. An investigation of mitochondrial inner membranes by rapid-freeze deep-etch techniques. *J. Cell Biol.* 108:2233-2240.
- Allen, R. D., and L. A. Staehelin. 1981. Digestive system membranes: freeze-fracture evidence for differentiation and flow in Paramecium. *J. Cell Biol.* 89:9-20.
- Allen, R. D., M. S. Ueno, and A. K. Fok. 1986. Monoclonal antibodies differentiate between various membrane pools of the phagosomal-phagolysosomal system in Paramecium. *J. Cell Biol.* 103:356a.
- Allen, R. D., D. G. Weiss, J. H. Hayden, D. T. Brown, H. Fujiwake and M. Simpson. 1985. Gliding movement of and bidirectional transport along single native microtubules from squid axoplasm: evidence for an active role of microtubules in cytoplasmic transport. *J. Cell Biol.* 100:1736-1752.
- Allen, R. D., and R. W. Wolf. 1974. The cytoproct of Paramecium caudatum: structure and function, microtubules, and fate of food vacuole membranes. *J. Cell Sci.* 14:611-631.
- Aufderheide, K. J. 1977. Saltatory motility of uninserted trichocysts and mitochondria in Paramecium tetraurelia. *Science* 198:299-300.
- Aufderheide, K. J. 1978. Motility events of trichocyst insertion in Paramecium tetraurelia. *J. Protozool.* 25:362-365.
- Bell, C. W., E. Fronk, and I. R. Gibbons. 1979. Polypeptide subunits of dynein-1 from sea urchin sperm flagella. *J. Supramol. Struct.* 11:311-317.
- Bershadsky A. D. and J. M. Vasiliev. 1988. Cytoskeleton. Plenum Press. New York.
- Bird, M. M. 1976. Microtubule-synaptic vesicle associations in cultured rat spinal cord neurons. *Cell Tissue Res.* 168:101-116.
- Bloom, G. S., M. C. Wagner, K. K. Pfister, and S. T. Brady. 1988. Native structure and physical properties of bovine brain kinesin, and identification of the ATP-binding subunit polypeptide. *Biochem.* 27:3409-3416.
- Brady, S. T., R. J. Lasek, and R. D. Allen. 1982. Fast axonal transport in extruded axoplasm from squid giant axon. *Science* 218:1129-1131.
- Brady, S. T., R. J. Lasek, and R. D. Allen. 1985. Video microscopy of fast axonal transport in extruded axoplasm: a new model for study of molecular mechanisms. *Cell Motil.* 5:81-101.
- Burton, P. R., and H. L. Fernandez. 1973. Delineation by lanthanum staining of filamentous elements associated with the surfaces of axonal microtubules. *J. Cell Sci.* 12:567-584.

- Burton, P. R., and J. L. Paige. 1981. Polarity of axoplasmic microtubules in the olfactory nerve of the frog. *Proc. Natl. Acad. Sci. (USA)* 78:3269-3273.
- Cleveland, D. W., S-Y. Hwo, and M. W. Kirschner. 1977. Purification of tau, a microtubule-associated protein that induces assembly of microtubules from purified tubulin. *J. Mol. Biol.* 116:207-225.
- Cohen, J., A. Adoutte, S. Grandchamp, L.-M. Houdebine, and J. Beisson. 1982. Immunocytochemical study of microtubular structures throughout the cell cycle of Paramecium. *Biol. Cell* 44:35-44.
- Cohen, J., N. Garreau de Loubresse, and J. Beisson. 1984. Actin microfilaments in Paramecium: Localization and role in intracellular movements. *Cell Motil.* 4:443-468.
- Cohn, S. A., A. L. Ingold, and J. M. Scholey. 1987. Correlation between the ATPase and microtubule translocating activities of sea urchin egg kinesin. *Nature (London)* 328:160-163.
- Cohn, S. A., A. L. Ingold, and J. M. Scholey. 1989. Quantitative analysis of sea urchin egg kinesin-driven microtubule motility. *J. Biol. Chem.* 264:4290-4297.
- Collins, C. A., and R. B. Vallee. 1988. Abundant cytoplasmic dynein related to brain dynein (MAP 1C) in rat liver and testis but not in sea urchin eggs. *Cell Motil. Cytoskel.* 11:195a.
- Cooper, P. D., and R. S. Smith. 1974. The movement of optically detectable organelles in myelinated axons of Xenopus laevis. *J. Physiol.* 242:77-97.
- Crang, R. F. E., and K. L. Klomparens. 1988. Artifacts in Biological Electron Microscopy. Plenum Press, New York.
- Dabora, S. L., and M. P. Sheetz. 1988a. Cultured cell extracts support organelle movement on microtubules in vitro. *Cell Motil. Cytoskel.* 10:482-495.
- Dabora, S. L., and M. P. Sheetz. 1988b. The microtubule-dependent formation of a tubulovesicular network with characteristics of the ER from cultured cell extracts. *Cell* 54:27-35.
- Dentler, W. L., S. Granett, and J. L. Rosenbaum. 1974. Ultrastructural localization of the high molecular weight proteins associated with in vitro-assembled brain microtubules. *J. Cell Biol.* 65:237-241.
- Dustin, P. 1978. Microtubules. Springer-Verlag, New York.

- Euteneuer, U., M. P. Koonce, K. K. Pfister, and M. Schliwa. 1988. An ATPase with properties expected for the organelle motor of the giant amoeba, Reticulomyxa. *Nature (London)* 332:176-178.
- Fok, A. K., and R. D. Allen. 1979. Axenic Paramecium caudatum. I. Mass culture and structure. *J. Protozool.* 26:463-470.
- Fok, A. K., and R. D. Allen. 1988. The Lysosome System. In: Paramecium. (H.-D. Görtz, Ed.). Springer-Verlag, Berlin.
- Fok, A. K., Y. Lee, and R. D. Allen. 1982. The correlation of digestive vacuole pH and size with the digestive cycle in Paramecium caudatum. *J. Protozool.* 29:409-414.
- Fok, A. K., J. H. Muraoka, and R. D. Allen. 1984. Acid phosphatase in the digestive vacuoles and lysosomes of Paramecium caudatum: a timed study. *J. Protozool.* 31:216-220.
- Fok, A. K., B. C. Sisson, Jr., M. S. Ueno, and R. D. Allen. 1988. Phagosome formation in Paramecium: effects of solid particles. *J. Cell Sci.* 90:517-524.
- Fok, A. K., M. S. Ueno, and R. D. Allen. 1986. Differentiation of Paramecium phagosome membrane and stages using monoclonal antibodies. *Eur. J. Cell Biol.* 40:1-8.
- Forman, D. S., A. L. Padjen, and G. R. Siggins. 1977. Axonal transport of organelles visualized by light microscopy: cinemicrographic and computer analysis. *Brain Res.* 136:197-213.
- Gelles, J., B. J. Schnapp, and M. P. Sheetz. 1988. Tracking kinesin-driven movements with nanometre-scale precision. *Nature (London)* 331:450-453.
- Gibbons, I. R. 1966. Studies on the adenosine triphosphatase activity of 14 S and 30 S dynein from cilia of Tetrahymena. *J. Biol. Chem.* 241:5590-5596.
- Gibbons, I. R. 1981. Cilia and flagella of eukaryotes. *J. Cell Biol.* 91:107s-124s.
- Gibbons, I. R. 1988. Microtubule-based motility: an overview of a fast moving field. In: Cell Movement, Volume 1, The Dynein ATPases. (F. D. Warner, P. Satir, and I. R. Gibbons, Eds.). Alan R. Liss, Inc., New York.
- Gibbons, I. R., A. Lee-Eiford, G. Mocz, C. A. Phillipson, W.J.Y. Tang, and B. H. Gibbons. 1987. Photosensitized cleavage of dynein heavy chains. *J. Biol. Chem.* 262:2780-2786.
- Goodenough, U. W., and J. E. Heuser. 1984. Structural comparison of purified dynein proteins with in situ dynein arms. *J. Mol. Biol.* 180:1083-1118.

- Grafstein, B., and D. S. Forman. 1980. Intracellular transport in neurons. *Physiol. Rev.* 60:1167-1283.
- Grissom, P. M., M. E. Porter, and J. R. McIntosh. 1988. Isoforms of cytoplasmic dynein in sea urchin eggs. *J. Cell Biol.* 107:246a.
- Hammond, G. R., and R. S. Smith. 1977. Inhibition of the rapid movements of optically detectable axonal particles by colchicine and vinblastine. *Brain Res.* 128:227-242.
- Hastie, A. T., S. P. Marchese-Ragona, K. A. Johnson, and J. S. Wall. 1988. Structure and mass of mammalian respiratory ciliary outer arm 19S dynein. *Cell Motil. Cytoskel.* 11:157-166.
- Hayden, J. H., and R. D. Allen. 1984. Detection of single microtubules in living cells: particle transport can occur in both directions along the same microtubule. *J. Cell Biol.* 99:1785-1793.
- Hayden, J. H., R. D. Goldman, and R. D. Allen. 1983. Cytoplasmic transport in keratocyte: direct visualization of particle translocation along microtubules. *Cell Motil.* 3:1-19.
- Heidemann, S. R., J. M. Landers, and M. A. Hamborg. 1981. Polarity orientation of axonal microtubules. *J. Cell Biol.* 91:661-665.
- Heidemann, S. R., and J. R. McIntosh. 1980. Visualization of the structural polarity of microtubules. *Nature (London)* 286:517-519.
- Heuser, J. E. 1981. Preparing biological samples for stereomicroscopy by the quick-freeze, deep-etch, rotary-replication technique. *Methods Cell Biol.* 22:97-122.
- Heuser, J. E. 1983. Procedure for freeze-drying molecules adsorbed to mica flakes. *J. Mol. Biol.* 169:155-195.
- Heuser, J. E., and M. W. Kirschner. 1980. Filament organization revealed in platinum replicas of freeze dried cytoskeletons. *J. Cell Biol.* 86:212-234.
- Heuser, J. E., T. S. Reese, M. J. Dennis, Y. Jan, L. Jan, and L. Evans. 1979. Synaptic vesicle exocytosis captured by quick freezing and correlated with quantal transmitter release. *J. Cell Biol.* 81:275-300.
- Hirokawa, N. 1982. Cross-linker system between neurofilaments, microtubules, and membranous organelles in frog axons revealed by the quick-freeze, deep-etching method. *J. Cell Biol.* 94:129-142.
- Hirokawa, N. 1986a. Quick freeze, deep etch of the cytoskeleton. *Methods Enzymol.* 134:598-612.
- Hirokawa, N. 1986b. 270 kD microtubule-associated protein cross-reacting with anti-MAP 2 IgG in the crayfish peripheral nerve axon. *J. Cell Biol.* 103:33-39.

- Hirokawa, N. 1988. Interactions between cytoskeletal polymers in neurons: quick-freeze deep-etch and immunocytochemical studies. In: Intrinsic determinants of neuronal form and function. Alan R. Liss, Inc., New York.
- Hirokawa, N., G. S. Bloom, and R. B. Vallee. 1985. Cytoskeletal architecture and immunocytochemical localization of microtubule-associated proteins in regions of axons associated with rapid axonal transport: the beta, beta'-iminodipropionitrile-intoxicated axon as a model system. *J. Cell Biol.* 101:227-239.
- Hirokawa, N., S. Hisanaga, and Y. Shiomura. 1988a. MAP 2 is a component of crossbridges between microtubules and neurofilaments in the neuronal cytoskeleton. Quick-freeze, deep-etch immunoelectron microscopy and reconstitutuion studies. *J. Neuroscience* 8:2769-2779.
- Hirokawa, N., K. K. Pfister, H. Yorifuji, M. C. Wagner, S. T. Brady, and G. S. Bloom. 1989. Submolecular domains of bovine brain kinesin identified by electron microscopy and monoclonal antibody decoration. *Cell* 56:867-878.
- Hirokawa, N., Y. Shiomura, and S. Okabe. 1988b. Tau proteins: the molecular structure and mode of binding on microtubules. *J. Cell Biol.* 107:1449-1459.
- Hirokawa, N., and H. Yorifuji. 1986. Cytoskeletal architecture of reactivated crayfish axons, with special reference to crossbridges among microtubules and between microtubules and membrane organelles. *Cell Motil. Cytoskel.* 6:458-468.
- Hirokawa, N., T. Yoshida, and R. Sato-Yoshitake. 1989. Brain Dynein (MAP 1C) localized on both anterogradely and retrogradely transported membranous organelles. *J. Cell Biol.* 109:157a.
- Hollenbeck, P. J. 1988. Kinesin: its properties and possible functions. *Protoplasma* 145:145-152.
- Huber, G., G. Pehling, and A. Matus. 1986. The novel microtubule-associated protein MAP 3 contributes to the in vitro assembly of brain microtubules. *J. Biol. Chem.* 261:2270-2273.
- Ingold, A. L., S. A. Cohn, and J. M. Scholey. 1988. Inhibition of kinesin-driven microtubule motility by monoclonal antibodies to kinesin heavy chains. *J. Cell Biol.* 107:2657-2667.
- Jalfors, U., and D. S. Smith. 1969. Association between synaptic vesicles and neurotubules. *Nature (London)* 224:710-711.
- Jurand, A., and G. G. Selman. 1969. The Anatomy of Paramecium aurelia. St. Martin's Press, New York.
- Kachar, B., P. C. Bridgman, and T. S. Reese. 1987. Dynamic shape changes of cytoplasmic organelles translocating along microtubules. *J. Cell Biol.* 105:1267-1271.

- Karlsson, J. O., and J. Sjöstrand. 1969. The effects of colchicine on the axonal transport in the optic nerve and tract of the rabbit. *Brain Res.* 13:617-619.
- Kirkpatrick, J. B., J. J. Bray, and S. M. Palmer. 1972. Visualization of axoplasmic flow in vitro by Nomarski microscopy. Comparison to rapid flow of radioactive proteins. *Brain Res.* 43:1-10.
- Kirschner, M. W. 1989. Biological implications of microtubule dynamics. The Harvey Lectures, Series 83, pages 1-20. Alan R. Liss, Inc., New York.
- Kondo, H. 1985. Reexamination of the reality or artifacts of the microtrabeculae. *J. Ultrastruc. Res.* 87:124-135.
- Koonce, M. P., U. Euteneuer, K. L. McDonald, D. Menzel, and M. Schliwa. 1986. Cytoskeletal architecture and motility in a giant freshwater amoeba, Reticulomyxa. *Cell Motil. Cytoskel.* 6:521-533.
- Kreutzberg, G. W., and G. W. Gross. 1977. General morphology and axonal ultrastructure of the olfactory nerve of the pike, Esox lucius. *Cell Tissue Res.* 181:443-457.
- Kuznetsov, S. A., and V. I. Gelfand. 1986. Bovine brain kinesin is a microtubule-activated ATPase. *Proc. Natl. Acad. Sci. (USA)* 83:8530-8534.
- Langford, G. M., R. D. Allen, and D. G. Weiss. 1987. Substructure of sidearms on squid axoplasmic vesicles and microtubules visualized by negative contrast electron microscopy. *Cell Motil. Cytoskel.* 7:20-30.
- Laemmli, U. K. 1970. Cleavage of structural proteins during the assembly of the head of bacteriophage T4. *Nature (London)* 227:680-685.
- Lanzetta, P. A., L. J. Alvarez, P. S. Reinach, and O. A. Candia. 1979. An improved assay for nanomole amounts of inorganic phosphate. *Anal. Biochem.* 100:95-97.
- Lasek, R. J. 1970. Protein transport in neurons. *Int. Rev. Neurobiol.* 13:289-321.
- Lasek, R. J., and S. T. Brady. 1985. Attachment of transported vesicles to microtubules in axoplasm is facilitated by AMP-PNP. *Nature (London)* 316:645-647.
- Lye, R. J., M. E. Porter, J. M. Scholey, and J. R. McIntosh. 1987. Identification of a microtubule-based cytoplasmic motor in the nematode C. elegans. *Cell* 51:309-318.
- Marchbanks, R. M., and M. Israel. 1972. The heterogeneity of bound acetylcholine and synaptic vesicles. *Biochem. J.* 129:1049-1061.

- Martin, R. G., and B. N. Ames. 1961. A method for determining the sedimentation behavior of enzymes: application to protein mixtures. *J. Biol. Chem.* 236:1372-1379.
- Mast, S. O. 1947. The food-vacuole in Paramecium. *Biol. Bull.* 92:31-72.
- Matteoni, R., and T. E. Kreis. 1987. Translocation and clustering of endosomes and lysosomes depends on microtubules. *J. Cell Biol.* 105:1253-1265.
- McEwen, B. S., and B. Grafstein. 1968. Fast and slow components in axonal transport. *J. Cell Biol.* 38:494-508.
- McNiven, M. A., and K. R. Porter. 1984. Chromatophores--models for studying cytomatrix translocations. *J. Cell Biol.* 99:152s-158s.
- Merril, C. R., D. Goldman, S. A. Sedman and M. H. Ebert. 1981. Ultrasensitive stain for proteins in polyacrylamide gels shows regional variation in cerebrospinal fluid proteins. *Science* 211:1437-1438.
- Miller, R. H., and R. J. Lasek. 1985. Cross-bridges mediate anterograde and retrograde vesicle transport along microtubules in squid axoplasm. *J. Cell Biol.* 101:2181-2193.
- Murphy, D. B., R. R. Hiesch, and K. T. Wallis. 1983. Identity and origin of the ATPase activity associated with neuronal microtubules. I. The ATPase activity is associated with membrane vesicles. *J. Cell Biol.* 96:1298-1305.
- Neely, M. D., and K. Boekelheide. 1988. Sertoli cell processes have axoplasmic features: an ordered microtubule distribution and an abundant high molecular weight microtubule-associated protein (cytoplasmic dynein). *J. Cell Biol.* 107:1767-1776.
- Neighbors, B. W., R. C. Williams, and J. R. McIntosh. 1988. Localization of kinesin in cultured cells. *J. Cell Biol.* 106:1193-1204.
- Obika, M. 1986. Intracellular transport of pigment granules in fish chromatophores. *Zool. Sci.* 3:1-11.
- Ochs, S. 1971. Characteristics and a model for fast axoplasmic transport in the nerve. *J. Neurobiol.* 2:331-346.
- Ochs, S., and D. Hollingsworth. 1971. Dependence of fast axoplasmic transport in nerve on oxidative metabolism. *J. Neurochem.* 18:107-114.
- Ochs, S., and R. Ranish. 1969. Characteristics of the fast transport system in mammalian nerve fibers. *J. Neurobiol.* 1:247-261.

- Parysek, L. M., C. F. Asnes, and J. B. Olmsted. 1984. MAP 4: occurrence in mouse tissues. *J. Cell Biol.* 99:1309-1315.
- Paschal, B. M., H. S. Shpetner, and R. B. Vallee. 1987. MAP 1C is a microtubule-activated ATPase which translocates microtubules in vitro and has dynein-like properties. *J. Cell Biol.* 105:1273-1282.
- Paschal, B. M., and R. B. Vallee. 1987. Retrograde transport by the microtubule-associated protein MAP 1C. *Nature (London)* 330:181-183.
- Paulson, J. C., and W. O. McClure. 1975. Inhibition of axoplasmic transport by colchicine, podophyllotoxin, and vinblastine: an effect on microtubules. *Ann. N. Y. Acad. Sci.* 253:517-527.
- Pfarr, C., and J. R. McIntosh. 1988. HeLa cytoplasmic dynein is a microtubule translocator. *Cell Motil. Cytoskel.* 11:198a.
- Pfister, K. K., R. B. Fay, and G. B. Witman. 1982. Purification and polypeptide composition of dynein ATPases from Chlamydomonas flagella. *Cell Motil.* 2:525-547.
- Pfister, K. K., M. C. Wagner, D. L. Stenoiien, S. T. Brady, and G. S. Bloom. 1989. Monoclonal antibodies to kinesin heavy chains and light chains stain vesicle-like structures, but not microtubules, in cultured cells. *J. Cell Biol.* 108:1453-1463.
- Plattner, H., C. Westphal, and R. Tiggemann. 1982. Cytoskeleton-secretory vesicle interactions during the docking of secretory vesicles at the cell membrane in Paramecium tetraurelia cells. *J. Cell Biol.* 92:368-377.
- Porter, M. E., J. M. Scholey, D. L. Stemple, G. P. A. Vigers, R. D. Vale, M. P. Sheetz, and J. R. McIntosh. 1987. Characterization of the microtubule movement produced by sea urchin egg kinesin. *J. Biol. Chem.* 262:2794-2802.
- Porter, M. E., P. M. Grissom, J. M. Scholey, E. D. Salmon, and J. R. McIntosh. 1988. Dynein isoforms in sea urchin eggs. *J. Biol. Chem.* 263:6759-6771.
- Pratt, M. M. 1981. The identification of a dynein ATPase in unfertilized sea urchin eggs. *Dev. Biol.* 74:364-378.
- Raine, C. S., G. Ghetti, and L. M. Shelanski. 1971. On the association between tubules and mitochondria in axons. *Brain Res.* 34:389-393.
- Rebhun, L. I. 1972. Polarized intracellular transport: saltatory movements and cytoplasmic streaming. *Int. Rev. Cytol.* 32:92-137.
- Reynolds, E. S. 1963. The use of lead citrate at high pH as an electron-opaque stain in electron microscopy. *J. Cell Biol.* 17:208-213.

- Ris, H. 1985. The cytoplasmic filament system in critical point-dried whole mounts and plastic-embedded sections. *J. Cell Biol.* 100:1474-1487.
- Sandoval, I. V., J. S. Bonifacino, R. D. Klausner, M. Henkary, and J. Wehland. 1984. Role of microtubules in the organization and localization of the Golgi apparatus. *J Cell Biol.* 99:113s-118s.
- Saxton, W. M., M. E. Porter, S. A. Cohn, J. M. Scholey, E. C. Raff, and J. R. McIntosh. 1988. Drosophila kinesin: characterization of microtubule motility and ATPase. *Proc. Natl. Acad. Sci. (USA)* 85:1109-1113.
- Saxton, W. M., and E. C. Raff. 1988. Drosophila kinesin: looking for a function. *J. Cell Biol.* 107:672a.
- Schliwa, M. 1984. Mechanisms of intracellular organelle transport. In: Cell and Muscle Motility, Vol. 5 (J. W. Shay, Ed.), Plenum, New York.
- Schliwa, M. 1986. The Cytoskeleton. Springer-Verlag, New York.
- Schnapp, B. J. 1986. Viewing single microtubules by video light microscopy. *Methods Enzymol.* 134:561-573.
- Schnapp, B. J., and T. S. Reese. 1982. Cytoplasmic structure in rapid frozen axons. *J. Cell Biol.* 94:667-679.
- Schnapp, B. J., and T. S. Reese. 1989. Dynein is the motor for retrograde axonal transport of organelles. *Proc. Natl. Acad. Sci. (USA)* 86:1548-1552.
- Schnapp, B. J., R. D. Vale, M. P. Sheetz, and T. S. Reese. 1985. Single microtubules from squid axoplasm support bidirectional movement of organelles. *Cell* 40:455-462.
- Scholey, J. M., M. E. Porter, P. M. Grissom, and J. R. McIntosh. 1985. Identification of kinesin in sea urchin eggs, and evidence for its localization in the mitotic spindle. *Nature (London)* 318:483-486.
- Schroer, T. A., B. J. Schnapp, T. S. Reese, and M. P. Sheetz. 1988. The role of kinesin and other soluble factors in organelle movement along microtubules. *J. Cell Biol.* 107:1785-1792.
- Schroer, T. A., E. R. Steuer, and M. P. Sheetz. 1989. Cytoplasmic dynein is a minus end-directed motor for membranous organelles. *Cell* 56:937-946.
- Shelanski, M. L., and E. W. Taylor. 1967. Isolation of a protein sub-unit from microtubules. *J. Cell Biol.* 34:549-554.
- Shiomura, Y., and N. Hirokawa. 1987. The molecular structure of microtubule-associated protein 1A (MAP 1A) in vivo and in vitro. An immunoelectron microscopy and quick-freeze, deep-etch study. *J. Neurosci.* 7:1461-1469.

- Shpetner, H. S., B. M. Paschal, and R. B. Vallee. 1988. Characterization of the microtubule-activated ATPase of brain cytoplasmic dynein (MAP 1C). *J. Cell Biol.* 107:1001-1009.
- Shpetner, H. S., and R. B. Vallee. 1989. Identification of dynamin, a novel mechanochemical enzyme that mediates interactions between microtubules. *Cell* 59:421-432.
- Sitte, H., L. Edelmann, and K. Neumann. 1987. Cryofixation without pretreatment at ambient pressure. In: Cryotechniques in Biological Electron Microscopy. (R. A. Steinbrecht and K. Zierold, Eds.) Springer-Verlag, Berlin.
- Sloboda, R. D., W. L. Dentler, and J. L. Rosenbaum. 1976. Microtubule-associated proteins and the stimulation of tubulin assembly in vitro. *Biochemistry* 15:4497-4505.
- Smith, B. H. 1971. Neuroplasmic transport in the nervous system of the cockroach Periplaneta americana. *J. Neurobiol.* 2:107-118.
- Smith, D. S., U. Jalfors, and R. Beraneck. 1970. The organization of synaptic axoplasm in the lamprey (Petromyzon myrinus) central nervous system. *J. Cell Biol.* 46:199-219.
- Smith, D. S., U. Jalfors, and B. F. Cameron. 1975. Morphological evidence for the participation of microtubules in axonal transport. *Ann. N. Y. Acad. Sci.* 253:472-506.
- Stephens, R. E. 1983. Reconstitution of ciliary membranes containing tubulin. *J. Cell Biol.* 96:68-75.
- Stephens, R. E. 1986. Membrane tubulin. *Biol. Cell.* 57:95-110.
- Teresaki, M., L. B. Chen, and K. Fujiwara. 1986. Microtubules and the endoplasmic reticulum are highly interdependent structures. *J. Cell Biol.* 103:1557-1568.
- Travis, S. M., and D. L. Nelson. 1988. Purification and properties of dyneins from Paramecium cilia. *Biochim. Biophys. Acta.* 966:73-83.
- Tucker, J. B. 1984. Spatial organization of microtubule-organizing centers and microtubules. *J. Cell Biol.* 99:55s-62s.
- Tyler, J. M., and D. Branton. 1980. Rotary shadowing of extended molecules dried from glycerol. *J. Ultrastruct. Res.* 71:95-102.
- Vale, R. D. 1987. Intracellular transport using microtubule-based motors. *Ann. Rev. Cell Biol.* 3:347-378.
- Vale, R. D., and H. Hotani. 1988. Formation of membrane networks in vitro by kinesin-driven microtubule movement. *J. Cell Biol.* 107:2233-2241.

- Vale, R. D., T. S. Reese, and M. P. Sheetz. 1985a. Identification of a novel force-generating protein, kinesin, involved in microtubule-based motility. *Cell* 42:39-50.
- Vale, R. D., B. J. Schnapp, T. Mitchison, E. Steuer, T. S. Reese, and M. P. Sheetz. 1985b. Different axoplasmic proteins generate movement in opposite directions along microtubules in vitro. *Cell* 43:623-632.
- Vale, R. D., B. J. Schnapp, T. S. Reese, and M. P. Sheetz. 1985c. Movement of organelles along filaments dissociated from the axoplasm of the squid giant axon. *Cell* 40:449-454.
- Vale, R. D., B. J. Schnapp, T. S. Reese, and M. P. Sheetz. 1985d. Organelle, bead, and microtubule translocations promoted by soluble factors from the squid giant axon. *Cell* 40:559-569.
- Vale, R. D., and Y. Y. Toyoshima. 1989. Microtubule translocation properties of intact and proteolytically digested dyneins from *Tetrahymena* cilia. *J. Cell Biol.* 108:2327-2334.
- Vallee, R. B. 1982. A taxol-dependent procedure for the isolation of microtubules and microtubule-associated proteins (MAPs). *J. Cell Biol.* 92:435-442.
- Vallee, R. B. 1986. Purification of brain microtubules and microtubule-associated protein-1 using taxol. *Methods Enzymol.* 134:104-115.
- Vallee, R. B., and G. S. Bloom. 1983. Isolation of sea urchin egg microtubules with taxol and identification of mitotic spindle microtubule-associated proteins with monoclonal antibodies. *Proc. Natl. Acad. Sci. (USA)* 80:6259-6263.
- Vallee, R. B., G. S. Bloom, and W. E. Theurkauf. 1984. Microtubule-associated protein subunits of the cytomatrix. *J. Cell Biol.* 99:39s-44s.
- Vallee, R. B., J. S. Wall, B. M. Paschal, and H. S. Shpetner. 1988. Microtubule-associated protein 1C from brain is a two-headed cytosolic dynein. *Nature (London)* 332:561-563.
- Vallee, R. B., B. M. Paschal, and H. S. Shpetner. 1989. Characterization of microtubule-associated protein (MAP) 1C as the motor for retrograde organelle transport and its identification as dynein. In: Cell Movement, Volume 2, Kinesin, Dynein, and Microtubule Dynamics. (F. D. Warner and J. R. McIntosh, Eds.). Alan R. Liss, Inc., New York.
- Voter, W. A., and H. P. Erikson. 1982. Electron microscopy of MAP 2 (microtubule associated protein 2). *J. Ultrastruct. Res.* 80:374-382.
- Yang, J. T., R. A. Laymon, and L. S. B. Goldstein. 1989. A three-domain structure of kinesin heavy chain revealed by DNA sequence and microtubule binding analyses. *Cell* 56:879-889.

- Wang, E., and R. D. Goldman. 1978. Functions of cytoplasmic fibers in intracellular movements in BHK-21 cells. *J. Cell Biol.* 79:708-726.
- Weingarten, M. D., A. H. Lockwood, S.-Y. Hwo, and M. W. Kirschner. 1975. A protein factor essential for microtubule assembly. *Proc. Natl. Acad. Sci. (USA)* 72:1858-1862.
- Weisenberg, R. C. 1972. Microtubule formation in vitro in solutions containing low calcium concentrations. *Science* 177:1104-1105.
- Weiss, D. G. 1986. The mechanism of axoplasmic transport. In: Axoplasmic Transport. (Z. Iqbal, Ed.) CRC Press, Boca Raton.
- Wiche, G. 1989. High-M_r microtubule-associated proteins: properties and functions. *Biochem. J.* 259:1-12.